Contents

1 Changes since Last Version of AN

- Version v2
  - Update results to 976 pb^{-1}
  - Add model-dependent upper limits (Sec. 16)

2 Introduction

In this note we describe a search for new physics in the opposite sign isolated dilepton sample (ee, $e\mu$, and $\mu\mu$) based on 976 pb^{-1} of 2011 data. The main sources of isolated dileptons at CMS are Drell Yan and $t\bar{t}$. Here we concentrate on dileptons with invariant mass inconsistent with $Z \to ee$ and $Z \to \mu\mu$, thus $t\bar{t}$ is the most important background. A separate search for new physics in the Z sample is performed as a separate analysis. This is an update of a (soon to be) published analysis performed on 2010 data [1, 2].

The search strategy is the following

- We start out with a pre-selection which is as close as possible to the published $t\bar{t}$ dilepton analysis [3] (same lepton ID, same jet definitions, etc.). We do make a couple of substantive modifications:
  1. The top analysis requires two leptons of $P_T > 20$ GeV. In this analysis we search for new physics in 2 data samples. The first data sample is collected with high p_T dilepton triggers; for this sample we require leptons with $p_T >$ (20,10) GeV (leading lepton $p_T > 20$ GeV, trailing lepton $p_T > 10$ GeV). The second data sample is collected with dilepton-H_T cross triggers. For this sample we require ee dileptons with $p_T >$ (10,10) GeV, $\mu\mu$ dileptons with $p_T >$ (10,5) GeV, and for $e\mu$ dileptons we require $p_T >$ (10,5) GeV and that the electron has $p_T > 10$ GeV. This is motivated by our desire to maintain sensitivity to possible SUSY signals with relatively low p_T leptons generated in the cascade decays of heavy objects.
  2. The top analysis requires at least two jets of $p_T > 30$ GeV with $\mathrm{E_T^{miss}} > 30$ GeV (ee and $\mu\mu$) or $\mathrm{E_T^{miss}} > 20$ GeV ($e\mu$). We tighten the $\mathrm{E_T^{miss}}$ cut to 50 GeV and we also require that the scalar sum of the p_T of all jets with $p_T > 30$ GeV be > 100 GeV. These requirements considerably reduce backgrounds to the $t\bar{t}$ sample, *e.g.*, backgrounds from Drell Yan and W+jets.
- The pre-selection consists mostly of $t\bar{t}$ events. Kinematic distributions in data are compared against Monte Carlo. Assuming reasonable agreeement for the bulk of $t\bar{t}$ we move on to a search for new physics in the tails of the $t\bar{t}$ $\mathrm{E_T^{miss}}$ and H_T distributions.
- Our prejudice is that new physics would manifest itself in an excess of events with high $\mathrm{E_T^{miss}}$ and significant hadronic activity. We define search regions a-priori by tightening the $\mathrm{E_T^{miss}}$ and hadronic activity requirements.
- We perform a counting experiment in the signal regions. We compare observed yields with expectations from Monte Carlo and with three independent data driven techniques (see Sections 11.1, 11.3 and 11.4).

3 Datasets, Triggers, Luminosity

A data sample corresponding to 976 pb^{-1} was analyzed, using the the official May10ReReco and July 1st PromptReco json files:

- `Cert_160404-163869_7TeV_May10ReReco_Collisions11_JSON`
- `Cert_160404-167784_7TeV_PromptReco_Collisions11_JSON`

We use two data samples, one collected with high p_T dilepton triggers and the other with dilepton-H_T cross triggers. These samples are complementary, since the dilepton-H_T trigger sample extends to lower lepton p_T, while the high p_T dilepton trigger sample does not include requirements on the hadronic activity in the event.

Currently we use data reconstructed in CMSSW 4_2_X and Spring11 MC reconstructed in CMSSW 3_11_X. We will update the MC when the Summer11 madgraph MC samples become available.

- Datasets
  - High p_T dilepton trigger sample
    * DoubleElectron_Run2011A-May10ReReco-v1_AOD
    * DoubleMu_Run2011A-May10ReReco-v1_AOD
    * MuEG_Run2011A-May10ReReco-v1_AOD
    * DoubleElectron_Run2011A-PromptReco-v4_AOD
    * DoubleMu_Run2011A-PromptReco-v4_AOD
    * MuEG_Run2011A-PromptReco-v4_AOD
  - Dilepton-H_T cross trigger sample
    * ElectronHad_Run2011A-May10ReReco-v1_AOD
    * MuHad_Run2011A-May10ReReco-v1_AOD
    * ElectronHad_Run2011A-PromptReco-v4_AOD
    * MuHad_Run2011A-PromptReco-v4_AOD
- Monte Carlo samples
  - TTJets_TuneZ2_7TeV-madgraph-tauola_Spring11-PU_S1_START311_V1G1-v1
  - DYToEE_M-10To20_TuneZ2_7TeV-pythia6_Spring11-PU_S1_START311_V1G1-v1
  - DYToMuMu_M-10To20_TuneZ2_7TeV-pythia6_Spring11-PU_S1_START311_V1G1-v1
  - DYToTauTau_M-10To20_CT10_TuneZ2_7TeV-powheg-pythia-tauola_Spring11-PU_S1_START311_V1G1-v2
  - DYToEE_M-20_CT10_TuneZ2_7TeV-powheg-pythia_Spring11-PU_S1_START311_V1G1-v1
  - DYToMuMu_M-20_CT10_TuneZ2_7TeV-powheg-pythia_Spring11-PU_S1_START311_V1G1-v1
  - DYToTauTau_M-20_CT10_TuneZ2_7TeV-powheg-pythia-tauola_Spring11-PU_S1_START311_V1G1-v1
  - DYJetsToLL_TuneD6T_M-50_7TeV-madgraph-tauola_Spring11-PU_S1_START311_V1G1-v1
  - WWTo2L2Nu_TuneZ2_7TeV-pythia6_Spring11-PU_S1_START311_V1G1-v1
  - WZtoAnything_TuneZ2_7TeV-pythia6-tauola_Spring11-PU_S1_START311_V1G1-v1
  - ZZtoAnything_TuneZ2_7TeV-pythia6-tauola_Spring11-PU_S1_START311_V1G1-v1
  - WJetsToLNu_TuneZ2_7TeV-madgraph-tauola_Spring11-PU_S1_START311_V1G1-v1
  - TToBLNu_TuneZ2_s-channel_7TeV-madgraph_Spring11-PU_S1_START311_V1G1-v1
  - TToBLNu_TuneZ2_t-channel_7TeV-madgraph_Spring11-PU_S1_START311_V1G1-v1
  - TToBLNu_TuneZ2_tW-channel_7TeV-madgraph_Spring11-PU_S1_START311_V1G1-v1

4 Event Preselection

The purpose of the preselection is to reject backgrounds other than $t\bar{t} \rightarrow$ dileptons. We compare the kinematical properties of this sample with expectations from $t\bar{t}$ Monte Carlo.

The preselection is based on the $t\bar{t}$ analysis [3]. We select events with two opposite sign, well-identified and isolated leptons (ee, $e\mu$, or $\mu\mu$); one of the leptons must have $p_T > 20$ GeV, the other one must have $p_T > 10$ GeV. Events with dilepton mass consistent with $Z \rightarrow ee/\mu\mu$ are rejected. In case of events with more than two such leptons, we select the pair that maximizes the scalar sum of lepton p_T's. There must be at least two pfjets of $p_T > 30$ GeV and $|\eta| < 3.0$; jets must pass loose `pfJetId` and be separated by $\Delta R > 0.4$ from any lepton with $p_T > 10$ GeV passing the selection. The scalar sum H_T of the p_T of all such jets must exceed 100 GeV, for the dilepton-H_T sample this requirement is increased to 200 GeV since these triggers have large inefficiency below this threshold. Finally, we require $\mathrm{E_T^{miss}} > 50$ GeV (pfmet). More details are given in the subsections below.

4.1 Event Cleanup

- Require at least one good deterministic annealing (DA) vertex
  - not fake
  - ndof > 4
  - $|\rho| < 2$ cm
  - $|z| < 24$ cm.

4.2 Muon Selection

Muon candidates are RECO muon objects passing the following requirements:

- $p_T > 5$ GeV and $|\eta| < 2.4$
- Global Muon and Tracker Muon
- χ^2/ndof of global fit < 10
- At least 11 hits in the tracker fit
- Impact parameter with respect to the first DA vertex $d_0 < 200$ μm and $d_z < 1$ cm
- $Iso \equiv E_T^{\rm iso}/p_T < 0.15$, $E_T^{\rm iso}$ is defined as the sum of transverse energy/momentum deposits in ecal, hcal, and tracker, in a cone of 0.3
- At least one of the hits from the standalone muon must be used in the global fit
- Tracker $\Delta p_T/p_T < 0.1$

4.3 Electron Selection

Electron candidates are RECO GSF electrons passing the following requirements:

- $p_T > 10$ GeV and $|\eta| < 2.5$.
- Veto electrons with a supercluster in the transition region $1.4442 < |\eta| < 1.556$.
- VBTF90 identification[4] with requirements tightened to match the CaloIdT and TrkIdVL HLT requirements:
  - $\sigma_{i\eta i\eta} < 0.01$ (EB), 0.03 (EE)
  - $\Delta\phi < 0.15$ (EB), 0.10 (EE)
  - $\Delta\eta < 0.007$ (EB), 0.009 (EE)
  - $H/E < 0.1$ (EB), 0.075 (EE)
- Impact parameter with respect to the first DA vertex $d_0 < 400$ μm and $d_z < 1$ cm.
- $Iso \equiv E_T^{\rm iso}/p_T < 0.15$. $E_T^{\rm iso}$ is defined as the sum of transverse energy/momentum deposits in ecal, hcal, and tracker, in a cone of 0.3. A 1 GeV pedestal is subtracted from the ecal energy deposition in the EB, however the ecal energy is never allowed to go negative.
- Electrons with a tracker or global muon within ΔR of 0.1 are vetoed.
- The number of missing expected inner hits must be less than two [5].
- Conversion removal via partner track finding: any electron where an additional GeneralTrack is found with dist < 0.02 cm and $\Delta \cot\theta < 0.02$ is vetoed [5].

We estimate the contributions from fake leptons using the data-driven fake rate (FR) method [11]. The requirements defining the fakeable objects are listed in App. A.

4.4 Invariant mass requirement

We remove e^+e^- and $\mu^+\mu^-$ events with invariant mass between 76 and 106 GeV. We also remove events with invariant mass < 12 GeV, since this kinematical region is not well reproduced in CMS Monte Carlo and to remove events with Upsilons.

In addition, we remove $Z \to \mu\mu\gamma$ candidates with the γ collinear with one of the muons. This is done as follows: if the ecal energy associated with one of the muons is greater than 6 GeV, we add this energy to the momentum of the initial muon, and we recompute the $\mu\mu$ mass. If this mass is between 76 and 106 GeV, the event is rejected.

4.5 Trigger Selection

We do not make any requirements on HLT bits in the Monte Carlo. Instead, as discussed in Section 5, a trigger efficiency weight is applied to each event, based on the trigger efficiencies measured on data (see Sec. 5).

We select data events using the following triggers. An event in the ee channel is required to pass a DoubleElectron trigger, an event in the $\mu\mu$ channel is required to pass a DoubleMu trigger, and an event in the $e\mu$ channel is required to pass a Ele-Mu trigger.

- High p_T dilepton trigger sample
  - `HLT_Ele17_CaloIdL_CaloIsoVL_Ele8_CaloIdL_CaloIsoVL`
  - `HLT_DoubleMu7`
  - `HLT_Mu13_Mu8`
  - `HLT_Mu17_Ele8_CaloIdL`
  - `HLT_Mu8_Ele17_CaloIdL`
- Lepton H_T cross trigger sample
  - `HLT_DoubleMu3_HT150`
  - `HLT_DoubleMu3_HT160`
  - `HLT_Mu3_Ele8_CaloIdL_TrkIdVL_HT150`
  - `HLT_Mu3_Ele8_CaloIdT_TrkIdVL_HT150`
  - `HLT_Mu3_Ele8_CaloIdL_TrkIdVL_HT160`
  - `HLT_Mu3_Ele8_CaloIdT_TrkIdVL_HT160`
  - `HLT_DoubleEle8_CaloIdL_TrkIdVL_HT150`
  - `HLT_DoubleEle8_CaloIdT_TrkIdVL_HT150`
  - `HLT_DoubleEle8_CaloIdL_TrkIdVL_HT160`
  - `HLT_DoubleEle8_CaloIdT_TrkIdVL_HT160`

5 Trigger efficiency

For the high p_T dilepton triggers, the efficiencies have been measured to be approximately 100% (DoubleEle), 90% (DoubleMu), and 95% (Mu-Ele) [6]. In the following, unless otherwise specified we weight the ee, $\mu\mu$ and $e\mu$ MC events by these efficiencies. We do not apply any efficiency correction for the hadronic part of the dilepton-H_T triggers. We have verified that the efficiencies for these triggers with respect to an offline selection of $H_T >$ 200 GeV is high ($\sim$90–95%), as shown in Fig. 1.

6 Dilepton Yields

Table 1: The data and MC yields in the ee and $\mu\mu$ final states for events with 2 selected leptons with invariant mass 76–106 GeV.

Sample	ee	$\mu\mu$
data	312963	394119
MC	299819	352879
data/MC	1.04	1.12

The data and MC dilepton mass distributions for events with 2 leptons passing the dilepton triggered $p_T >$ (20,10) GeV selection are displayed in Fig. 2. The yields of Z events in the mass range 76–106 GeV are indicated in Table 1. In data we observe a slight excess with respect to MC expectations, of 4% (12%) in the ee ($\mu\mu$) channel, which we attribute to uncertainties in trigger efficiency, lepton selection efficiency, and integrated luminosity. We use the ratio of $Z \to \mu^+\mu^-$ to $Z \to e^+e^-$ yields in data to estimate the ratio of muon to electron selection efficiencies, and find $R_{\mu e} = \mathrm{eff}(\mu)/\mathrm{eff(e)} = 1.12$.

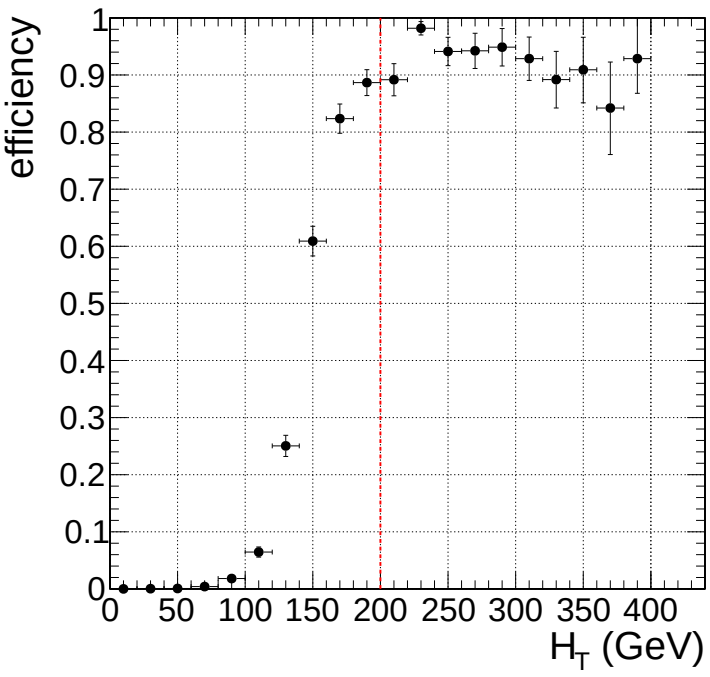

Figure 1: Efficiency for the dimuon-H_T trigger HLT_DoubleMu3_HT150 as a function of the offline H_T. Events are selected with the high p_T dilepton trigger HLT_DoubleMu7 and required to have 2 muons passing analysis selection. The vertical dashed line indicates the requirement $H_T > 200$ GeV, which is used in the preselection for the dilepton-H_T trigger sample.

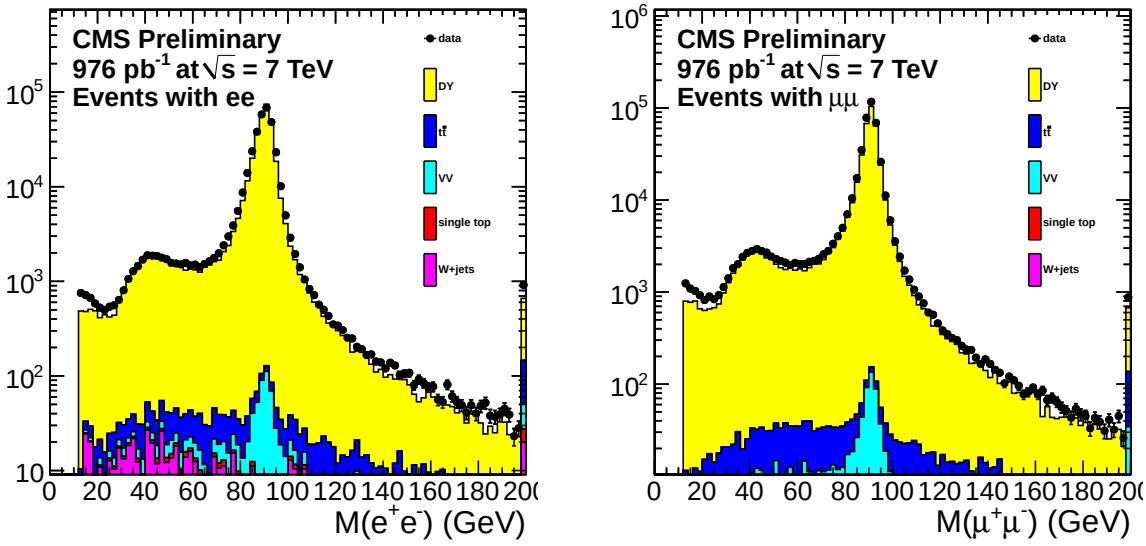

Figure 2: Distributions of dilepton mass in data and MC, in the ee channel (left) and $\mu\mu$ channel (right).

7 Preselection yields: Data/MC Comparison

The data yields and the MC predictions for the dilepton trigger sample are given in Table 2. As anticipated, the MC predicts that the preselection is dominated by $t\bar{t}$. We observe a slight excess in data with respect to MC expectations, which may be related to a possible under-estimate of the luminosity at the level of 5–10%. We also look for an excess of low lepton p_T events using the dilepton-H_T trigger sample. In this sample the leptons are required have $p_T >$ (10,5) GeV and not to have $p_T >$ (20,10) GeV. This is done to remove overlap with the dilepton trigger sample, as summarized in Table 3. We observe reasonable agreement between the data and MC

yields in this region. Finally, we compare in Table 4 the data samples collected with high p_T dilepton triggers and lepton-H_T cross triggers, including the requirements $H_T > 200$ GeV and lepton $p_T >$ (20,10) GeV. The yields in the high-p_T dilepton and dilepton-H_T trigger samples are very similar.

The MC yields are normalized to 976 pb^{-1} using the cross-sections from Reference [7]. The MC is scaled by the approximate trigger efficiency (100% for ee, 95% for $\mu\mu$, and 95% for $e\mu$) and has been reweighted such that the distribution of reconstructed DA vertices matches that in data. The DY contribution is dominated by DY$\rightarrow \tau^+\tau^-$, and we have verified with the data-driven $R_{out/in}$ method [3] that the contributions from DY$\rightarrow e^+e^-$ and DY$\rightarrow \mu^+\mu^-$ are negligible. Also shown are the yields for LM1 and LM3, two of the LM points which are benchmarks for SUSY analyses at CMS. The LM yields are calculated at NLO using process-dependent k-factors computed from Prospino.

Table 2: High p_T dilepton trigger data and Monte Carlo yields for the preselection (njets ≥ 2, H_T>100 GeV, $\mathrm{E_T^{miss}}$ > 50 GeV, lepton $p_T >$ (20,10) GeV).

Sample	ee	$\mu\mu$	$e\mu$	tot
$t\bar{t} \rightarrow \ell^+\ell^-$	335.8 ± 8.0	372.3 ± 8.0	895.7 ± 12.8	1603.8 ± 17.1
$t\bar{t} \rightarrow \ell^\pm\tau^\mp/\tau^+\tau^-$	77.0 ± 3.9	93.0 ± 4.0	199.9 ± 6.1	369.9 ± 8.3
$t\bar{t} \rightarrow$ fake	12.6 ± 1.6	3.7 ± 0.8	22.7 ± 2.0	39.0 ± 2.7
DY	18.6 ± 5.0	26.6 ± 6.0	37.6 ± 7.1	82.8 ± 10.6
W^+W^-	4.0 ± 0.5	4.3 ± 0.4	9.5 ± 0.7	17.7 ± 0.9
$W^\pm Z^0$	0.8 ± 0.1	1.0 ± 0.1	1.9 ± 0.1	3.8 ± 0.2
Z^0Z^0	0.3 ± 0.0	0.4 ± 0.0	0.4 ± 0.0	1.2 ± 0.1
single top	12.6 ± 0.6	14.0 ± 0.6	33.2 ± 1.0	59.9 ± 1.3
$W +$ jets	12.6 ± 5.4	0.0 ± 0.0	7.8 ± 4.6	20.5 ± 7.1
tot SM MC	474.5 ± 11.7	515.4 ± 10.8	1208.6 ± 16.7	2198.5 ± 23.1
data	524	576	1381	2481
LM1	62.3 ± 1.6	69.5 ± 1.6	35.8 ± 1.2	167.5 ± 2.6
LM3	22.1 ± 0.8	26.9 ± 0.9	39.7 ± 1.1	88.6 ± 1.7
LM6	4.5 ± 0.1	5.0 ± 0.1	5.7 ± 0.1	15.3 ± 0.2

Table 3: Dilepton-H_T trigger data and Monte Carlo yields for the preselection (njets ≥ 2, $H_T > 200$ GeV, $\mathrm{E_T^{miss}}$ > 50 GeV, lepton $p_T >$ (10,5) GeV and not lepton $p_T >$ (20,10) GeV).

Sample	ee	$\mu\mu$	$e\mu$	tot
$t\bar{t} \rightarrow \ell^+\ell^-$	1.6 ± 0.6	10.5 ± 1.4	11.4 ± 1.5	23.4 ± 2.1
$t\bar{t} \rightarrow \ell^\pm\tau^\mp/\tau^+\tau^-$	1.7 ± 0.6	10.8 ± 1.4	9.7 ± 1.3	22.2 ± 2.0
$t\bar{t} \rightarrow$ fake	0.4 ± 0.3	3.6 ± 0.8	4.1 ± 0.9	8.1 ± 1.2
DY	0.0 ± 0.0	10.3 ± 4.0	1.8 ± 1.6	12.1 ± 4.3
W^+W^-	0.0 ± 0.0	0.0 ± 0.0	0.1 ± 0.1	0.1 ± 0.1
$W^\pm Z^0$	0.0 ± 0.0	0.1 ± 0.0	0.1 ± 0.0	0.1 ± 0.0
Z^0Z^0	0.0 ± 0.0	0.0 ± 0.0	0.0 ± 0.0	0.1 ± 0.0
single top	0.1 ± 0.0	0.7 ± 0.1	1.0 ± 0.2	1.8 ± 0.2
$W +$ jets	0.0 ± 0.0	0.0 ± 0.0	0.0 ± 0.0	0.0 ± 0.0
tot SM MC	3.7 ± 0.9	36.0 ± 4.5	28.1 ± 2.7	67.9 ± 5.3
data	1	26	34	61
LM1	1.5 ± 0.3	13.8 ± 0.7	11.0 ± 0.7	26.3 ± 1.0
LM3	0.3 ± 0.1	2.6 ± 0.3	2.3 ± 0.3	5.2 ± 0.4
LM6	0.0 ± 0.0	0.5 ± 0.0	0.3 ± 0.0	0.8 ± 0.0

8 Properties of data passing the preselection

A number of kinematical distributions for events passing the preselection in data are compared with MC in Appendix C. Although we observe a slight overall excess of data, in general we find that the MC does a good job of reproducing the shapes of the kinematical distributions. We keep in mind that the CMS luminosity estimate is expected to increase by a few percent. Given good observed agreement between data and expectation, we turn our

Table 4: Comparison of data yields in the high-p_T dilepton and dilepton-H_T trigger samples, passing the selection njets ≥ 2, $\mathrm{E_T^{miss}} > 50$ GeV, H_T>200 GeV, lepton p_T> (20,10) GeV.

Sample	ee	$\mu\mu$	$e\mu$	tot
high-p_T dilepton trigger	218	212	537	967
dilepton-H_T trigger	210	214	531	955

attention to events in the tails of the $t\bar{t}$ distributions.

9 Definition of the signal region

We define signal regions to look for possible new physics contributions in the opposite sign isolated dilepton sample. The choice of signal region is driven by three observations:

1. astrophysical evidence for dark matter suggests that we concentrate on the region of high $\mathrm{E_T^{miss}}$;
2. new physics signals should have high $\sqrt{\hat{s}}$;
3. observable high cross section new physics signals are likely to be produced strongly; thus, we expect significant hadronic activity in conjunction with the two leptons.

Following these observations, we define the following 3 signal regions (shown in figure 3) by adding requirements of large hadronic activity and missing transverse energy to the preselection of Section 4.

- 2010 signal region: $H_T > 300$ GeV and $y > 8.5$ GeV$^{1/2}$.
- high $\mathrm{E_T^{miss}}$ signal region: $H_T > 300$ GeV and $\mathrm{E_T^{miss}} > 275$ GeV
- high H_T signal region: $H_T > 600$ GeV and $\mathrm{E_T^{miss}} > 200$ GeV

In our 2010 analysis, we cut on the quantity $y \equiv \mathrm{E_T^{miss}}/\sqrt{\mathrm{H_T}}$ rather than $\mathrm{E_T^{miss}}$ because the variables H_T and y are largely uncorrelated for the dominant $t\bar{t}$ background. This allows us to use a data-driven ABCD method to estimate the background (see Section 11.1). Here, we include 2 additional tighter signal regions using requirements on on $\mathrm{E_T^{miss}}$ and H_T, since we observe that $\mathrm{E_T^{miss}}$ is a better discriminant between $t\bar{t}$ vs. SUSY. We have developed a novel technique, which is a variation of the ABCD method, to estimate the background in a signal region defined by $\mathrm{E_T^{miss}}$ and H_T requirements (see App. B).

The 2010 signal region is the same as the one used in the 2010 analysis, and was chosen to preserve about 1% of the $t\bar{t}$ sample. The additional signal regions (high $\mathrm{E_T^{miss}}$ and high H_T) have tightened requirements on $\mathrm{E_T^{miss}}$and H_T, respectively, which reduce the expected background by roughly an order of magnitude.

For each signal region, we search in the high p_T dilepton trigger sample requiring lepton $p_T >$ (20,10) GeV, and separately in the dilepton-H_T trigger sample requiring lepton $p_T >$ (10,5) GeV and not passing lepton $p_T >$ (20,10) GeV, to remove overlap with the high p_T dilepton trigger sample. For the high p_T dilepton sample, for which we have prior experience with the 2010 analysis, we apply the ABCD, $p_T(\ell\ell)$, and OF subtraction background estimates. For the dilepton-H_T sample we currently apply only the OF subtraction background estimate.

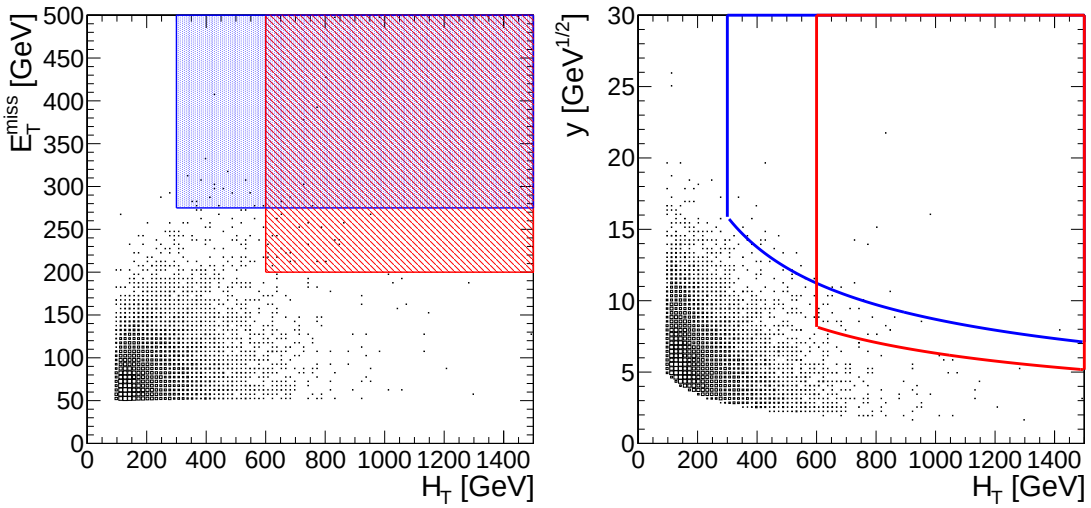

Figure 3: Illustration of signal regions for the 2011 analysis; $t\bar{t}$ MC is plotted. Left: $\mathrm{E_T^{miss}}$ vs. H_T. The high $\mathrm{E_T^{miss}}$ signal region ($\mathrm{E_T^{miss}} > 275$ GeV, $H_T > 300$ GeV) is shown in blue. The high H_T signal region ($\mathrm{E_T^{miss}} > 200$ GeV, $H_T > 600$ GeV) is shown in red. Right: The 2011 signal regions shown on the left are represented in the y vs. H_T plane.

Data yields are compared against Monte Carlo expectations in the following tables:

- High p_T dilepton trigger sample:
  - Table 5: 2010 signal region
  - Table 6: 2011 high $\mathrm{E_T^{miss}}$signal region
  - Table 7: 2011 high $H_T$signal region
- Dilepton-H_T cross trigger sample (events with $p_T >$ (20,10) are excluded):
  - Table 8: 2010 signal region
  - Table 9: 2011 high $\mathrm{E_T^{miss}}$signal region
  - Table 10: 2011 high $H_T$signal region

Yields for the 2010 signal regions are presented in tables 5 and 8 to ensure that results from the 2011 analysis are consistent with the 2010 results.

Table 5: High p_T dilepton trigger data and MC yields in the 2010 signal region. MC errors are statistical only.

Sample	ee	$\mu\mu$	$e\mu$	tot
$t\bar{t} \to \ell^+\ell^-$	4.4 ± 0.9	6.9 ± 1.1	12.6 ± 1.5	23.9 ± 2.1
$t\bar{t} \to \ell^\pm\tau^\mp/\tau^+\tau^-$	1.9 ± 0.6	2.0 ± 0.6	5.6 ± 1.0	9.5 ± 1.3
$t\bar{t} \to$ fake	0.5 ± 0.3	0.0 ± 0.0	0.7 ± 0.4	1.2 ± 0.5
DY	0.9 ± 0.9	1.9 ± 1.9	2.0 ± 2.0	4.8 ± 2.9
W^+W^-	0.2 ± 0.1	0.2 ± 0.1	0.4 ± 0.1	0.8 ± 0.2
$W^\pm Z^0$	0.0 ± 0.0	0.0 ± 0.0	0.1 ± 0.0	0.1 ± 0.0
Z^0Z^0	0.0 ± 0.0	0.0 ± 0.0	0.0 ± 0.0	0.1 ± 0.0
single top	0.2 ± 0.1	0.0 ± 0.0	0.1 ± 0.1	0.3 ± 0.1
$W +$ jets	0.0 ± 0.0	0.0 ± 0.0	0.0 ± 0.0	0.0 ± 0.0
tot SM MC	8.1 ± 1.4	11.1 ± 2.3	21.5 ± 2.7	40.7 ± 3.8
data	11	8	26	45
LM1	30.7 ± 1.1	36.4 ± 1.2	18.6 ± 0.9	85.7 ± 1.9
LM3	8.9 ± 0.5	10.8 ± 0.6	15.0 ± 0.7	34.6 ± 1.0
LM6	2.9 ± 0.1	3.2 ± 0.1	3.7 ± 0.1	9.7 ± 0.2

Table 6: High p_T dilepton trigger data and MC yields in the high $\mathrm{E_T^{miss}}$ signal region. MC errors are statistical only.

Sample	ee	$\mu\mu$	$e\mu$	tot
$t\bar{t} \to \ell^+\ell^-$	1.2 ± 0.5	1.0 ± 0.4	2.2 ± 0.7	4.3 ± 0.9
$t\bar{t} \to \ell^\pm\tau^\mp/\tau^+\tau^-$	0.3 ± 0.2	0.0 ± 0.0	0.4 ± 0.3	0.7 ± 0.4
$t\bar{t} \to$ fake	0.0 ± 0.0	0.0 ± 0.0	0.0 ± 0.0	0.0 ± 0.0
DY	0.0 ± 0.0	0.0 ± 0.0	2.0 ± 2.0	2.0 ± 2.0
W^+W^-	0.1 ± 0.1	0.1 ± 0.1	0.0 ± 0.0	0.2 ± 0.1
$W^\pm Z^0$	0.0 ± 0.0	0.0 ± 0.0	0.0 ± 0.0	0.0 ± 0.0
Z^0Z^0	0.0 ± 0.0	0.0 ± 0.0	0.0 ± 0.0	0.0 ± 0.0
t	0.0 ± 0.0	0.0 ± 0.0	0.0 ± 0.0	0.0 ± 0.0
$W +$ jets	0.0 ± 0.0	0.0 ± 0.0	0.0 ± 0.0	0.0 ± 0.0
tot SM MC	1.6 ± 0.6	1.1 ± 0.4	4.6 ± 2.1	7.3 ± 2.2
data	5	0	3	8
LM1	17.5 ± 0.9	20.3 ± 0.9	10.9 ± 0.7	48.7 ± 1.4
LM3	4.8 ± 0.4	5.8 ± 0.4	7.4 ± 0.5	18.0 ± 0.7
LM6	2.4 ± 0.1	2.6 ± 0.1	3.0 ± 0.1	8.1 ± 0.2

Table 7: High p_T dilepton trigger data and MC yields in the high H_T signal region. MC errors are statistical only.

Sample	ee	$\mu\mu$	$e\mu$	tot
$t\bar{t} \to \ell^+\ell^-$	0.4 ± 0.3	0.9 ± 0.4	1.8 ± 0.6	3.2 ± 0.8
$t\bar{t} \to \ell^\pm\tau^\mp/\tau^+\tau^-$	0.3 ± 0.2	0.5 ± 0.3	1.0 ± 0.4	1.9 ± 0.6
$t\bar{t} \to$ fake	0.0 ± 0.0	0.0 ± 0.0	0.0 ± 0.0	0.0 ± 0.0
DY	0.0 ± 0.0	0.0 ± 0.0	2.0 ± 2.0	2.0 ± 2.0
W^+W^-	0.0 ± 0.0	0.0 ± 0.0	0.0 ± 0.0	0.0 ± 0.0
$W^\pm Z^0$	0.0 ± 0.0	0.0 ± 0.0	0.0 ± 0.0	0.0 ± 0.0
Z^0Z^0	0.0 ± 0.0	0.0 ± 0.0	0.0 ± 0.0	0.0 ± 0.0
single top	0.0 ± 0.0	0.0 ± 0.0	0.0 ± 0.0	0.0 ± 0.0
$W +$ jets	0.0 ± 0.0	0.0 ± 0.0	0.0 ± 0.0	0.0 ± 0.0
tot SM MC	0.7 ± 0.4	1.5 ± 0.5	4.9 ± 2.1	7.1 ± 2.2
data	1	0	3	4
LM1	14.9 ± 0.8	15.9 ± 0.8	7.0 ± 0.5	37.7 ± 1.3
LM3	5.2 ± 0.4	5.8 ± 0.4	7.7 ± 0.5	18.8 ± 0.8
LM6	2.2 ± 0.1	2.5 ± 0.1	2.7 ± 0.1	7.4 ± 0.1

Table 8: Dilepton-$H_T$trigger data and MC yields in the 2010 signal region. MC errors are statistical only.

Sample	ee	$\mu\mu$	$e\mu$	tot
$t\bar{t} \to \ell^+\ell^-$	0.0 ± 0.0	0.4 ± 0.3	1.1 ± 0.5	1.5 ± 0.5
$t\bar{t} \to \ell^\pm\tau^\mp/\tau^+\tau^-$	0.0 ± 0.0	0.6 ± 0.3	0.2 ± 0.2	0.8 ± 0.4
$t\bar{t} \to$ fake	0.0 ± 0.0	0.0 ± 0.0	0.3 ± 0.2	0.3 ± 0.2
DY	0.0 ± 0.0	0.0 ± 0.0	0.0 ± 0.0	0.0 ± 0.0
W^+W^-	0.0 ± 0.0	0.0 ± 0.0	0.0 ± 0.0	0.0 ± 0.0
$W^\pm Z^0$	0.0 ± 0.0	0.0 ± 0.0	0.0 ± 0.0	0.0 ± 0.0
Z^0Z^0	0.0 ± 0.0	0.0 ± 0.0	0.0 ± 0.0	0.0 ± 0.0
single top	0.0 ± 0.0	0.0 ± 0.0	0.0 ± 0.0	0.0 ± 0.0
$W +$ jets	0.0 ± 0.0	0.0 ± 0.0	0.0 ± 0.0	0.0 ± 0.0
tot SM MC	0.0 ± 0.0	1.1 ± 0.4	1.6 ± 0.5	2.7 ± 0.7
data	0	2	2	4
LM1	0.8 ± 0.2	7.4 ± 0.5	5.9 ± 0.5	14.2 ± 0.8
LM3	0.1 ± 0.0	1.2 ± 0.2	1.0 ± 0.2	2.2 ± 0.3
LM6	0.0 ± 0.0	0.3 ± 0.0	0.2 ± 0.0	0.5 ± 0.0

Table 9: Dilepton-H_T trigger data and MC yields in the high $\mathrm{E_T^{miss}}$ signal region. MC errors are statistical only.

Sample	ee	$\mu\mu$	$e\mu$	tot
$t\bar{t} \to \ell^+\ell^-$	0.0 ± 0.0	0.1 ± 0.1	0.0 ± 0.0	0.1 ± 0.1
$t\bar{t} \to \ell^\pm\tau^\mp/\tau^+\tau^-$	0.0 ± 0.0	0.0 ± 0.0	0.2 ± 0.2	0.2 ± 0.2
$t\bar{t} \to$ fake	0.0 ± 0.0	0.0 ± 0.0	0.0 ± 0.0	0.0 ± 0.0
DY	0.0 ± 0.0	0.0 ± 0.0	0.0 ± 0.0	0.0 ± 0.0
W^+W^-	0.0 ± 0.0	0.0 ± 0.0	0.0 ± 0.0	0.0 ± 0.0
$W^\pm Z^0$	0.0 ± 0.0	0.0 ± 0.0	0.0 ± 0.0	0.0 ± 0.0
Z^0Z^0	0.0 ± 0.0	0.0 ± 0.0	0.0 ± 0.0	0.0 ± 0.0
single top	0.0 ± 0.0	0.0 ± 0.0	0.0 ± 0.0	0.0 ± 0.0
$W +$ jets	0.0 ± 0.0	0.0 ± 0.0	0.0 ± 0.0	0.0 ± 0.0
tot SM MC	0.0 ± 0.0	0.1 ± 0.1	0.2 ± 0.2	0.3 ± 0.2
data	0	0	0	0
LM1	0.4 ± 0.1	4.4 ± 0.4	3.5 ± 0.4	8.3 ± 0.6
LM3	0.1 ± 0.0	0.7 ± 0.1	0.6 ± 0.1	1.3 ± 0.2
LM6	0.0 ± 0.0	0.3 ± 0.0	0.1 ± 0.0	0.4 ± 0.0

Table 10: Dilepton-H_T trigger data and MC yields in the high H_T signal region. MC errors are statistical only.

Sample	ee	$\mu\mu$	$e\mu$	tot
$t\bar{t} \to \ell^+\ell^-$	0.0 ± 0.0	0.0 ± 0.0	0.0 ± 0.0	0.0 ± 0.0
$t\bar{t} \to \ell^\pm\tau^\mp/\tau^+\tau^-$	0.0 ± 0.0	0.0 ± 0.0	0.0 ± 0.0	0.0 ± 0.0
$t\bar{t} \to$ fake	0.0 ± 0.0	0.0 ± 0.0	0.0 ± 0.0	0.0 ± 0.0
DY	0.0 ± 0.0	0.0 ± 0.0	0.0 ± 0.0	0.0 ± 0.0
W^+W^-	0.0 ± 0.0	0.0 ± 0.0	0.0 ± 0.0	0.0 ± 0.0
$W^\pm Z^0$	0.0 ± 0.0	0.0 ± 0.0	0.0 ± 0.0	0.0 ± 0.0
Z^0Z^0	0.0 ± 0.0	0.0 ± 0.0	0.0 ± 0.0	0.0 ± 0.0
single top	0.0 ± 0.0	0.0 ± 0.0	0.0 ± 0.0	0.0 ± 0.0
$W +$ jets	0.0 ± 0.0	0.0 ± 0.0	0.0 ± 0.0	0.0 ± 0.0
tot SM MC	0.0 ± 0.0	0.1 ± 0.0	0.0 ± 0.0	0.1 ± 0.0
data	0	0	1	1
LM1	0.4 ± 0.1	3.8 ± 0.4	2.1 ± 0.3	6.3 ± 0.5
LM3	0.1 ± 0.1	0.8 ± 0.2	0.4 ± 0.1	1.3 ± 0.2
LM6	0.0 ± 0.0	0.3 ± 0.0	0.1 ± 0.0	0.4 ± 0.0

These results are summarized as:

- High p_T dilepton trigger sample
  - 2010 signal region ($y > 8.5$ GeV$^{1/2}$, $H_T > 300$ GeV)
    - observed yield : 45
    - MC prediction : 40.7 ± 3.8
  - high $\mathrm{E_T^{miss}}$ signal region ($\mathrm{E_T^{miss}} > 275$ GeV, $H_T > 300$ GeV)
    - observed yield : 8
    - MC prediction : 7.3 ± 2.2
  - high H_T signal region ($\mathrm{E_T^{miss}} > 200$ GeV, $H_T > 600$ GeV)
    - observed yield : 4
    - MC prediction : 7.1 ± 2.2
- Dilepton-H_T trigger sample (events with $p_T >$ (20,10) are excluded)
  - 2010 signal region ($y > 8.5$ GeV$^{1/2}$, $H_T > 300$ GeV)
    - observed yield : 4
    - MC prediction : 2.7 ± 0.7
  - high $\mathrm{E_T^{miss}}$ signal region ($\mathrm{E_T^{miss}} > 275$ GeV, $H_T > 300$ GeV)
    - observed yield : 0
    - MC prediction : 0.3 ± 0.2
  - high H_T signal region ($\mathrm{E_T^{miss}} > 200$ GeV, $H_T > 600$ GeV)
    - observed yield : 1
    - MC prediction : 0.0 ± 0.0

For all signal regions, we observe reasonable agreement between data and MC expectations. A data/MC comparison of the kinematic distributions of the 45 events passing the 2010 signal region selection is presented in App. D.

10 Estimation of Drell Yan and QCD backgrounds

For the 2010 signal region, we observe 3 ee, 1 $\mu\mu$, and 3 $e\mu$ events in the Z mass window, confirming the expectation from MC that the DY background is negligible. We also confirm the MC expectation that the contribution of fake leptons is small, using the data-driven fake rate method [11]. The results are summarized as (all errrors are statistical only):

- High p_T dilepton trigger sample
  - 2010 signal region ($y > 8.5$ GeV$^{1/2}$, $H_T > 300$ GeV)
    - single fakes : 3.8 ± 1.4
    - double fakes : $0.0^{+0.4}_{-0.0}$
  - high $\mathrm{E_T^{miss}}$ signal region ($\mathrm{E_T^{miss}} > 275$ GeV, $H_T > 300$ GeV)
    - single fakes : 0.4 ± 0.4
    - double fakes : $0.0^{+0.4}_{-0.0}$
  - high H_T signal region ($\mathrm{E_T^{miss}} > 200$ GeV, $H_T > 600$ GeV)
    - single fakes : 1.1 ± 0.7
    - double fakes : $0.0^{+0.4}_{-0.0}$

- Dilepton-H_T trigger sample (events with $p_T >$ (20,10) are excluded)
  - 2010 signal region ($y > 8.5$ GeV$^{1/2}$, $H_T > 300$ GeV)
    - single fakes : 1.2 ± 0.9
    - double fakes : 0.1 ± 0.1
  - high $\mathrm{E_T^{miss}}$ signal region ($\mathrm{E_T^{miss}} > 275$ GeV, $H_T > 300$ GeV)
    - single fakes : $0.0^{+0.6}_{-0.0}$
    - double fakes : $0.0^{+0.4}_{-0.0}$
  - high H_T signal region ($\mathrm{E_T^{miss}} > 200$ GeV, $H_T > 600$ GeV)
    - single fakes : $0.0^{+0.6}_{-0.0}$
    - double fakes : $0.0^{+0.4}_{-0.0}$

Based on these results, we treat the contributions from fakes leptons in our signal regions as negligible.

11 Data Driven Background Estimation Methods for $t\bar{t}$

For the high p_T dilepton trigger sample, we use 3 data-driven methods to estimate the background in the signal regions. In the first method, ABCD, one exploits the fact that H_T and y are nearly uncorrelated for the $t\bar{t}$ background. When predicting the backgrounds in the signal regions defined in the $\mathrm{E_T^{miss}}$ vs. H_T plane, we use a variation of the ABCD method which we refer to as the ABCD' method (see Appendix B). The second method, $p_T(\ell\ell)$, is based on the fact that in $t\bar{t}$ the p_T of the dilepton pair is on average nearly the same as the p_T of the pair of neutrinos from W-decays, which is reconstructed as $\mathrm{E_T^{miss}}$ in the detector. The third method exploits the fact that in $t\bar{t}$ events the rates of same-flavor vs. opposite-flavor dilepton events are the same. For the low lepton p_T events collected by the dilepton-H_T triggers, we use the opposite-flavor subtraction technique only.

We study the closure of these methods using our madgraph $t\bar{t}$ sample, as well as the powheg sample TTTo2L2Nu2B_7TeV-powheg-pythia6_Spring11-PU_S1_START311_V1G1-v1 which has approximately 10 times more events in the dilepton channel than the madgraph sample. We use these samples to estimate correction factors and systematic uncertainties for the background predictions. However, the final choice of correction factors and uncertainties will be extracted from the Summer11 $t\bar{t}$ madgraph sample which will have 50 times as many events as the current madgraph sample. For the studies presented in this section, we do not apply trigger efficiency corrections or reweighting for number of reconstructed vertices since are not comparing MC to data.

11.1 ABCD method

We find that in $t\bar{t}$ events H_T and y are nearly uncorrelated, as demonstrated in Fig. 4 (left). Thus, we can use an ABCD method in the y vs. H_T plane to estimate the background in a data driven way. We define 4 regions in the plane of y vs. H_T, as shown in Fig. 4 (right). The region D is the signal region, and the regions A, B and C are control regions. The predicted background in region D is given by $N_A \times N_C / N_B$.

In Table 11, we quote the $t\bar{t}$ MC expected results for 1 fb^{-1}. We find that the prediction agrees with the observed yield in the signal region within $\sim$20%, and we assign a corresponding systematic uncertainty. We also study the dependence of the ratio of observed to predicted signal yields, as a function of the y and H_T requirements used to define the signal region, shown in Fig. 5.

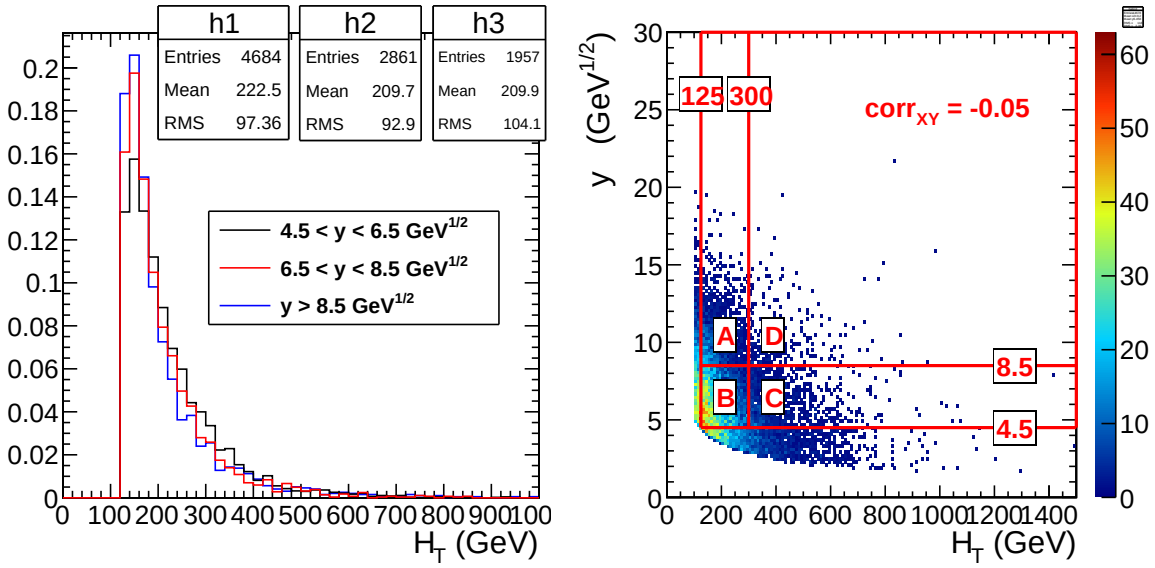

Figure 4: Illustration that y and H_T are not very correlated in MC for the 2010 signal region. Left: distributions of H_T in MC $t\bar{t}$ events for different intervals of y. h1, h2, and h3 refer to the y intervals 4.5 - 6.5, 6.5 - 8.5 and > 8.5, respectively. Right: Distributions of y vs. H_T for $t\bar{t}$ MC. Here we also show our choice of ABCD regions. The correlation coefficient $\mathrm{corr_{XY}}$ is computed for events falling in the ABCD regions.

Table 11: Expected yields from $t\bar{t}$ MC in 1 fb^{-1} in the four ABCD regions for the signal region depicted in Figs. 8, as well as the predicted yield in region D given by $N_A \times N_C/N_B$ and the ratio of the observed signal yield to the prediction. The quoted uncertainties are statistical only.

signal region	sample	A	B	C	D	$N_A \times N_C/N_B$	obs/pred
2010 signal region	madgraph	251.3 ± 6.1	951.5 ± 11.9	165.2 ± 4.9	38.3 ± 2.4	43.6 ± 1.8	0.88 ± 0.07
	powheg	231.7 ± 2.0	850.6 ± 3.7	157.8 ± 1.6	37.0 ± 0.8	43.0 ± 0.6	0.86 ± 0.02

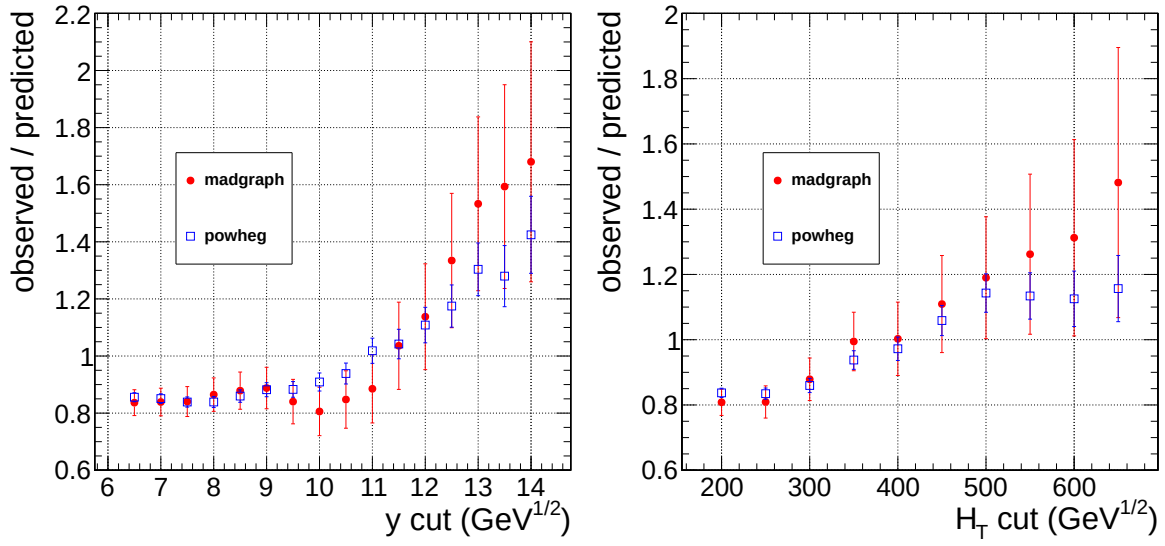

Figure 5: Variation of observed/predicted for the ABCD method as a function of the y (for $H_T > 300$ GeV) and H_T (for $y > 8.5$ GeV$^{1/2}$) cuts defining the signal region.

11.2 ABCD' Method

To estimate the background in a signal region defined in the $\not\!\!E_T^{miss}$ vs. H_T plane, we perform a variant of the ABCD method which we refer to as the ABCD' method. This method is discussed in detail in App. B. Based on these results, we apply the scale factors and systematic uncertainties summarized in Table 15 to the background prediction of the ABCD' method.

11.3 Dilepton p_T method

This method is based on a suggestion by V. Pavlunin [8], and was investigated by our group in 2009 [9] and in our 2010 analysis [2]. The idea is that in dilepton $t\bar{t}$ events the lepton and neutrinos from W decays have the same p_T spectrum (modulo W polarization effects). One can then use the observed $p_T(\ell\ell)$ distribution to model the sum of neutrino p_T's which is identified with the $\not\!\!E_T^{miss}$.

Then, in order to predict the $t\bar{t} \rightarrow$ dilepton contribution to a selection with $\not\!\!E_T^{miss}$+X, one applies a cut on $p_T(\ell\ell)$+X instead. In practice one has to rescale the result of the $p_T(\ell\ell)$+X selection to account for the fact that any dilepton selection must include a moderate $\not\!\!E_T^{miss}$ cut in order to reduce Drell Yan backgrounds. This is discussed in Section 5.3 of Reference [9]; for a $\not\!\!E_T^{miss}$ cut of 50 GeV, the rescaling factor is obtained from the MC as

$$K = \frac{\int_0^\infty \mathcal{N}(p_T(\ell\ell))\ dp_T(\ell\ell)}{\int_{50}^\infty \mathcal{N}(p_T(\ell\ell))\ dp_T(\ell\ell)} = 1.5.$$

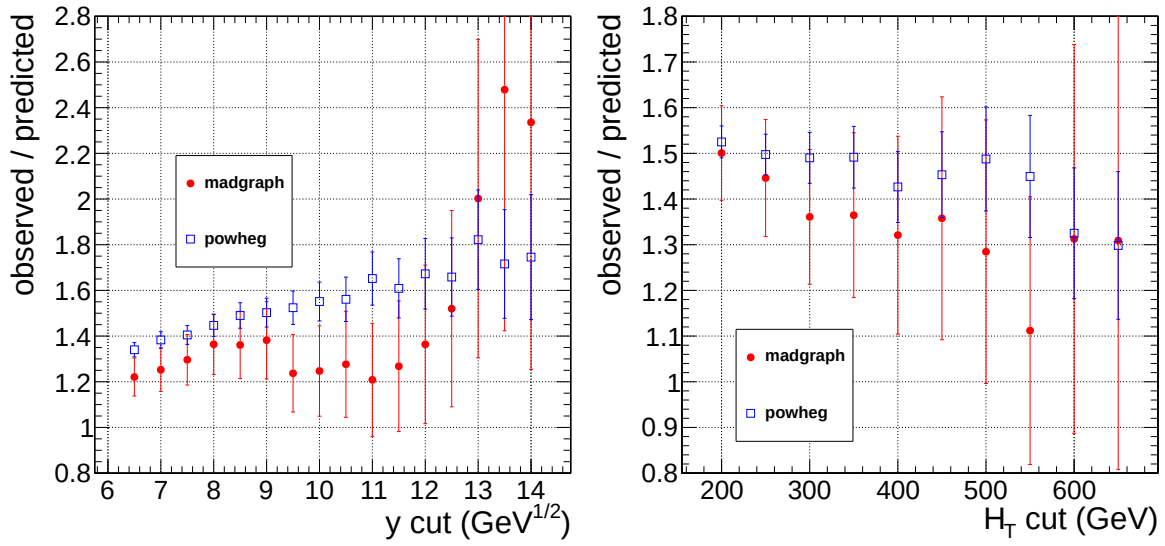

Figure 6: Variation of observed/predicted for the $p_T(\ell\ell)$ method as a function of the y (for $H_T >$ 300 GeV) and H_T (for $y >$ 8.5 GeV$^{1/2}$) cuts defining the signal region.

We summarize the expected results of the $p_T(\ell\ell)$ method in 1 fb^{-1} $t\bar{t}$ MC in Table 12, and we show the dependence of observed/predicted vs. the signal region requirements in Fig. 6. Based on these results, we apply the scale factors and uncertainties summarized in Table 15 to the predicted background from the $p_T(\ell\ell)$ method. In [1], we have studied extensively the origin of the excess of observed vs. predicted events from this method. We found that it is due mostly to the W polarization, which results in a harder p_T distribution for the W neutrinos than charged leptons.

As a validation of the $p_T(\ell\ell)$ method, we also apply the background estimate to the H_T sideband region 125–300 GeV, where we expect the events to be dominated by background and where the higher event yields allow us to test the method with higher statistcal precision. The results of the $p_T(\ell\ell)$ method applied to $t\bar{t}$ MC in the H_T sideband region with the requirements corresponding to the 2010 signal region ($y >$ 8.5 GeV$^{1/2}$) and the high $\not\!\!E_T^{miss}$ region ($\not\!\!E_T^{miss} >$ 200 GeV) are given in Table 13. Based on these results we will apply a correction factor $K_C = 1.4 \pm 0.1$ ($K_C = 1.3 \pm 0.2$) to data for the $y >$ 8.5 GeV$^{1/2}$ ($\not\!\!E_T^{miss} >$ 200 GeV) requirements in the H_T sideband region.

Table 12: Expected observed and predicted yields in 1 fb^{-1} for $t\bar{t}$ MC for the $p_T(\ell\ell)$ method applied to the 3 signal regions, and the ratio of the observed signal yield to the prediction. The quoted uncertainties are statistical only. Based on these results, we will apply the correction factor K_C to the prediction in data.

signal region	sample	predicted	observed	obs/pred	K_C
2010 signal region	madgraph	28.2 ± 2.5	38.3 ± 2.4	1.36 ± 0.15	1.4 ± 0.2
	powheg	24.8 ± 0.8	37.0 ± 0.8	1.49 ± 0.06	
high $\mathrm{E_T^{miss}}$signal region	madgraph	2.7 ± 0.8	4.6 ± 0.8	1.72 ± 0.59	1.5 ± 0.3
	powheg	3.3 ± 0.3	4.5 ± 0.3	1.39 ± 0.15	
high H_T signal region	madgraph	4.7 ± 1.0	5.5 ± 0.9	1.17 ± 0.31	1.3 ± 0.2
	powheg	4.7 ± 0.3	6.2 ± 0.3	1.33 ± 0.11	

Table 13: Expected observed and predicted yields in 1 fb^{-1} for $t\bar{t}$ MC for the $p_T(\ell\ell)$ method for the control regions in the H_T sideband region $125 < H_T < 300$ GeV, and the ratio of the observed signal yield to the prediction. The quoted uncertainties are statistical only, assuming Gaussian errors.

control region	sample	predicted	observed	obs/pred
$125 < H_T < 300$ GeV, $y > 8.5$ GeV$^{1/2}$	madgraph	35.8 ± 1.3	51.3 ± 1.2	1.43 ± 0.06
	powheg	33.4 ± 0.4	47.3 ± 0.4	1.42 ± 0.02
$125 < H_T < 300$ GeV, $\mathrm{E_T^{miss}} > 200$ GeV$^{1/2}$	madgraph	6.4 ± 1.3	9.9 ± 1.2	1.54 ± 0.36
	powheg	6.6 ± 0.4	8.4 ± 0.4	1.27 ± 0.10

Table 14: Dependence of the correction factor K_C on the hadronic energy scale. Based on these results, we apply the uncertainty in the rightmost column to K_C for the given signal region.

Signal Region	sample	nominal	+5%	-5%	uncertainty
2010 signal region	madgraph	1.36 ± 0.15	1.66 ± 0.17	1.07 ± 0.12	0.3
	powheg	1.49 ± 0.06	1.82 ± 0.07	1.18 ± 0.05	
high $\mathrm{E_T^{miss}}$ signal region	madgraph	1.72 ± 0.59	2.34 ± 0.76	1.11 ± 0.41	0.4
	powheg	1.39 ± 0.15	1.83 ± 0.18	1.05 ± 0.12	
high H_T signal region	madgraph	1.17 ± 0.31	1.42 ± 0.36	1.07 ± 0.29	0.3
	powheg	1.33 ± 0.11	1.58 ± 0.13	1.11 ± 0.10	

Table 15: Summary of correction factors and systematic uncertainties for the ABCD' and $p_T(\ell\ell)$ methods in the 3 signal regions. For the $p_T(\ell\ell)$ method, the correction factor is from Table 12, with the additional uncertainty from hadronic energy scale of Table 14.

signal region	ABCD'	$p_T(\ell\ell)$
2010 signal region	1.0 ± 0.2	1.4 ± 0.4
high $\mathrm{E_T^{miss}}$ signal region	1.2 ± 0.5	1.5 ± 0.5
high H_T signal region	1.0 ± 0.5	1.3 ± 0.4

11.4 Opposite-Flavor Subtraction

The opposite-flavor subtraction technique exploits the fact that in $t\bar{t}$, the flavor of the 2 leptons from W decay are uncorrelated. Hence we expect equal rates of same-flavor (SF) ee or $\mu\mu$ vs. opposite-flavor (OF) $e\mu$ lepton pairs. In SUSY, the lepton flavors may be correlated, producing an excess of SF over OF events. We use the observed yield in the OF final state to predict the yields in the SF final state according to:

$$N(ee) = \frac{1}{2R_{\mu e}} N(e\mu) \text{ and } N(\mu\mu) = \frac{R_{\mu e}}{2} N(e\mu)$$

where $R_{\mu e}$ is the ratio of muon to electron selection efficiencies. This quantity is evaluated by taking the ratio of the number of observed $Z \to \mu^+\mu^-$ to $Z \to e^+e^-$ events, in the mass range 76-106 GeV with no jets or $\mathrm{E_T^{miss}}$ requirements (see Fig. 2). Alternatively, we can quantify the excess of SF vs. OF events with the quantity:

$$\Delta = R_{\mu e} N(ee) + \frac{1}{R_{\mu e}} N(\mu\mu) - N(e\mu), \quad (1)$$

which is predicted to be 0 for processes with uncorrelated lepton flavors. In order for this technique to work, the kinematic selection applied to events in all dilepton flavor channels must be the same, which is not the case for our default selection because the Z mass veto is applied only to same-flavor channels. Therefore when applying the OF subtraction technique we also apply the Z mass veto also to the $e\mu$ channel.

We will apply this technique to both the high p_T dilepton trigger and dilepton-H_T trigger data samples. In the following, we first apply the technique to $t\bar{t}$ MC with high p_T leptons, and then to $t\bar{t}$ MC with low p_T leptons.

11.4.1 OF subtraction: Application to high p_T lepton sample

We begin by applying the OF subtraction technique to $t\bar{t}$ MC with leptons passing $p_T >$ (20,10) GeV. Here we extract $R_{e\mu}$ by taking the ratio of $Z \to \mu^+\mu^-$ vs. $Z \to e^+e^-$ events in the window 76–106 GeV in DY MC. For data, we have verified that the contribution from fake leptons in the high lepton p_T signal regions is small using the data-driven fake rate method, hence we do not need to correct for fake leptons here. The results are summarized in Table 16, where we find values of Δ consistent with 0, as expected.

Table 16: Expected yields in 1 fb^{-1} $t\bar{t}$ MC for the OF subtraction method, and the quantity Δ, defined in Eq. 1. The quoted systematic uncertainty refers to that of $R_{\mu e}$.

region	sample	$N(ee)$	$N(\mu\mu)$	$N(e\mu)$	Δ
preselection region	madgraph	431.1 $\pm$ 8.0	531.3 $\pm$ 8.9	945.8 $\pm$ 11.8	11.8 $\pm$ 16.8 (stat) $\pm$ 1.1 (syst)
	powheg	383.1 $\pm$ 2.5	492.9 $\pm$ 2.9	876.2 $\pm$ 3.8	-7.0 $\pm$ 5.4 (stat) $\pm$ 0.8 (syst)
2010 signal region	madgraph	7.4 $\pm$ 1.0	10.7 $\pm$ 1.3	14.5 $\pm$ 1.5	3.3 $\pm$ 2.2 (stat) $\pm$ 0.04 (syst)
	powheg	7.2 $\pm$ 0.3	8.6 $\pm$ 0.4	16.8 $\pm$ 0.5	-1.1 $\pm$ 0.7 (stat) $\pm$ 0.03 (syst)

11.4.2 OF subtraction: Application to low p_T lepton sample

In this section, we apply the OF subtraction technique to $t\bar{t}$ MC with leptons passing $p_T >$ (10,5) GeV but not passing $p_T >$ (20,10) GeV (in order to remove overlap with the high lepton p_T sample). The OF subtraction in the low lepton p_T regime is complicated by 2 factors:

- The ratio of muon to electron selection efficiencies $R_{\mu e}$ increases significantly at low p_T, due to a drop in the electron selection efficiency.
- We reconstruct muons down to $p_T > 5$ GeV but electrons only to $p_T > 10$ GeV.

Our strategy is the following:

- Evaluate $R_{\mu e}$ from $t\bar{t}$ MC.

- Parameterize $R_{\mu e}$ as a function of lepton p_T. For now we split in 2 bins, $10 < p_T < 20$ GeV and $p_T > 20$ GeV.
- For data, we will apply to $R_{\mu e}$ a trigger efficiency correction and subtract the expected contribution from fake leptons from the data-driven fake rate method (but neither correction is performed for the MC studies in this section).
- We first apply the OF subtraction to the preselection region, and then to the signal region.

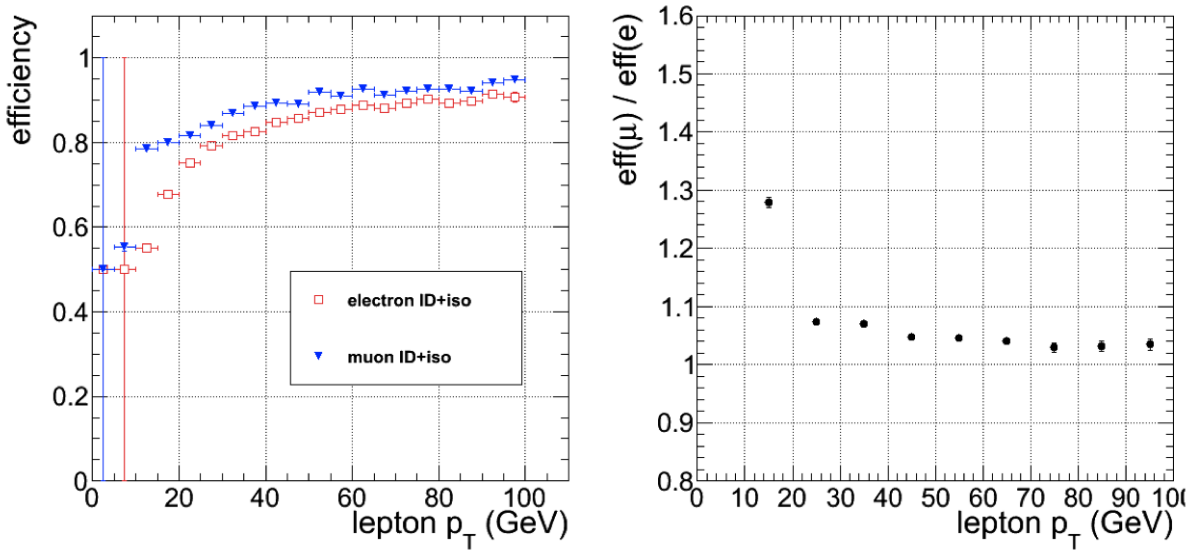

Figure 7: Left: the electron and muon selection efficiencies, as a function of lepton p_T, extracted from $t\bar{t}$ MC. Right: the ratio $R_{\mu e}$ of muon to electron selection efficiencies as a function of lepton p_T.

We begin by examining the dependence of $R_{\mu e}$ on lepton p_T, as shown in Fig. 7. We find that $R_{\mu e}$ increases in the region p_T 10–20 GeV, but is roughly constant for $p_T > 20$ GeV. Hence we take $R_{\mu e}^{10-20} = 1.28$ for p_T 10–20 GeV and $R_{\mu e}^{>20} = 1.08$ for $p_T > 20$ GeV, and assign a 5% systematic uncertainty.

Next, to take into account the fact the electrons and muons have a different p_T range, we split the low p_T sample into events with leptons passing $p_T >$ (10,10) GeV, denoted in the following as (10,10), and events with leptons passing $p_T >$ (10,5) GeV but not passing $p_T >$ (10,10) GeV, denoted in the following as (10,5). We find the following relations, expected for backgrounds with uncorrelated lepton flavors:

- $N(ee)(10,10) = 1/(2R_{\mu e}^{10-20})N(e\mu)(10,10)$
- $N(\mu\mu)(10,10) = (R_{\mu e}^{10-20}/2)N(e\mu)(10,10)$
- $N(\mu\mu)(10,5) = R_{\mu e}^{>20}N(e\mu)(10,5)$

Note that for (10,10) events, both leptons are in the range p_T 10–20 GeV, hence the relevant efficiency ratio is $R_{\mu e}^{10-20}$. For (10,5) events, both ee and $\mu\mu$ events have a muon with p_T 5–10 GeV and an additional lepton with $p_T > 10$ GeV. In most cases the leading lepton has $p_T > 20$ GeV, hence we use $R_{\mu e}^{>20}$ for these events.

In this case we find the following expression for Δ, quantifying the excess of SF vs. OF yields:

$$\Delta = R_{\mu e}^{10-20}N(ee)(10,10) + 1/R_{\mu e}^{10-20}N(\mu\mu)(10,10) + 1/R_{\mu e}^{>20}N(\mu\mu)(10,5) - N(e\mu)(10,10) - N(e\mu)(10,5) \quad (2)$$

In Table 17 we apply this technique to $t\bar{t}$ MC. As expected, we find Δ consistent with 0.

Table 17: Expected yields in 1 fb^{-1} $t\bar{t}$ MC for the OF subtraction method in the low lepton p_T regime, and the quantity Δ, defined in Eq. 2. The quoted systematic uncertainty refers to that of $R_{\mu e}$.

region	sample	$N(ee)(10,10)$	$N(\mu\mu)(10,10)$	$N(e\mu)(10,10)$	$N(\mu\mu)(10,5)$	$N(e\mu)(10,5)$	Δ
preselection region	madgraph	3.4 ± 0.7	4.9 ± 0.9	6.4 ± 1.0	22.9 ± 1.8	18.2 ± 1.6	4.8 ± 2.8 (stat) ± 1.0 (syst)
	powheg	2.5 ± 0.2	4.4 ± 0.3	7.0 ± 0.3	19.0 ± 0.6	16.6 ± 0.5	0.6 ± 0.9 (stat) ± 0.9 (syst)
2010 signal region	madgraph	0.0 ± 0.0	0.4 ± 0.3	0.6 ± 0.3	1.0 ± 0.4	0.7 ± 0.3	-0.0 ± 0.6 (stat) ± 0.1 (syst)
	powheg	0.1 ± 0.0	0.2 ± 0.1	0.4 ± 0.1	1.4 ± 0.2	1.1 ± 0.1	0.1 ± 0.2 (stat) ± 0.1 (syst)

12 Results

12.1 Background estimate from the ABCD method

We begin by applying the ABCD method to estimate the background in the 2010 signal region. The data yields in the four regions are summarized in Tables 19 and the y vs. H_T distributions are displayed in Fig. 8. The ABCD background prediction is $N_A \times N_C/N_B = 40.3 \pm 4.3$ (stat) $\pm$ 8.1 (syst), in agreement with the MC expectation. We also apply the ABCD' method to estimate the background in this region, following the procedure of App. B, and find a predicted background of 40.5 ± 5.0 (stat) $\pm$ 8.1 (syst), in good agreement with the ABCD prediction.

Next, we apply the ABCD' method to predict the yields in the high $\mathrm{E_T^{miss}}$ and high H_T signal regions. The y vs. H_T distributions for data are displayed in Fig. 9. The signal regions are indicated, as well as the control regions used to measure the $f(y)$ and $g(H_T)$ distributions. For the high $\mathrm{E_T^{miss}}$ signal region, we find a predicted yield of 4.0 ± 1.0 (stat) $\pm$ 0.8 (syst) (stat), in reasonable agreement with the observed yield of 8 events. For the high $\mathrm{E_T^{miss}}$ signal region, we find a predicted yield of 4.5 ± 1.6 (stat) $\pm$ 0.9 (syst) (stat), in good agreement with the observed yield of 4 events. These results are summarized in Table 18.

Table 18: Summary of results of the ABCD' method, applied to the 3 signal regions. The correction factors are given in Table 15.

Signal Region	ABCD' pred	correction factor	prediction
2010 signal region	40.5 ± 5.0	1.0 ± 0.2	40.5 ± 5.0 (stat) ± 8.1 (syst)
high $\mathrm{E_T^{miss}}$ signal region	3.3 ± 0.8	1.2 ± 0.2	4.0 ± 1.0 (stat) ± 0.8 (syst)
high H_T signal region	4.5 ± 1.6	1.0 ± 0.2	4.5 ± 1.6 (stat) ± 0.9 (syst)

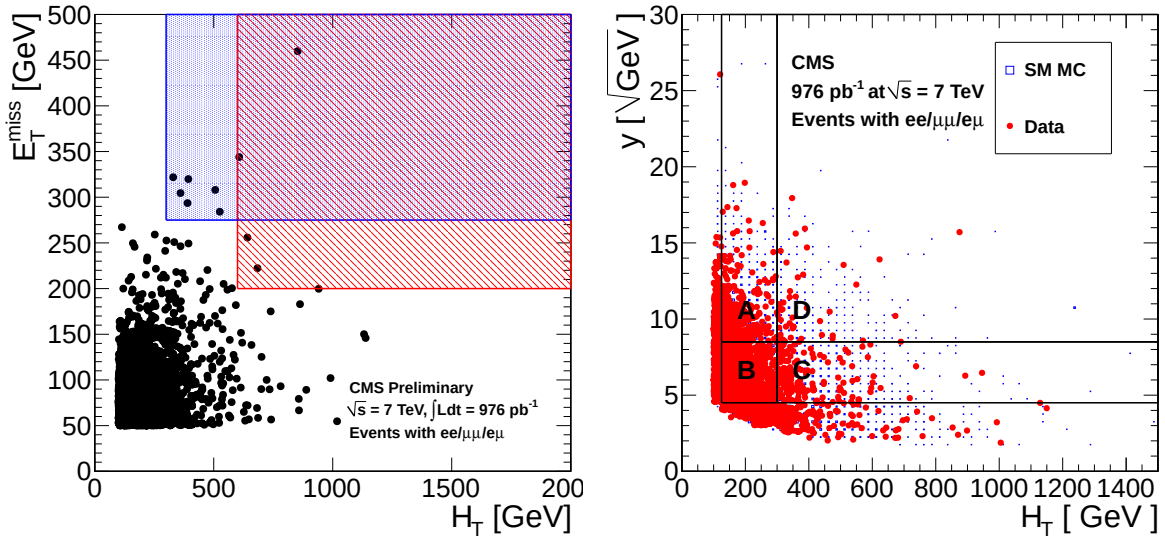

Figure 8: Left: Distribution of $\mathrm{E_T^{miss}}$ vs. H_T for SM Monte Carlo and data. The 2011 high H_T signal region is shown in red. The 2011 high $\mathrm{E_T^{miss}}$ signal region is shown in blue. Right: Distributions of y vs. H_T for SM Monte Carlo and data. The 2010 signal region boundaries are overlayed.

Table 19: Data yields in the four regions of Figure 8 for the 2010 signal region, as well as the predicted yield in region D given by $N_A \times N_C/N_B$. The quoted uncertainty on the prediction in data is statistical only, assuming Gaussian errors. We also show the SM Monte Carlo expectations with statistical errors only.

sample	N_A	N_B	N_C	N_D	$N_A \times N_C/N_B$
$t\bar{t}$	233.5 ± 6.5	880.2 ± 12.7	152.8 ± 5.3	34.6 ± 2.5	40.5 ± 1.9
DY	2.6 ± 1.8	38.9 ± 7.2	3.6 ± 2.2	4.8 ± 2.9	0.2 ± 0.2
W^+W^-	2.9 ± 0.4	7.6 ± 0.6	0.7 ± 0.2	0.8 ± 0.2	0.3 ± 0.1
$W^\pm Z^0$	0.4 ± 0.1	1.6 ± 0.1	0.2 ± 0.0	0.1 ± 0.0	0.1 ± 0.0
Z^0Z^0	0.1 ± 0.0	0.5 ± 0.0	0.1 ± 0.0	0.1 ± 0.0	0.0 ± 0.0
single top	9.2 ± 0.5	26.9 ± 0.9	1.0 ± 0.2	0.3 ± 0.1	0.3 ± 0.1
W + jets	2.8 ± 2.8	6.0 ± 3.2	0.0 ± 0.0	0.0 ± 0.0	0.0 ± 0.0
Total SM MC	251.5 ± 7.4	961.9 ± 15.0	158.4 ± 5.8	40.7 ± 3.8	41.4 ± 2.0
data	306	1071	141	45	40.3 ± 4.3

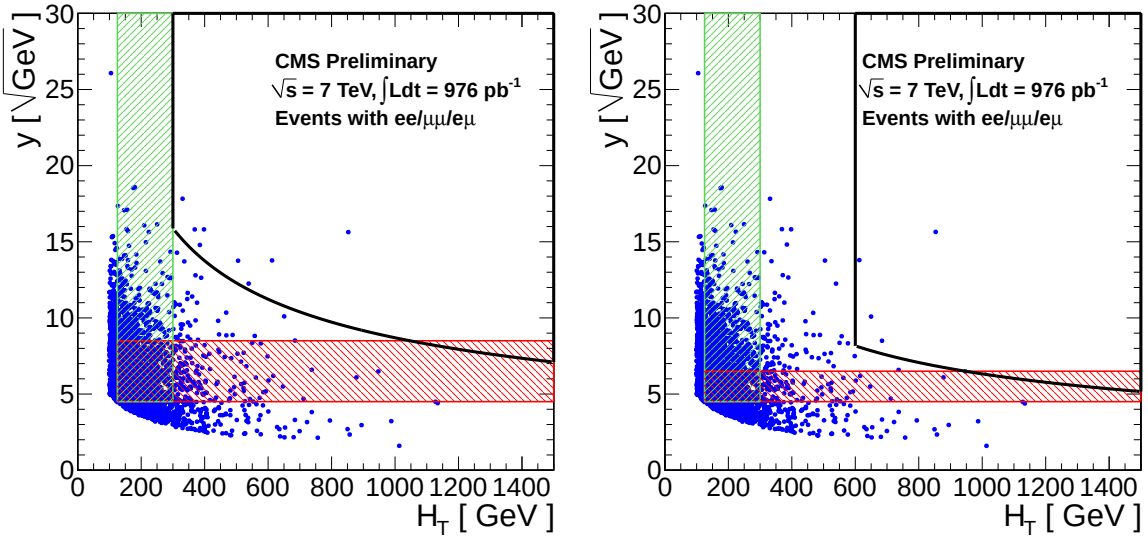

Figure 9: Distributions of y vs. H_T in data. The signal regions $\mathrm{E_T^{miss}} > 275$ GeV, $H_T > 300$ GeV (left) and $\mathrm{E_T^{miss}} > 200$ GeV, $H_T > 600$ GeV (right) are indicated with thick black lines. The $f(y)$ and $g(H_T)$ functions are measured using events in the green and red shaded areas, respectively.

12.2 Background estimate from the $P_T(\ell\ell)$ method

We begin by extracting the value of the $\mathrm{E_T^{miss}}$ acceptance scaling factor K from data, for the H_T control region 125–300 GeV and for the 2 signal regions $H_T > 300$ and $H_T > 600$ GeV. The quantity $1/K$ is the efficiency for events passing preselection and falling in the given H_T range to pass the requirement $p_T(\ell\ell) > 50$ GeV. The values of K extracted from data and $t\bar{t}$ MC are given in Table 20. For all 3 H_T regions, the value of K extracted from data agrees with the $t\bar{t}$ MC prediction, but for the $H_T > 600$ GeV region the statistical uncertainty in K from data is 56%. Therefore we use the value of K extracted from data for the control region 125–300 GeV and for the signal regions $H_T > 300$; for the $H_T > 600$ GeV region we use K from $t\bar{t}$ MC.

For each signal region D, we count the number of events falling in the region D', which is defined using the same requirements as D but switching the y requirement to a $p_T(\ell\ell)/\sqrt{H_T}$ requirement (2010 signal region) or switching the $\mathrm{E_T^{miss}}$ requirement to a $p_T(\ell\ell)$ requirement (high $\mathrm{E_T^{miss}}$ and high H_T signal regions). We subtract off the expected DY contribution using the data-driven $R_{out/in}$ technique, using $R_{out/in} = 0.13 \pm 0.07$. We then scale this yield by 2 corrections factors: K, the $\mathrm{E_T^{miss}}$ acceptance correction factor, and K_C, the correction factor determined in Sec. 11. Our final prediction N_P is given by:

$$N_P = (N(D') - N(DY)) \times K \times K_C,$$

as summarized in Table 21, and displayed in Figs. 11-13. We also perform the $p_T(\ell\ell)$ method in the H_T sideband

region 125–300 GeV, as a validation of the technique in a high statistics sample which is expected to be dominated by background. The results are summarized in Table 22 and displayed in Fig. 10. The prediction is extracted for the requirement $y > 8.5$ GeV$^{1/2}$ corresponding to the 2010 signal region, as well as for $\mathrm{E_T^{miss}} > 200$ GeV corresponding to the high H_T signal region. In both cases, we observe good agreement between the predicted and observed yields.

Table 20: Summary of the $\mathrm{E_T^{miss}}$ acceptance scaling factor K, extracted from data and $t\bar{t}$ MC.

region	data	$t\bar{t}$ MC
control region: $125 < H_T < 300$ GeV	1.65 ± 0.08	1.67 ± 0.03
signal region: $H_T > 300$ GeV	1.48 ± 0.17	1.50 ± 0.06
signal region: $H_T > 600$ GeV	1.24 ± 0.56	1.32 ± 0.20

Table 21: Summary of results of the dilepton p_T template method applied to the 3 signal regions. The quantities indicated in the table are discussed in the text. The quoted statistical uncertainty in the prediction N_P is due to that of $N(D')$, the quoted systematic uncertainty includes that of $N(DY)$, K, and K_C.

Signal Region	$N(D')$	$N(DY)$	K	K_C	N_P
2010 signal region	26	2.7 ± 1.2	1.5 ± 0.2	1.4 ± 0.4	48.2 ± 10.6 (stat) ± 15.1 (syst)
high $\mathrm{E_T^{miss}}$ signal region	8	1.6 ± 0.8	1.5 ± 0.2	1.5 ± 0.5	14.3 ± 6.3 (stat) ± 5.3 (syst)
high H_T signal region	6	0.1 ± 0.1	1.3 ± 0.2	1.3 ± 0.4	10.1 ± 4.2 (stat) ± 3.5 (syst)

Table 22: Summary of results of the dilepton p_T template method applied to the H_T sideband control region 125–300 GeV. The quantities indicated in the table are discussed in the text. The quoted statistical uncertainty in the prediction N_P is due to that of $N(D')$, the quoted systematic uncertainty includes that of $N(DY)$ and K_C. The predictions are compare with the observed yield N_O.

Control Region	$N(D')$	$N(DY)$	K	K_C	N_P	N_O
$y > 8.5$ GeV$^{1/2}$	165	5.3 ± 2.3	1.6 ± 0.1	1.4 ± 0.1	368.9 ± 29.7 (stat) ± 32.3 (syst)	306
$\mathrm{E_T^{miss}} > 200$ GeV	8	1.9 ± 0.9	1.6 ± 0.1	1.3 ± 0.2	13.0 ± 6.1 (stat) ± 2.9 (syst)	14

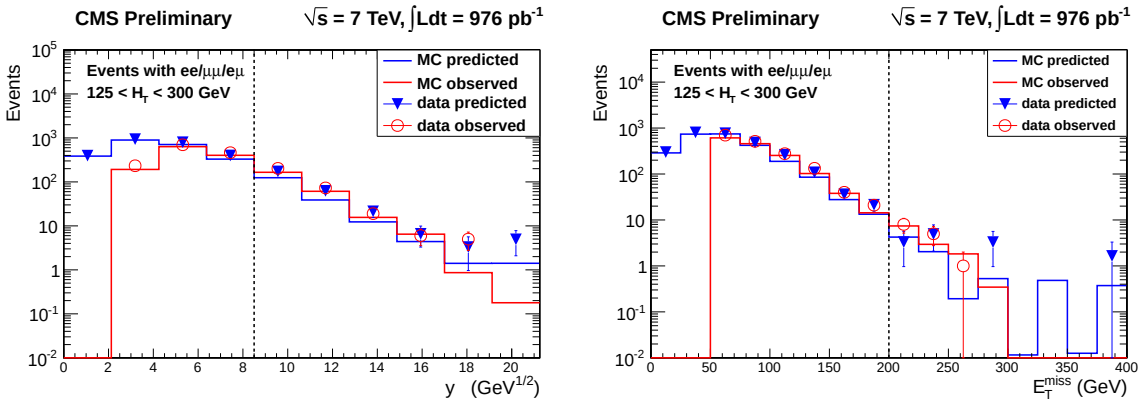

Figure 10: Results of the $p_T(\ell\ell)$ method in the H_T sideband region 125-300 GeV. Left: distributions of $p_T(\ell\ell)/\sqrt{H_T}$ (predicted) and y (observed) for SM MC and data. The vertical dashed lines indicate the requirement $y > 8.5$ GeV$^{1/2}$), corresponding to the 2010 signal region. Right: distributions of $p_T(\ell\ell)$ (predicted) and $\mathrm{E_T^{miss}}$ (observed) for SM MC and data. The vertical dashed lines indicate the requirement $\mathrm{E_T^{miss}} > 200$ GeV, corresponding to the high H_T signal region.

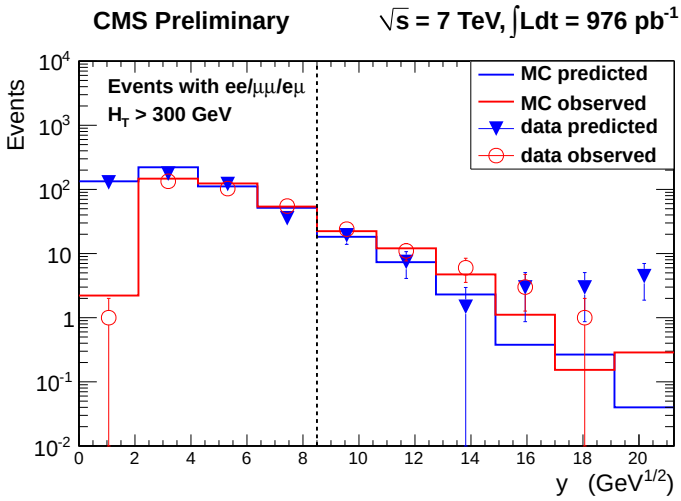

Figure 11: Distributions of $p_T(\ell\ell)/\sqrt{H_T}$ (predicted) and y (observed) for SM MC and data, for the $H_T>$ 300 GeV. The vertical dashed lines indicate the requirement $y > 8.5$ GeV$^{1/2}$ corresponding to the 2010 signal region.

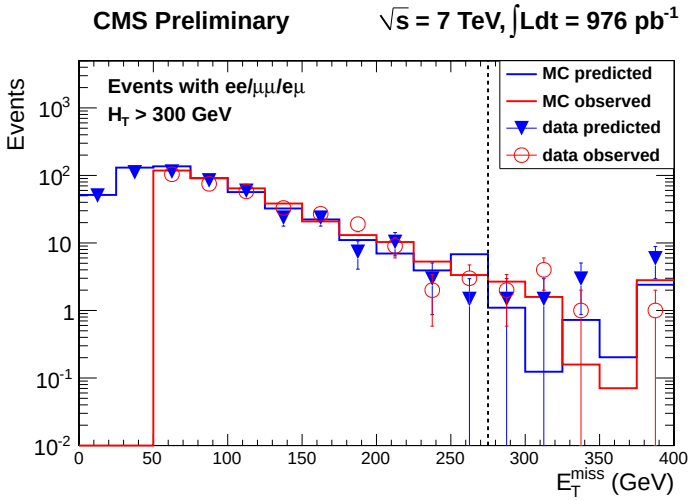

Figure 12: Distributions of $p_T(\ell\ell)$ (predicted) and $\mathrm{E_T^{miss}}$ (observed) for SM MC and data, for the region $H_T>$ 300 GeV. The vertical dashed lines indicate the requirement $\mathrm{E_T^{miss}} > 275$ GeV, corresponding to the high $\mathrm{E_T^{miss}}$ signal region.

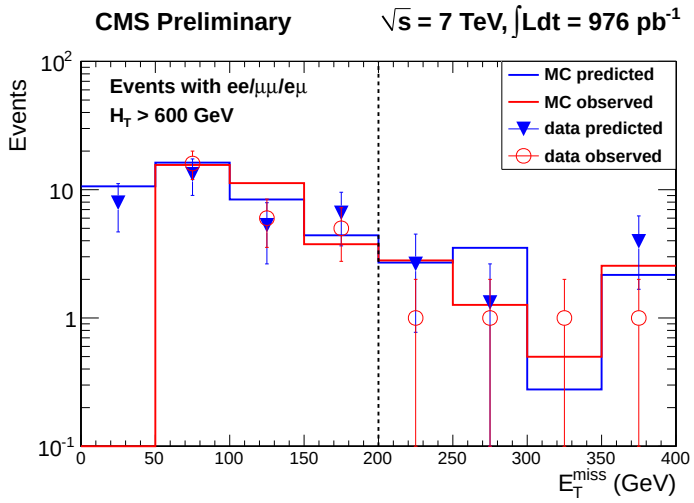

Figure 13: Distributions of $p_T(\ell\ell)$ (predicted) and $\mathrm{E_T^{miss}}$ (observed) for SM MC and data, for the region $H_T >$ 600 GeV. The vertical dashed lines indicate the requirement $\mathrm{E_T^{miss}} > 200$ GeV, corresponding to the high H_T signal region.

12.3 Background estimate from OF subtraction

The results of the OF subtraction technique applied to the high p_T dilepton trigger sample are summarized in Table 23. We evaluate the quantity $\Delta = R_{\mu e}N(ee) + \frac{1}{R_{\mu e}}N(\mu\mu) - N(e\mu)$ with $R_{\mu e} = 1.12 \pm 0.05$ extracted from the ratio of $Z \to \mu^+\mu^-$ vs. $Z \to e^+e^-$ events in data. We perform the OF subtraction first in the preselection region, and find Δ consistent with 0, as expected. We then perform the OF subtraction in all 3 signal regions, and do not observe any excess of same-flavor vs. opposite-flavor events. We do not correct the value of Δ for contributions from fake leptons; instead, we assess on uncertainty based on the results of Sec. 10.

Table 23: Summary of results for the OF subtraction technique. The quantity $\Delta = R_{\mu e}N(ee) + \frac{1}{R_{\mu e}}N(\mu\mu) - N(e\mu)$ is quoted with $R_{\mu e} = 1.12 \pm 0.05$. The quoted systematic uncertainty corresponds to that of $R_{\mu e}$ and the contribution from fake leptons. The $e\mu$ yields differ from those previously quoted because the Z mass veto is included here.

region	$N(ee)$	$N(\mu\mu)$	$N(e\mu)$	Δ
preselection region	524	576	1099	2.2 $\pm$ 47.1 (stat) $\pm$ 3.2 (syst)
2010 signal region	11	8	23	-3.5 $\pm$ 6.6 (stat) $\pm$ 3.8 (syst)
high $\mathrm{E_T^{miss}}$ signal region	5	0	2	3.6 $\pm$ 2.9 (stat) $\pm$ 0.4 (syst)
high H_T signal region	1	0	2	-0.9 $\pm$ 1.8 (stat) $\pm$ 1.1 (syst)

For the dilepton-H_T trigger sample, we observe 4 events in the 2010 signal region consistent with MC expectations, and 0 (1) events in the high $\mathrm{E_T^{miss}}$ (high H_T) signal regions. In the case of an excess of events at low lepton p_T, we will perform the OF subtraction technique of Sec. 11.4.2.

12.4 Summary of results

A summary of our results is presented in Table 24. In all 3 signal regions, we observe reasonable agreement between the observed yields and the predictions from MC and data-driven background estimates. We therefore do not observe evidence for an excess of events above SM expectations. After assessing systematic uncertainties in Sec. 13, we proceed to set upper limits on the non-SM contributions to the signal regions in Sec. 14.

Table 24: Summary of the observed and predicted yields in the 3 signal regions. MC errors are statistical only. The systematic uncertainty on the ABCD and $p_T(\ell\ell)$ method is from the scaling factors from MC closure only. For the OF subtraction, the quantity $\Delta = R_{\mu e}N(ee) + \frac{1}{R_{\mu e}}N(\mu\mu) - N(e\mu)$ is quoted; the systematic uncertainty here is from the ratio of muon to electron selection efficiencies and from the contribution from fake leptons.

	2010 signal region	high $\mathrm{E_T^{miss}}$ signal region	high H_T signal region
Observed yield	45	8	4
MC prediction	40.7 $\pm$ 3.8	7.3 $\pm$ 2.2	7.1 $\pm$ 2.2
ABCD prediction	40.3 $\pm$ 4.3 (stat) $\pm$ 8.1 (syst)		
ABCD' prediction	40.5 $\pm$ 5.0 (stat) $\pm$ 8.1 (syst)	4.0 $\pm$ 1.0 (stat) $\pm$ 0.8 (syst)	4.5 $\pm$ 1.6 (stat) $\pm$ 0.9 (syst)
$p_T(\ell\ell)$ prediction	48.2 $\pm$ 10.6 (stat) $\pm$ 15.1 (syst)	14.3 $\pm$ 6.3 (stat) $\pm$ 5.3 (syst)	10.1 $\pm$ 4.2 (stat) $\pm$ 3.5 (syst)
OF subtraction (Δ)	-3.5 $\pm$ 6.6 (stat) $\pm$ 3.8 (syst)	3.6 $\pm$ 2.9 (stat) $\pm$ 0.4 (syst)	-0.9 $\pm$ 1.8 (stat) $\pm$ 1.1 (syst)

13 Acceptance and efficiency systematics

This is a search for new physics contributions to events with high $\mathrm{E_T^{miss}}$and lots of jet activity. As seen in Section 12, there is no evidence for a contribution beyond SM expectations.

Strictly speaking it is impossible to talk about "acceptance and efficiency systematics" because these kinds of systematics only apply to a well defined final state. Nevertheless, we can make general statements about the systematic uncertainties, including quantitative estimates of the systematic uncertainties associated with a few specific processes.

The systematic uncertainty on the lepton acceptance consists of two parts: the trigger efficiency uncertainty and the ID and isolation uncertainty. We discuss these in turn.

The trigger efficiency for the high p_T dilepton triggers has been studied in [6] in detail. The efficiency is found to be approximately 100% for ee, 95% for $e\mu$, and 90% for $\mu\mu$. There is a small dependence of the efficiency on the lepton p_T, which we do not attempt to parameterize. Instead, we assign an uncertainty of 2%, based on the small variation of the efficiency on the lepton p_T.

To evaluate the uncertainty on the lepton ID and isolation efficiencies, we perform a tag and probe technique on Z data and MC. We calculate the efficiency for leptons passing isolation criteria to also pass the ID criteria, and the efficiency for leptons passing the ID criteria to also pass the isolation criteria. We observe agreement between data and MC within about 2%, and assign a corresponding systematic uncertainty.

Another significant source of systematic uncertainty is associated with the jet and $\mathrm{E_T^{miss}}$ energy scale. The impact of this uncertainty is final-state dependent. Final states characterized by lots of hadronic activity and $\mathrm{E_T^{miss}}$ are less sensitive than final states where the $\mathrm{E_T^{miss}}$ and H_T are typically close to the requirement. To be more quantitative, we have used the method of Reference [3] to evaluate the systematic uncertainties on the acceptance for $t\bar{t}$ and three benchmark SUSY points. The uncertainties are calculated assuming a 7.5% uncertainty to the hadronic energy scale in CMS.

Table 25: Summary of efficiency uncertainties due to the 7.5% uncertainty in the hadronic energy scale.

Signal Region	$t\bar{t}$	LM1	LM3	LM6
2010 signal region	0.39	0.09	0.10	0.06
high $\mathrm{E_T^{miss}}$ signal region	0.61	0.22	0.27	0.10
high H_T signal region	0.50	0.30	0.32	0.14

The uncertainty in the integrated luminosity is 6%.

14 Derivation of Upper Limits

We proceed to set upper limits on the non-SM contributions to the 3 signal regions. For all 3 regions, we find reasonable agreement between the observed yields and the predictions from MC and from the 2 data-driven methods. We choose here to extract the upper limits using the weighted average of the 2 data-driven predictions for the background estimate. The 95% CL upper limit is extracted using the CLs technique. The results are summarized in Table 26. The 3 benchmark points LM1, LM3 and LM6 are excluded by these results.

Table 26: Summary of 95% CL upper limits on the non-SM yield. The background estimate N_{bkg} is the weighted average of the 2 data-driven estimates. The LM1 and LM3 yields are shown, with uncertainties from the hadronic energy scale, lepton selection and trigger efficiencies, and integrated luminosity.

	2010 signal region	high $\mathrm{E_T^{miss}}$ signal region	high H_T signal region
Observed yield	45	8	4
N_{bkg}	42 ± 8.5	4.2 ± 1.3	5.1 ± 1.7
non-SM yield UL	22	10	5.8
LM1	85.7 ± 9.7	48.7 ± 11.2	37.7 ± 11.6
LM3	34.6 ± 4.2	18.0 ± 5.0	18.8 ± 6.2
LM6	9.7 ± 0.9	8.1 ± 1.0	7.4 ± 1.2

15 Outreach

Conveying additional useful information about the results of a generic "signature-based" search such as the one described in this note is a difficult issue. Here we attempt to present our result in the most general way.

Models of new physics in the dilepton final state can be confronted in an approximate way by simple generator-level studies that compare the expected number of events in 976 pb^{-1} with our upper limits in Sec. 14. The key ingredients of such studies are the kinematical cuts described in this note, the lepton efficiencies, and the detector responses for H_T, y, and $\mathrm{E_T^{miss}}$.

The muon identification efficiency is $\approx 96\%$; the electron identification efficiency varies approximately linearly from $\approx$ 60% at p_T= 10 GeV to 90% for $p_T>$ 30 GeV. The lepton isolation efficiency depends on the lepton

momentum, as well as on the jet activity in the event. In $t\bar{t}$ events, it varies approximately linearly from $\approx 73\%$ (muons) and $\approx 82\%$ (electrons) at p_T= 10 GeV to $\approx 97\%$ for $p_T>$ 60 GeV. In LM1 (LM3,LM6) events, this efficiency is decreased by $\approx$5–10% ($\approx$10%,$\approx$5%)over the whole momentum spectrum. The average detector responses (the reconstructed quantity divided by the generated quantity) for H_T, y and $\mathrm{E_T^{miss}}$ are consistent with 1 within the 5% jet energy scale uncertainty. The experimental resolutions on these quantities are 9%, 12% and 12%, respectively.

To justify the statements in the previous paragraph about the detector responses, we plot in Figure 14 the average response for H_T, y and $\mathrm{E_T^{miss}}$, as well as the efficiency for the cuts on these quantities used in defining the signal region.

The lepton identification and isolation efficiencies are displayed for the dominant $t\bar{t}$ background in Fig. 15. The isolation efficiencies for the LM1 and LM3 processes are displayed in Fig. 16, which shows the decrease in isolation efficiency resulting from the large hadronic activity in these events.

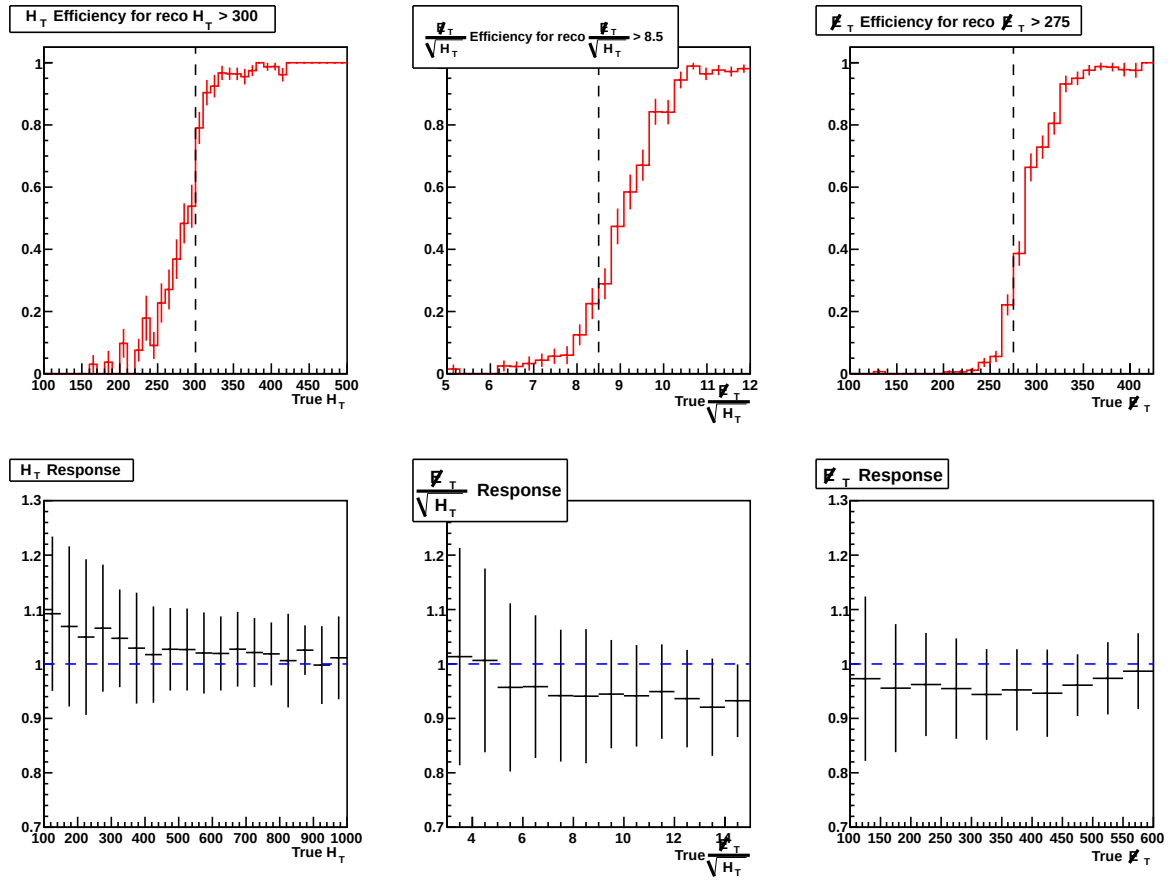

Figure 14: Top plots: the efficiencies to pass the signal region requirements (vertical dashed lines) on H_T (left), y (middle) and $\mathrm{E_T^{miss}}$ (right) as a function of the generated quantities. Bottom plots: the average detector responses for H_T, y and $\mathrm{E_T^{miss}}$ and the corresponding RMS (error bars), as a function of the generated quantities. The response is defined as the ratio of the reconstructed quantity to the true quantity in MC. These plots are done using the LM1 Monte Carlo, but they are not expected to depend strongly on the underlying physics.

16 Model Dependent Upper Limits

As an example of how the upper limit presented in Sec. 14 can be used to test if a specific model is excluded, in this section we consider the benchmark SUSY processes LM1, LM3 and LM6. We place upper limits on the quantity $\sigma \times A$, assuming efficiencies and uncertainties from these processes, and compare them to the expected values of $\sigma \times A$. Here σ is the signal production cross section and A is the signal acceptance.

The signal event yield N_{SIG} can be expressed as:

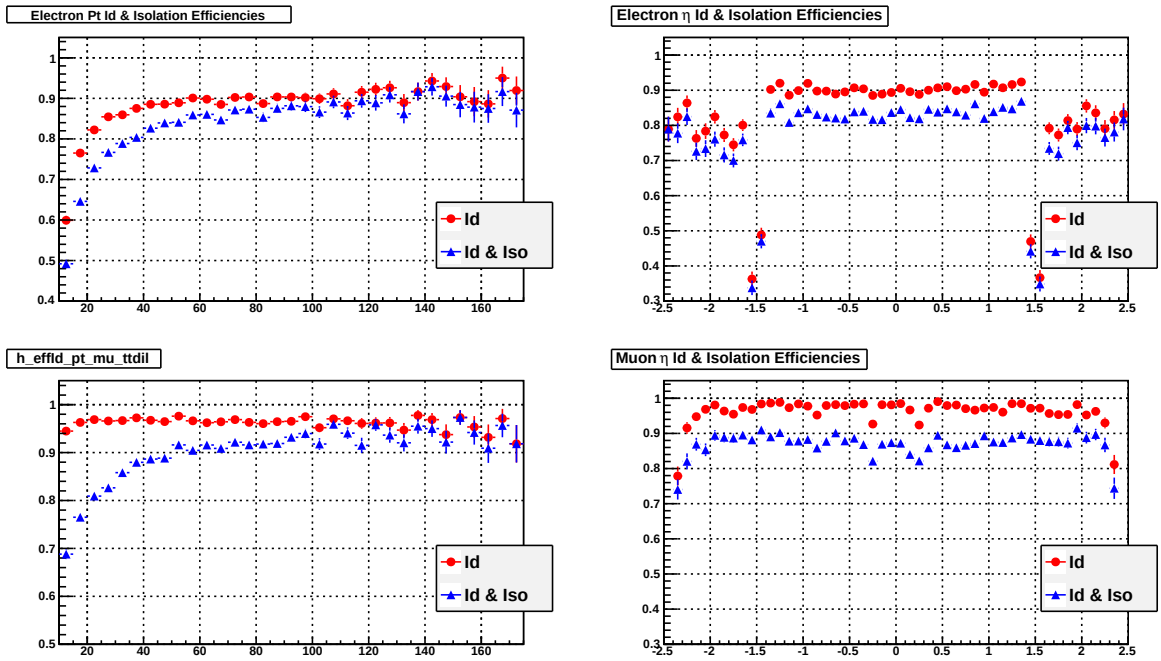

Figure 15: The lepton identification and isolation efficiencies in $t\bar{t}$ MC for electrons (top) and muons (bottom) vs. p_T (left) and η (right).

$$N_{SIG} = \sigma \times A \times \epsilon \times \mathcal{L}, \tag{3}$$

and we therefore have:

$$N_{SIG}/(\epsilon \times \mathcal{L}) = \sigma \times A. \tag{4}$$

Here ϵ is the signal efficiency and $\mathcal{L}$ is the integrated luminosity. Since we wish to place an upper limit on the quantity $\sigma \times A$, we must evaluate the quantity $N_{SIG}/(\epsilon \times \mathcal{L})$. Because of the efficiency in the denominator, this upper limit cannot be calculated in an entirely model-independent way; rather, it must be calculated with respect to a specific model. We therefore evaluate the upper limit on $\sigma \times A$ with respect to LM1, LM3 and LM6. For each process, we must calculate both the efficiency and its uncertainty.

We evaluate the signal efficiencies and acceptances using MC. The acceptance is defined by he following requirements which are applied on the generator-level quantities:

- 2 electrons or muons with $p_T > 10$ GeV and $|\eta| < 2.5$, at least 1 lepton must have $p_T > 20$ GeV
- Opposite-sign pair, veto same-flavor pairs with $76 < \mathrm{m}(\ell\ell) < 106$ GeV
- Count genjets with $p_T > 30$ GeV, $|\eta| < 3.0$, $\Delta R > 0.4$ from any selected lepton as defined above, require at least 2 genjets
- H_T^{gen} is the scalar sum of selected genjet p_T's, MET^{gen} is the event gen-level missing ET, and $y^{GEN} \equiv MET^{gen}/\sqrt{H_T^{gen}}$.

For the 2010, high $\mathrm{E_T^{miss}}$, and high H_T signal regions, we add the corresponding requirements on the generator-level quantities H_T^{gen}, MET^{gen} and y^{GEN}. The signal efficiency is defined as the fraction of events passing the above acceptance requirements, which also pass the full reco-level selection. The efficiency uncertainty is determined by the trigger uncertainty (2%), the lepton selection uncertainty (2%/lepton) and the hadronic energy scale uncertainties quoted in Table 25.

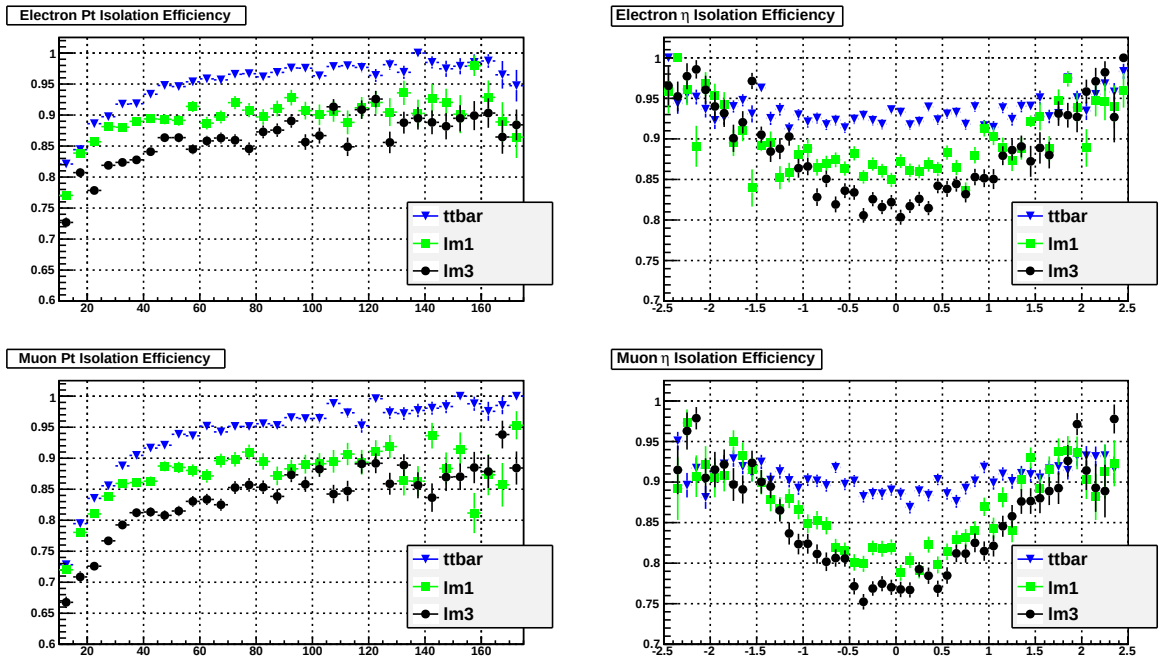

Figure 16: The lepton isolation efficiencies for $t\bar{t}$, LM1 and LM3 MC for electrons (top) and muons (bottom) vs. p_T (left) and η (right).

Armed with the efficiencies and uncertainties calculated in the previous 2 sections, we proceed to calculate upper limits on the quantity $\sigma \times A$ for the 3 benchmark SUSY scenarios. We calculate 95% CL upper limits using the CLs technique. We quote here the upper limits from the high H_T signal region. The results are summarized in Table 27. These results show that the LM1, LM3 and LM6 scenarios are excluded.

We also quote the result more generally in the context of the CMSSM. The CLs 95% CL limit in the $(m_0, m_{1/2})$ plane, for $\tan\beta = 10$, $A_0 = 0$ and $\mu > 0$ is shown in Figure 17. The high $\mathrm{E_T^{miss}}$ and high $H_T$signal regions have similar sensitivity to the CMSSM; here we choose to show results based on the high-$H_T$signal regions. The SUSY particle spectrum is calculated using SoftSUSY [22], and the signal events are generated at leading order (LO) with PYTHIA6.4.22. NLO cross sections, obtained with the program Prospino [24], are used to calculate the observed exclusion contour. At each point in the $(m_0, m_{1/2})$ plane, the acceptance uncertainty is calculated by summing in quadrature the uncertainties from jet and $\mathrm{E_T^{miss}}$ energy scale using the procedure discussed in Section 13, the uncertainty in the NLO cross section due to the choice of factorization and renormalization scale, and the uncertainty from the parton distribution functions and α_S, evaluated using the prescription from the PDF4LHC recommendation [25]. The luminosity, trigger efficiency, and lepton selection efficiency uncertainties are also included, giving a total relative acceptance uncertainty which varies in the range ∼0.3–0.4. A point is considered to be excluded if the NLO yield exceeds the 95% CL CLs upper limit calculated with this acceptance uncertainty, using a log-normal model for the nuisance parameter integration.

The excluded regions for the CDF search for jets + missing energy final states [26] were obtained for $\tan\beta = 5$, while those from D0 [27] were obtained for $\tan\beta = 3$, each with approximately 2 fb^{-1} of data and for $\mu < 0$. The LEP-excluded regions are based on searches for sleptons and charginos [28]. The D0 exclusion limit, valid for $\tan\beta = 3$ and obtained from a search for associated production of charginos $\chi_1^{\pm}$ and neutralinos χ_2^0 in trilepton final states [29], is also included in Figure 17. In contrast to the other limits presented in Figure 17, the results of our search and of the trilepton search are strongly dependent on the choice of $\tan\beta$ and they reach the highest sensitivity in the CMSSM for $\tan\beta$ values below 10.

17 Summary

We have presented a search for BSM physics in the opposite-sign dilepton final state using a data sample of proton-proton collisions at 7 TeV centre-of-mass energy corresponding to an integrated luminosity of 976 pb^{-1}, recorded by the CMS detector in 2011. The search focused on dilepton events with large missing transverse energy and

Table 27: Summary of model-dependent limits. The efficiency and acceptance are defined in the text; the efficiency uncertainty is dominated by the uncertainty in the hadronic energy scale. The 95% CL CLs UL on the quantity $\sigma \times A$ is indicated, as well as the value of this quantity for the LM1, LM3 and LM6 scenarios.

	LM1	LM3	LM6
2010 signal region			
efficiency (%)	48 ± 5	45 ± 5	51 ± 4
acceptance (%)	2.55	1.4	3.9
UL($\sigma \times A$) (fb)	48	52	45
$\sigma \times A$ (fb)	177	73	18
high $\mathrm{E_T^{miss}}$ signal region			
efficiency (%)	45 ± 10	41 ± 11	52 ± 6
acceptance (%)	1.6	0.84	3.3
UL($\sigma \times A$) (fb)	27	31	21
$\sigma \times A$ (fb)	108	43	16
high H_T signal region			
efficiency (%)	42 ± 13	38 ± 12	50 ± 7
acceptance (%)	1.2	0.85	3.0
UL($\sigma \times A$) (fb)	16	18	12
$\sigma \times A$ (fb)	83	46	15

significant hadronic activity, motivated by many models of BSM physics, such as supersymmetric models. Good agreement with standard model predictions was found, both in terms of event yields and shapes of various relevant kinematic distributions. In the absence of evidence for BSM physics, we have set upper limits on the non-SM contributions to yields in the signal regions.

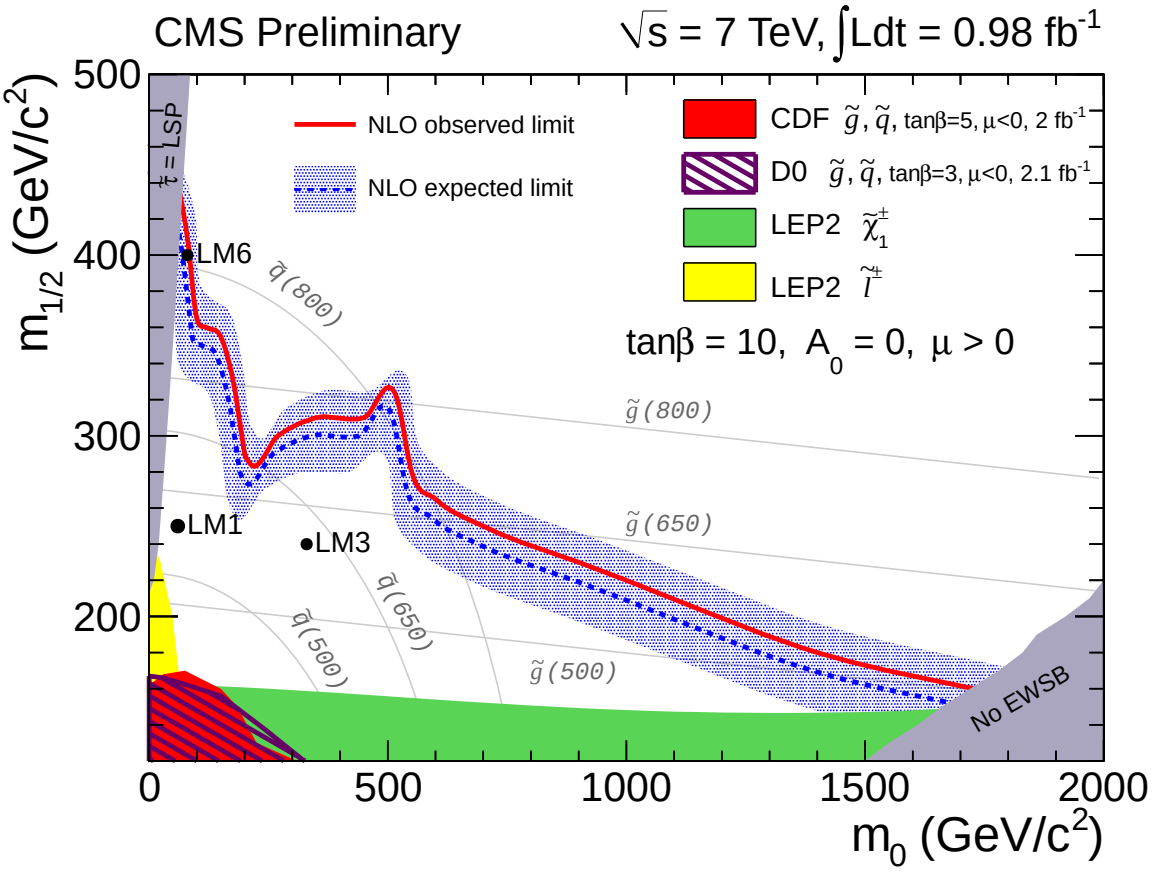

Figure 17: The observed 95% CL exclusion contour at NLO (solid red line) and the expected exclusion contour (dashed blue line) in the CMSSM $(m_0, m_{1/2})$ plane for $\tan\beta = 10$, $A_0 = 0$ and $\mu > 0$. The area below the curve is excluded by this measurement. Exclusion limits obtained from previous experiments are presented as filled areas in the plot. Thin grey lines correspond to constant squark and gluino masses.

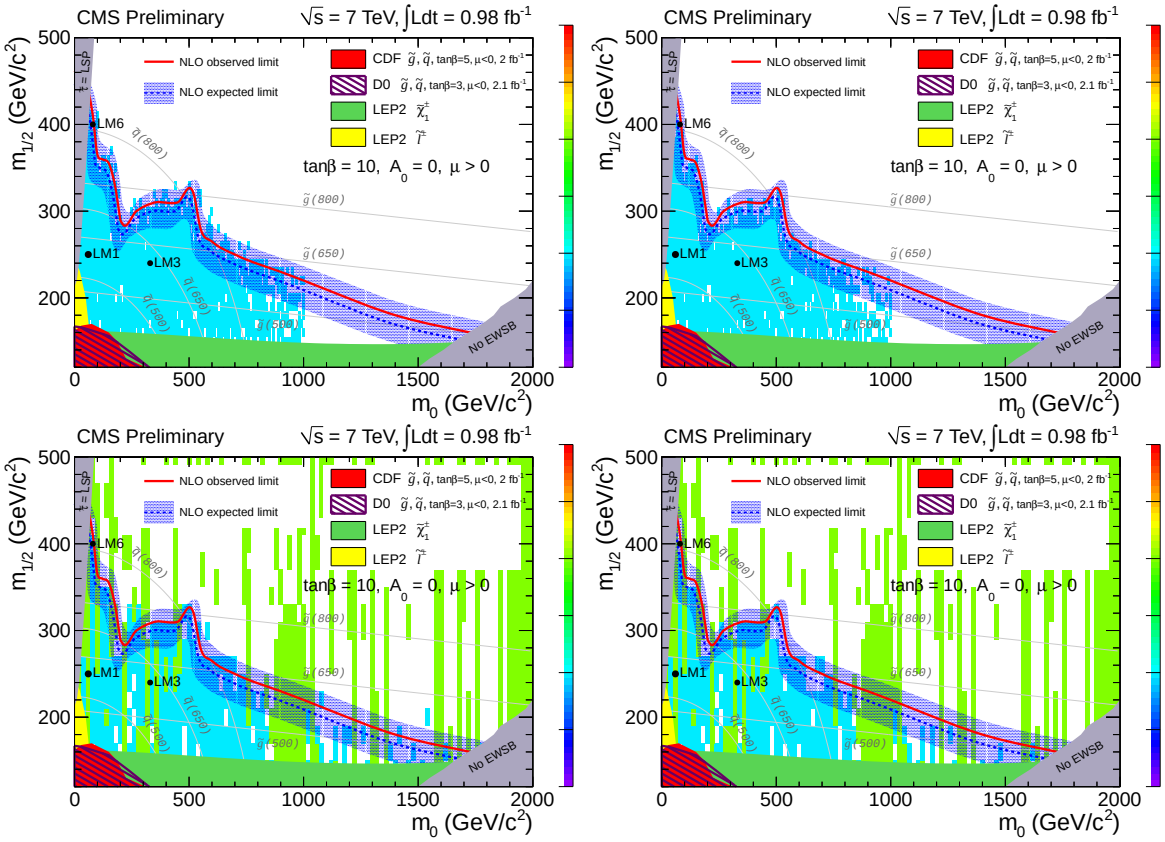

Figure 18: CMSSM exclusion contour, overlaid with the excluded points (blue) from the 38X CMSSM scan (top) and 41X CMSSM scan (bottom) for the observed (left) and expected (right) limit. For the 41X scan, the green points are those that don't have the correct number of entries due to data processing errors, these points are ignored.

References

[1] CMS AN-2010/370

[2] arXiv:1103.1348v1 [hep-ex], "Search for Physics Beyond the Standard Model in Opposite-Sign Dilepton Events at $\sqrt{s} = 7$ TeV."

[3] Phys.Lett.B695:424-443,2011

[4] https://twiki.cern.ch/twiki/bin/viewauth/CMS/SimpleCutBasedEleID

[5] D. Barge *at al.*, AN-CMS2009/159.

[6] CMS AN-2011/155

[7] https://twiki.cern.ch/twiki/bin/view/CMS/ProductionReProcessingSpring10

[8] V. Pavlunin, Phys. Rev. **D81**, 035005 (2010).

[9] D. Barge *at al.*, AN-CMS2009/130.

[10] W. Andrews *et al.*, AN-CMS2009/023.

[11] D. Barge *at al.*, AN-CMS2010/257.

[12] W. Andrews *et al.*, AN-CMS2010/274.

[13] J. Conway, `http://www-cdf.fnal.gov/physics/statistics/code/bayes.f`.

[14] G. Landsberg, `https://twiki.cern.ch/twiki/pub/CMS/EXOTICA/cl95cms.c`

[15] `https://hypernews.cern.ch/HyperNews/CMS/get/susy/617/2/1.html`

[16] `https://twiki.cern.ch/twiki/bin/view/CMS/SUSY38XSUSYScan`

[17] arXiv:hep-ph/0605240v2

[18] CMS Collaboration, "Measurement of CMS luminosity", *CMS-PAS* **EWK-10-004** (2010).

[19] `CleanExclusion.cc` available at `https://twiki.cern.ch/twiki/bin/viewauth/CMS/SUSYLimitTools`

[20] R. Cousins, `http://www.physics.ucla.edu/c̃ousins/stats/cousins_lognormal_prior.pdf`

[21] S. Harper, private communication (relayed to us by M. Chiorboli.).

[22] B.C. Allanach, Comput.Phys.Commun. 305, SOFTSUSY: a program for calculating supersymmetric spectra.

[23] P. M. Nadolsky and H.-L. Lai and Q.-H. Cao and J. Huston and J. Pumplin and D. Stump and W.-K. Tung and C.-P. Yuan, "Implications of CTEQ global analysis for collider", "Phys. Rev.", "D78", "2008", "013004",

[24] W. Beenakker and others, Nucl.Phys., 51, Squark and Gluino Production at Hadron Colliders, B492, 1997, http://dx.doi.org/10.1016/S0550-3213(97)00084-9

[25] PDF4LHC Working Group, `http://www.hep.ucl.ac.uk/pdf4lhc/PDF4LHCrecom.pdf`

[26] CDF Collaboration, 2011-01-12 16:21:11 +0100, 10.1103/PhysRevLett.102.121801, Phys. Rev. Lett., Mar, 7, 121801, American Physical Society, Inclusive Search for Squark and Gluino Production in $p\bar{p}$ Collisions at $\sqrt{s} = 1.96\ TeV$, 102, 2009, http://dx.doi.org/10.1103/PhysRevLett.102.121801

[27] D0 Collaboration, 2011-01-12 16:21:58 +0100, 10.1016/j.physletb.2008.01.042, 0370-2693, Physics Letters B, 449, Search for squarks and gluinos in events with jets and missing transverse energy using 2.1 fb^{-1} of collision data at $\sqrt{s} = 1.96$ TeV, http://www.sciencedirect.com/science/article/B6TVN-4RPTJ5K-1/2/e292da021dc1d62b049dab7f57f50e61, 660, 2008, http://www.sciencedirect.com/science/article/B6TVN-4RPTJ5K-1/2/e292da021dc1d62b049dab7f57f50e61, http://dx.doi.org/10.1016/j.physletb.2008.01.042

[28] LEPSUSYWG, ALEPH, DELPHI, L3 and OPAL experiments, 2011-01-12 15:58:46 +0100, 2011-01-12 16:02:40 +0100, LEPSUSYWG/02-06.2, LSP mass limit in Minimal SUGRA, http://lepsusy.web.cern.ch/lepsusy/Welcome.html, http://lepsusy.web.cern.ch/lepsusy/Welcome.html

[29] D0 Collaboration, 2011-01-12 16:22:11 +0100, 10.1016/j.physletb.2009.08.011, 0370-2693, Physics Letters B, 34, Search for associated production of charginos and neutralinos in the trilepton final state using 2.3 fb^{-1} of data, http://www.sciencedirect.com/science/article/B6TVN-4X0F3RJ-8/2/4e2c160d19488f249889d531ee97a94b, 680, 2009, http://www.sciencedirect.com/science/article/B6TVN-4X0F3RJ-8/2/4e2c160d19488f249889d531ee97a94b, http://dx.doi.org/10.1016/j.physletb.2009.08.011

[30] A. Barr *at al.*, J.Phys.G29:2343-2363,2003; Cheng, H.C., Han, arXiv:hep-ph/0810.5178v2. `http://indico.cern.ch/contributionDisplay.py?contribId=3&confId=66410`

[31] `http://indico.cern.ch/contributionDisplay.py?contribId=5&confId=93837`

[32] M. Narain *et al.*, CMS AN-2010/259; we thank the Brown group for providing their code to us.

Appendix A Fakeable Object Definitions

We estimate the contributions from leptons not originating from W/Z decay (fake leptons) using the data-driven fake rate method [3]. We define the following 'fakeable object' selections, by taking the electron and muon requirements listed in Sec. 4 and loosening the following requirements:

- electrons
  - $d_0 < 0.2$ cm
  - $Iso \equiv E_T^{\rm iso}/p_T < 0.4$, $E_T^{\rm iso}$ is defined as the sum of transverse energy/momentum deposits in ecal, hcal, and tracker, in a cone of 0.3 A 1 GeV pedestal is subtracted from the ecal energy deposition in the EB, however the ecal energy is never allowed to go negative.
- muons
  - $d_0 < 0.2$ cm
  - χ^2/ndof of global fit < 50
  - $Iso \equiv E_T^{\rm iso}/p_T < 0.4$, $E_T^{\rm iso}$ is defined as the sum of transverse energy/momentum deposits in ecal, hcal, and tracker, in a cone of 0.3

Appendix B The ABCD' Technique

We have developed a novel technique, based on the ABCD technique which we perform in the plane of y vs. H_T, which allows us to estimate the background in a signal region defined in the $\mathrm{E_T^{miss}}$ vs. H_T plane. We refer to this as the ABCD' technique.

First, we extract the y and H_T distributions $f(y)$ and $g(H_T)$ from data, using events from control regions which we expect to be dominated by background. Under the assumption that y and H_T are weakly-correlated (the same assumption which allows the use of the ABCD technique), we can predict the distribution of events in the y vs. H_T plane as:

$$\frac{\partial^2 N}{\partial y \partial H_T} = f(y)g(H_T) \tag{5}$$

Once the distribution of events in the y vs. H_T plane is known, the number of events falling in any region of this plane can be deduced. In particular, we can deduce the number of events falling in a region defined by requirements on $\mathrm{E_T^{miss}}$ and H_T.

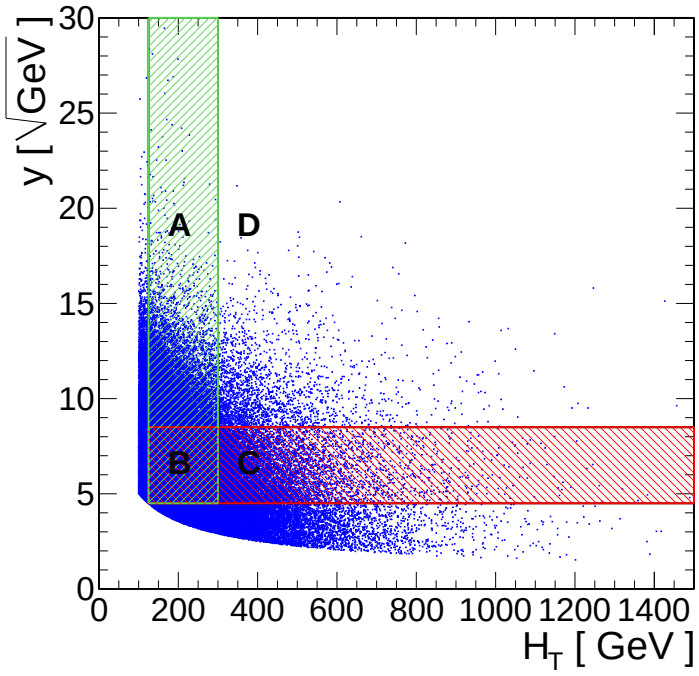

Figure 19: Distributions of y vs. H_T for $t\bar{t}$ MC. The $f(y)$ and $g(H_T)$ functions are measured using events in the green and red shaded areas, respectively.

In this section, we study the ABCD' technique by applying it to $t\bar{t}$ MC (we use the powheg sample which has 10 times the number of dilepton events as the madgraph sample). As a cross-check, we first use the ABCD' technique to estimate the background in the 2010 signal region defined as $y > 8.5$ GeV$^{1/2}$ and $H_T > 300$ GeV, which may be compared to the prediction of the standard ABCD technique. We measure the $f(y)$ and $g(H_T)$ distributions using events in the regions indicated in Fig. 19, yielding the distributions shown in Fig. 20. Next, we randomly sample values of y and H_T from these distributions; each pair of y and H_T values is a pseudo-event. We generate 1 million pseudo-events, and find the ratio $R_{S/C}$, the ratio of the number of pseudo-events falling in the 2010 signal region (ie. region D) to the number of pseudo-events falling in a control region, defined as the OR of the A, B and C regions. We then multiply this ratio by the number of $t\bar{t}$ MC events which fall in the control region to get the predicted yield, ie. $N_{pred} = R_{S/C} \times N(\mathrm{control})$. To estimate the statistical uncertainty in the predicted background, we smear the bin contents of $f(y)$ and $g(H_T)$ according to their uncertainties. We repeat the prediction 20 times with these smeared distributions, and take the RMS of the deviation from the nominal prediction as the statistical uncertainty. The results are summarized in Table 18, which show that the prediction of the ABCD' method is consistent with that of the ABCD method within the statistical uncertainty.

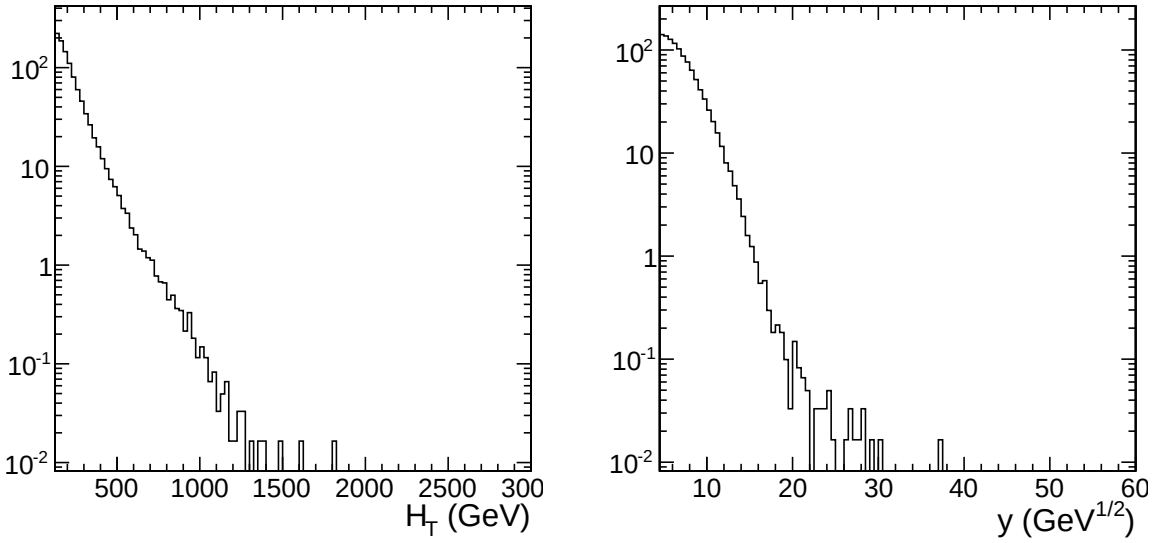

Figure 20: The distributions $f(y)$ and $g(H_T)$ extracted from $t\bar{t}$ MC.

We next apply the ABCD' technique to estimate the background in the regions:

- SR1: $\mathrm{E_T^{miss}} > 275$ GeV, $H_T > 300$ GeV
- SR2: $\mathrm{E_T^{miss}} > 200$ GeV, $H_T > 600$ GeV.

Note that we are unable to predict the yield in this region using the standard ABCD technique, since $\mathrm{E_T^{miss}}$ and H_T are not weakly correlated. The signal regions are shown in Fig. 21. There is a sizable overlap between SR2 and region C, hence when estimating the background for this signal region we restrict the control region used to measure $g(H_T)$ and to determine $N(\mathrm{control})$ to $4.5 < y < 6.5$ GeV$^{1/2}$. As summarized in Table 18, we find values of observed / predicted of 1.30 ± 0.10 and 1.05 ± 0.07 for SR1 and SR2, respectively.

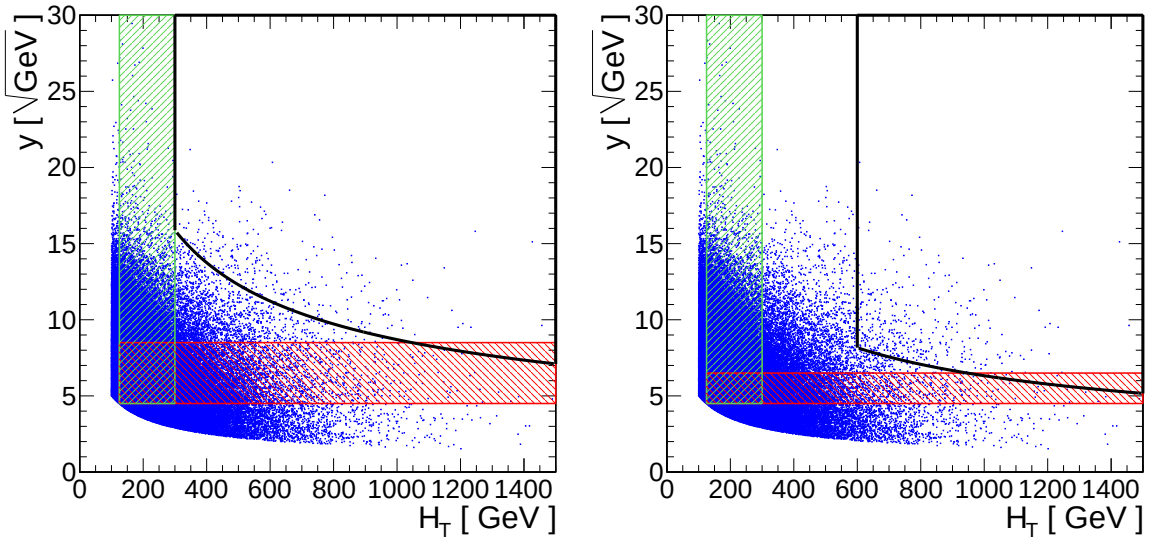

Figure 21: Distributions of y vs. H_T for $t\bar{t}$ MC. The signal regions $\mathrm{E_T^{miss}} > 275$ GeV, $H_T > 300$ GeV (left) and $\mathrm{E_T^{miss}} > 200$ GeV, $H_T > 600$ GeV (right) are indicated with thick black lines. The $f(y)$ and $g(H_T)$ functions are measured using events in the green and red shaded areas, respectively.

Next, we study the ABCD' technique by applying it to samples with size comparable to the expected number of events in 1 fb^{-1} of data. We take the full powheg data sample, and split it into subsamples of ~2500 events

Table 28: Expected results from $t\bar{t}$ MC in 1 fb^{-1} for the ABCD' method. The quoted uncertainties are statistical only.

signal region	sample	predicted	observed	obs/pred
2010 signal region	madgraph	44.0 ± 1.5	38.3 ± 2.4	0.87 ± 0.06
	powheg	43.3 ± 0.5	37.0 ± 0.8	0.85 ± 0.02
high $\mathrm{E_T^{miss}}$ signal region	madgraph	3.1 ± 0.4	4.6 ± 0.8	1.47 ± 0.31
	powheg	3.5 ± 0.1	4.5 ± 0.3	1.30 ± 0.10
high H_T signal region	madgraph	5.3 ± 0.8	5.5 ± 0.9	1.03 ± 0.23
	powheg	5.9 ± 0.3	6.2 ± 0.3	1.05 ± 0.07

each, which corresponds roughly to the number of expected events in data passing preselection, for an integrated luminosity of 1 fb^{-1}. For each sample, we use the ABCD' technique to predict the background in the SR1 and SR2 regions. In Fig. 22, we plot the quantity <observed>/predicted for the SR1 and SR2 regions, where <observed> indicates the observed yield in the signal yield, average over the number of toy MC subsamples. Based on these studies, we apply a correction factor of 1.2 ± 0.5 and 1.0 ± 0.5 for the SR1 and SR2 regions.

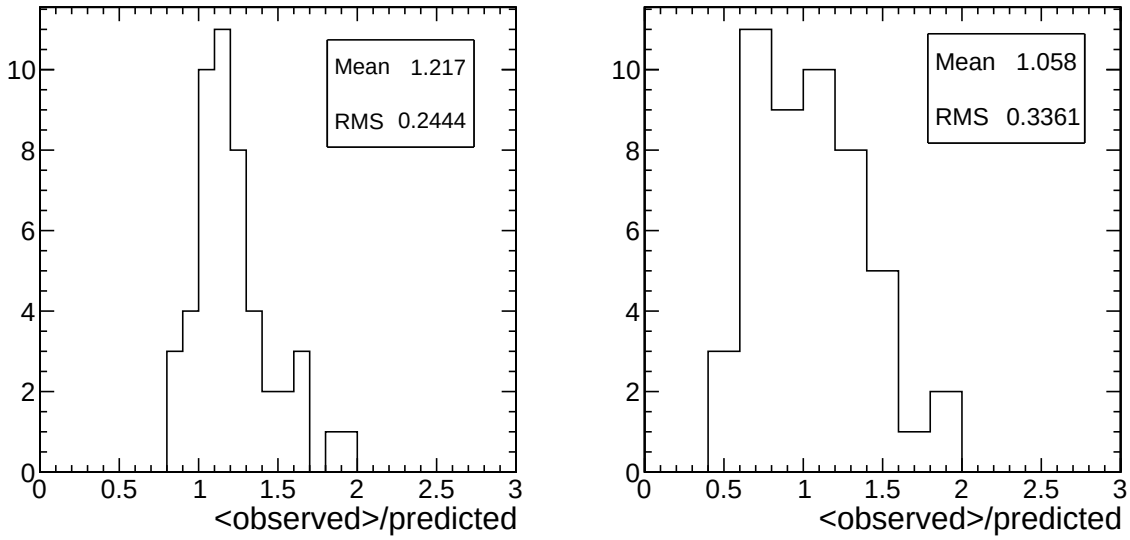

Figure 22: Distributions of <observed>/predicted for the toy MC subsamples.

Appendix C Data/MC Comparison: Preselection Region

Here we compare data and MC distributions for data passing the preselection requirements. The high p_T dilepton trigger data is used.

All MC samples are scaled by an overall factor 1.13, the ratio of the observed data yield in the preselection region to the prediction from MC. For illustration purposes, we overlay the distributions from the LM1 SUSY benchmakr point.

The meaning of most of the variables plotted in the following figures should be obvious. There are some exceptions that we exlain below:

- $MT2$ is a kinematical quantity built from the two leptons and the $\mathrm{E}_{\mathrm{T}}^{\mathrm{miss}}$. For events with two $W \to \ell$ decays it should have a sharp kinematical cutoff at W mass. For more details, see Reference [30].
- $MT2J$ is very much like $MT2$ but it is built out of the leptons, the $\mathrm{E}_{\mathrm{T}}^{\mathrm{miss}}$ and the two jets. For $t\bar{t}$ events it has a kinematical cutoff at M_{top}, with tails due to the fact that occasionally one of the b-jets is not found and is replaced by a gluon jet from ISR or FSR. For more details, see Reference [31].

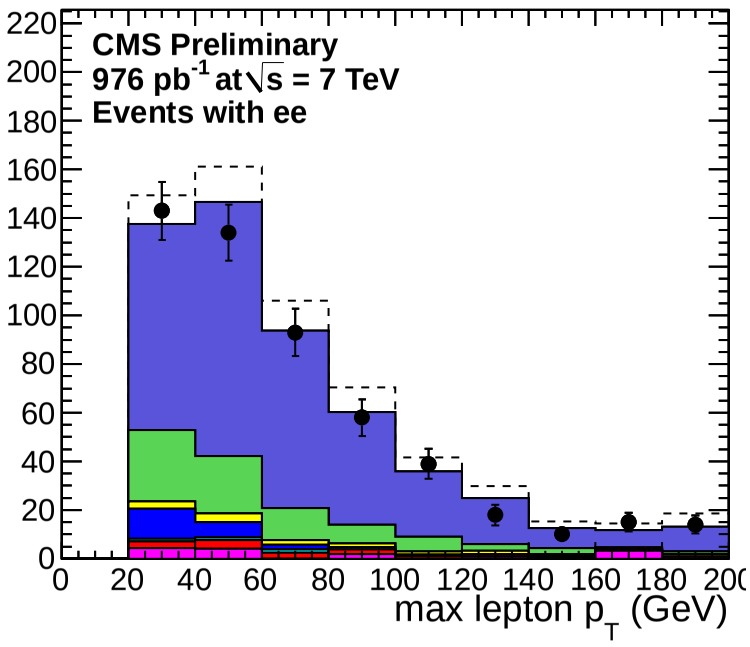
CMS Preliminary
976 pb-1 at √s = 7 TeV
Events with ee
max lepton pT (GeV)

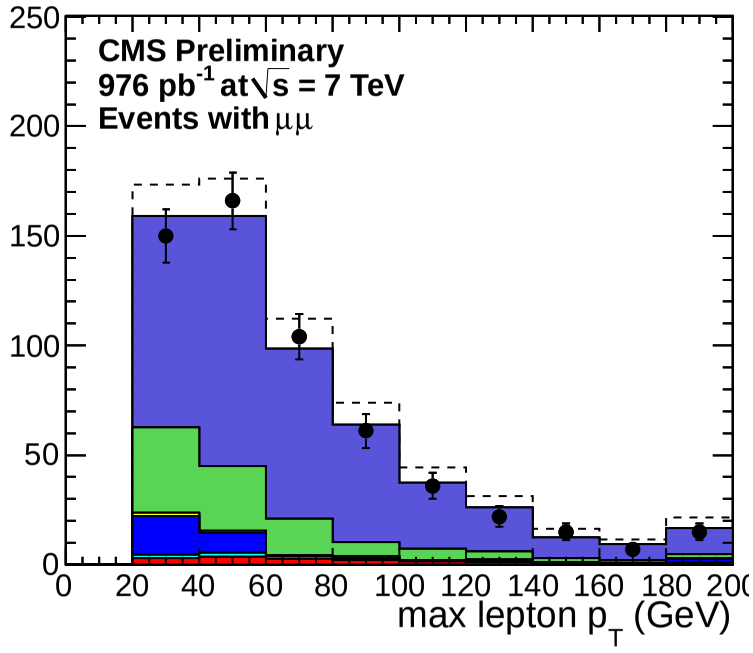
CMS Preliminary
976 pb-1 at √s = 7 TeV
Events with μμ
max lepton pT (GeV)

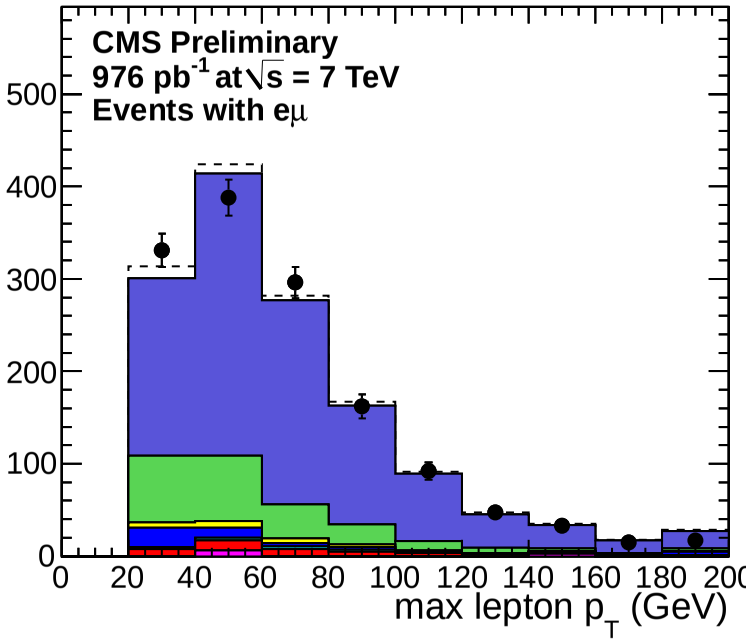
CMS Preliminary
976 pb-1 at √s = 7 TeV
Events with eμ
max lepton pT (GeV)

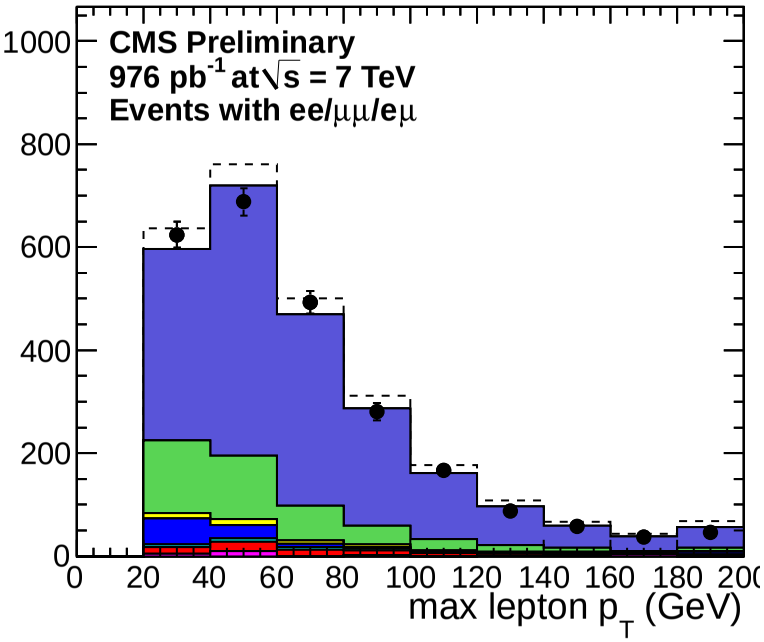
CMS Preliminary
976 pb-1 at √s = 7 TeV
Events with ee/μμ/eμ
max lepton pT (GeV)

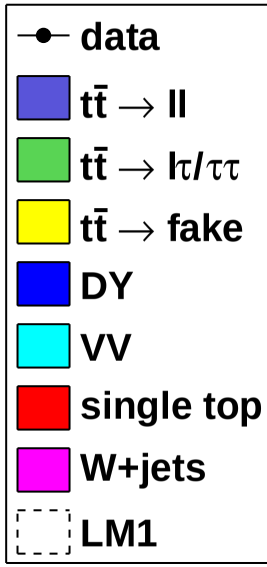
data
tt̄ → ll
tt̄ → lτ/ττ
tt̄ → fake
DY
VV
single top
W+jets
LM1

652

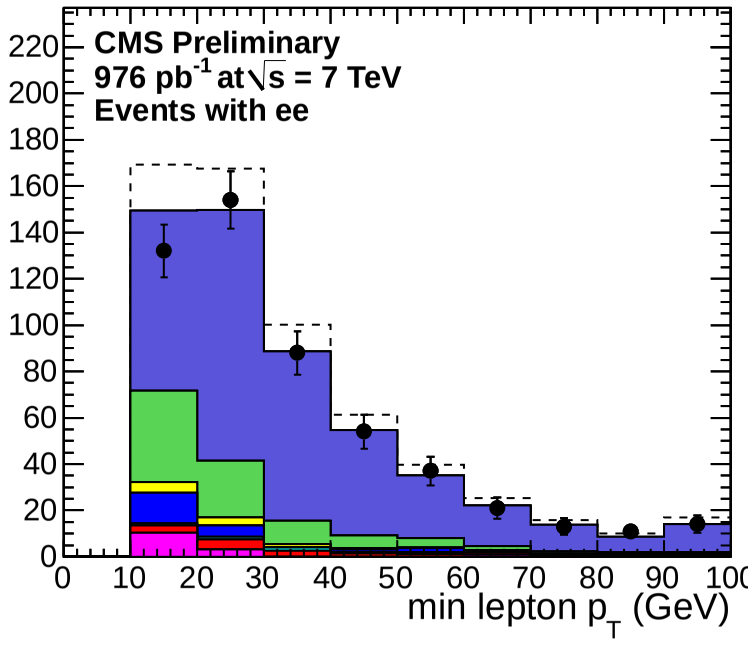
CMS Preliminary
976 pb-1 at √s = 7 TeV
Events with ee
min lepton pT (GeV)

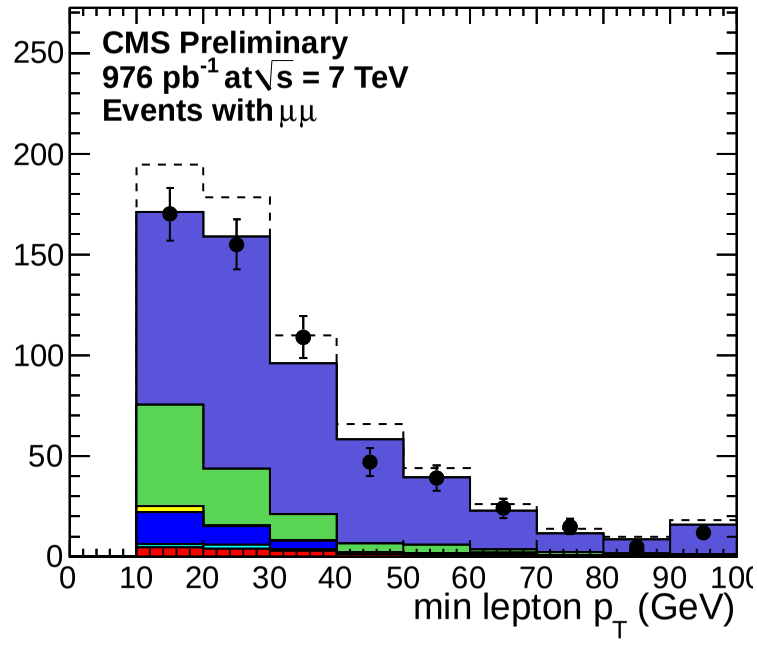
CMS Preliminary
976 pb-1 at √s = 7 TeV
Events with μμ
min lepton pT (GeV)

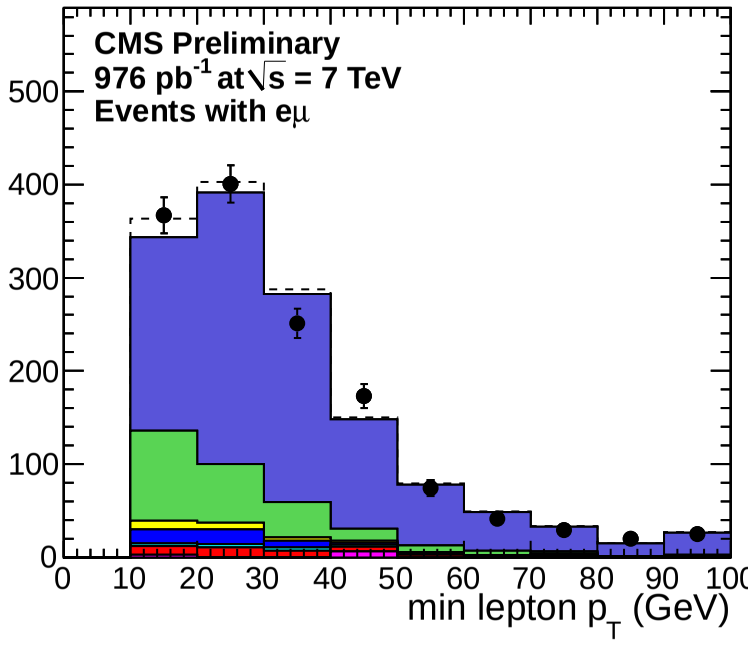
CMS Preliminary
976 pb-1 at √s = 7 TeV
Events with eμ
min lepton pT (GeV)

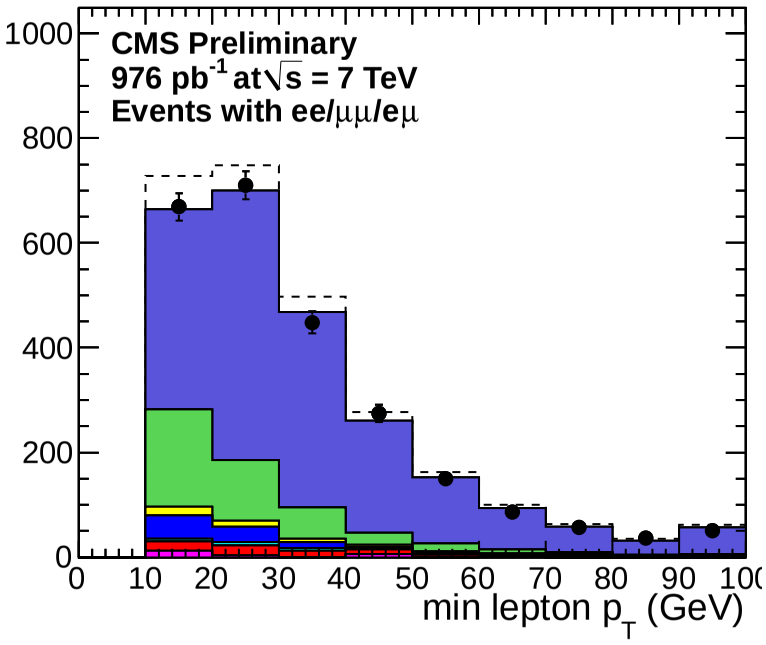
CMS Preliminary
976 pb-1 at √s = 7 TeV
Events with ee/μμ/eμ
min lepton pT (GeV)

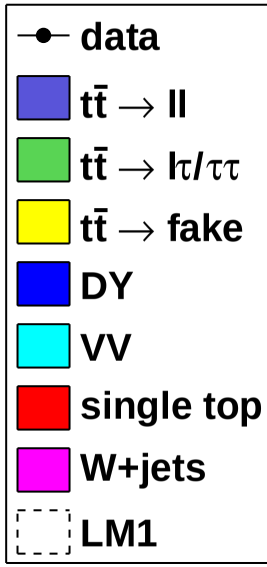
data
tt̄ → ll
tt̄ → lτ/ττ
tt̄ → fake
DY
VV
single top
W+jets
LM1

653

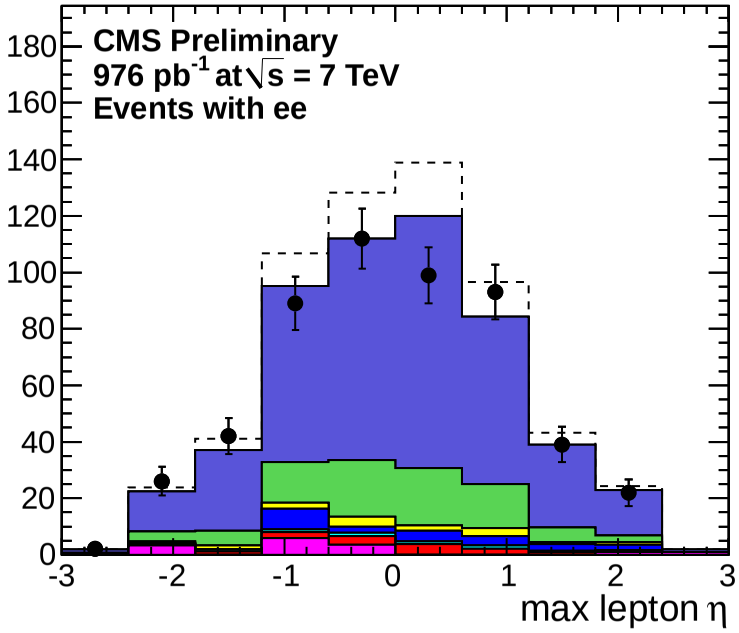
CMS Preliminary
976 pb-1 at √s = 7 TeV
Events with ee
max lepton η

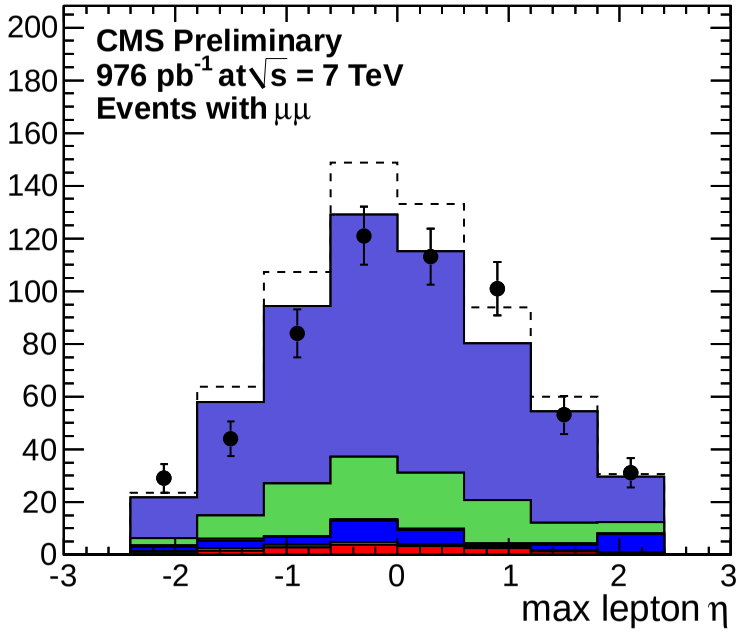
CMS Preliminary
976 pb-1 at √s = 7 TeV
Events with μμ
max lepton η

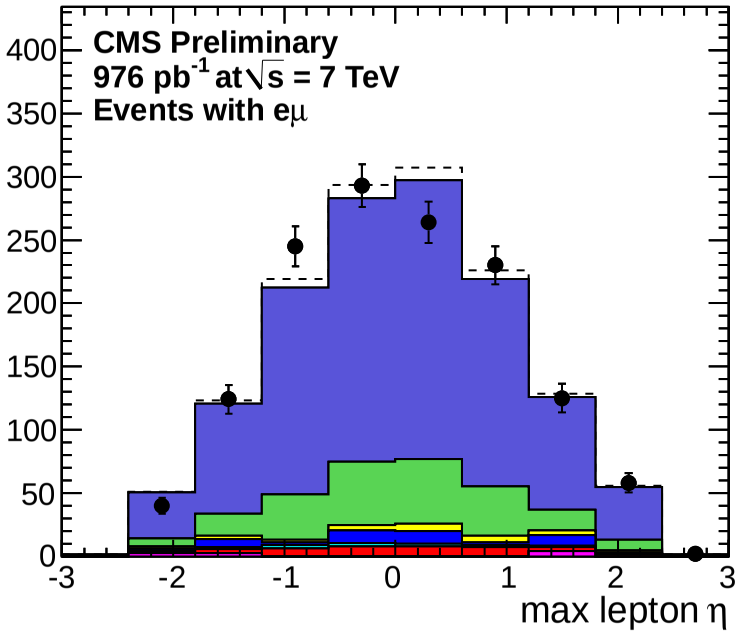
CMS Preliminary
976 pb-1 at √s = 7 TeV
Events with eμ
max lepton η

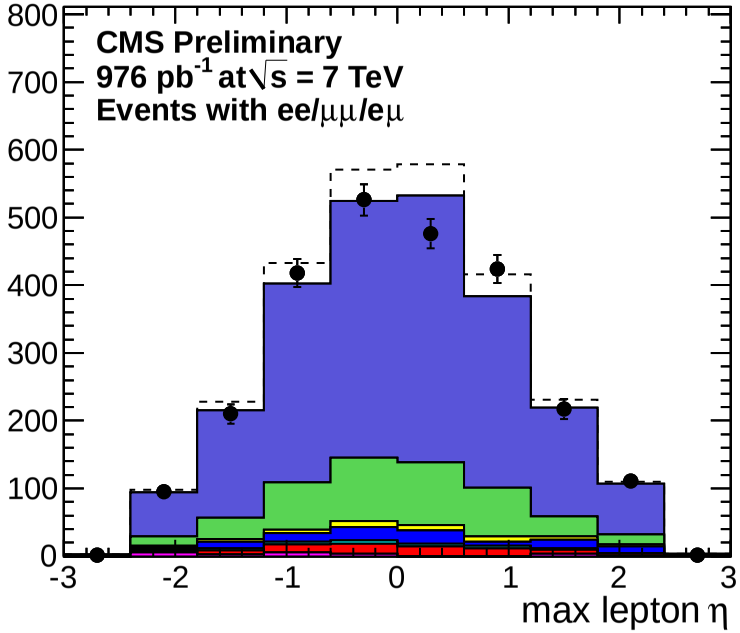
CMS Preliminary
976 pb-1 at √s = 7 TeV
Events with ee/μμ/eμ
max lepton η

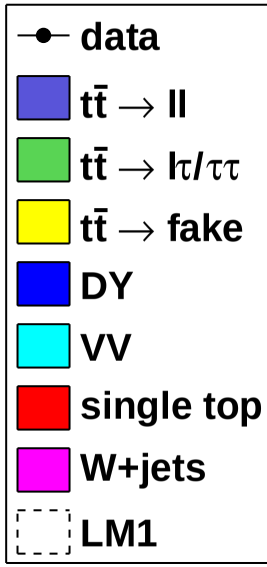
data
tt̄ → ll
tt̄ → lτ/ττ
tt̄ → fake
DY
VV
single top
W+jets
LM1

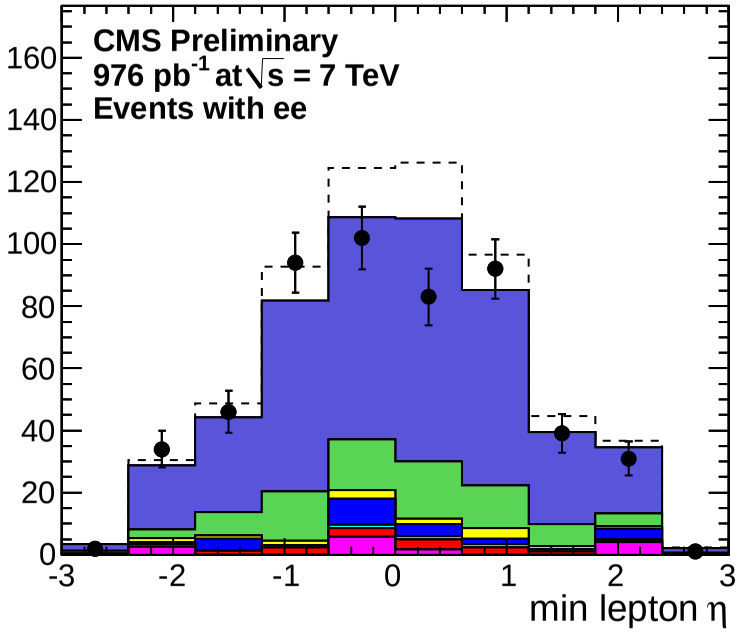
CMS Preliminary
976 pb-1 at √s = 7 TeV
Events with ee
min lepton η

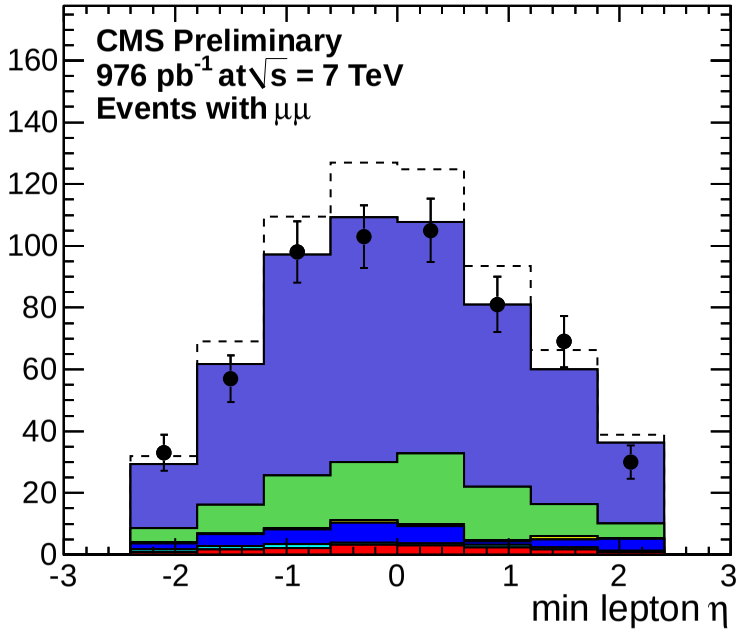
CMS Preliminary
976 pb-1 at √s = 7 TeV
Events with μμ
min lepton η

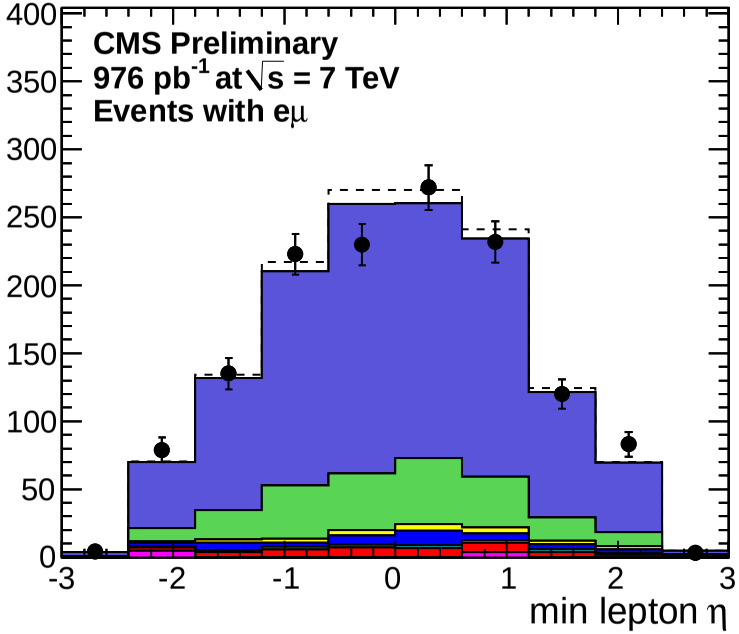
CMS Preliminary
976 pb-1 at √s = 7 TeV
Events with eμ
min lepton η

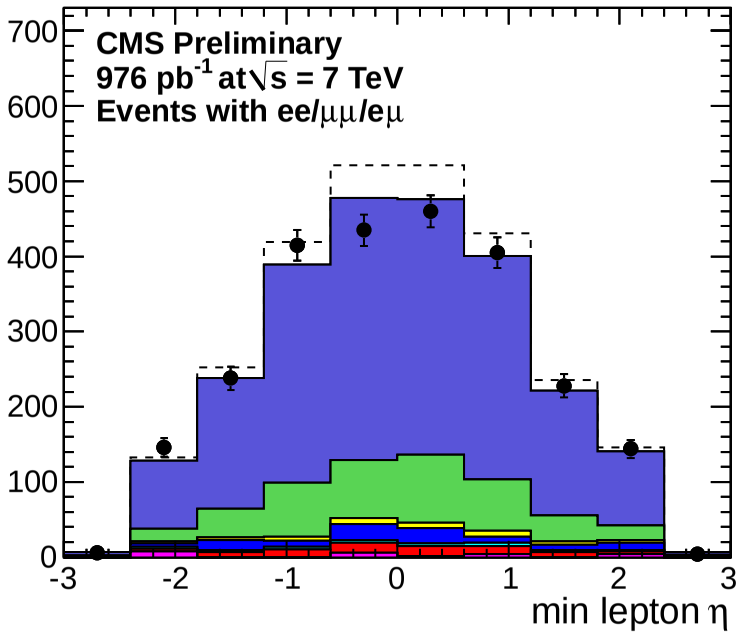
CMS Preliminary
976 pb-1 at √s = 7 TeV
Events with ee/μμ/eμ
min lepton η

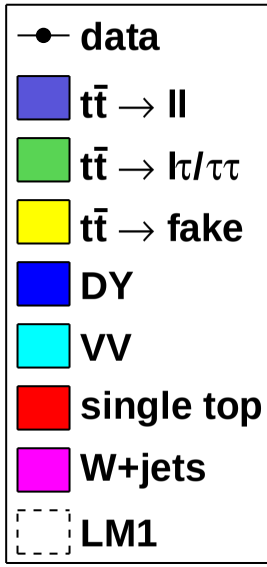
data
tt̄ → ll
tt̄ → lτ/ττ
tt̄ → fake
DY
VV
single top
W+jets
LM1

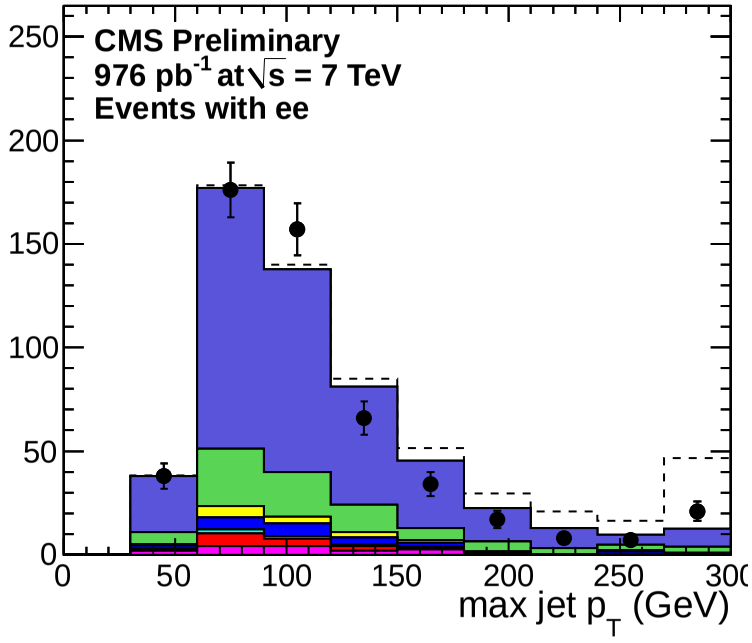
CMS Preliminary
976 pb-1 at √s = 7 TeV
Events with ee
max jet pT (GeV)

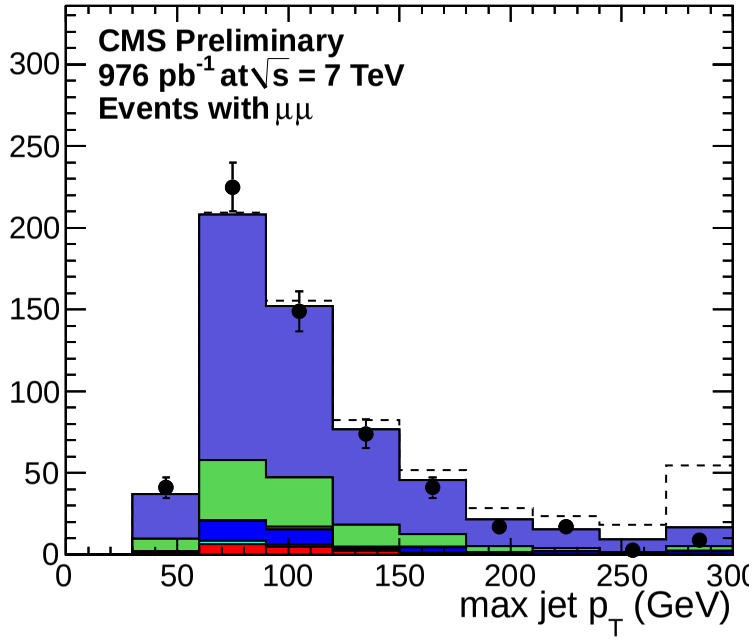
CMS Preliminary
976 pb-1 at √s = 7 TeV
Events with μμ
max jet pT (GeV)

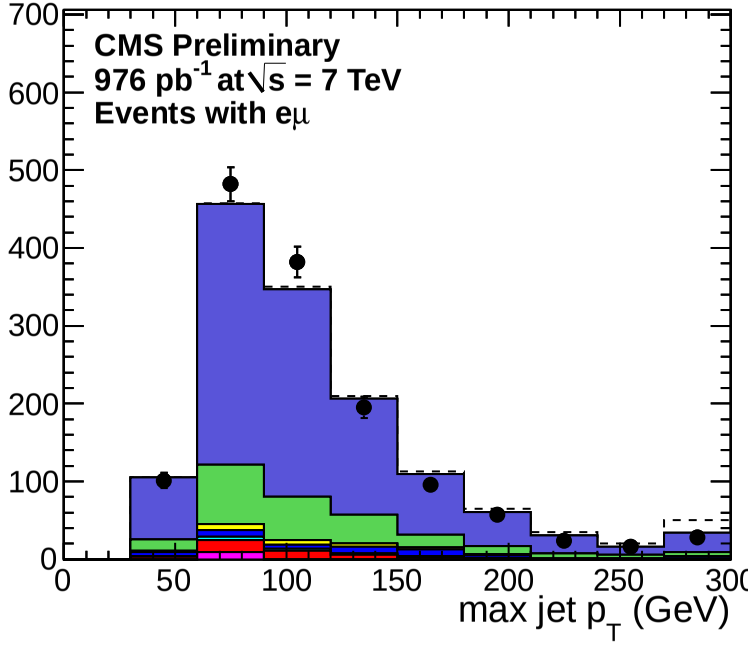
CMS Preliminary
976 pb-1 at √s = 7 TeV
Events with eμ
max jet pT (GeV)

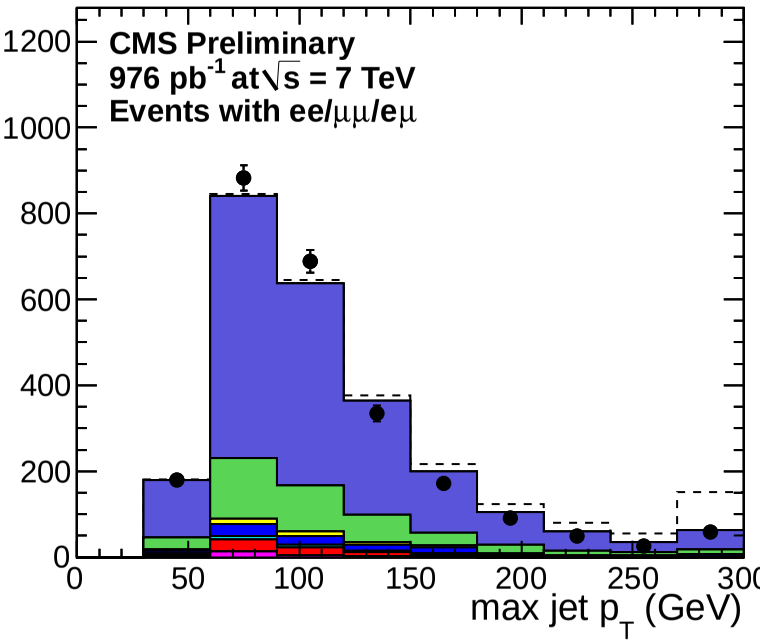
CMS Preliminary
976 pb-1 at √s = 7 TeV
Events with ee/μμ/eμ
max jet pT (GeV)

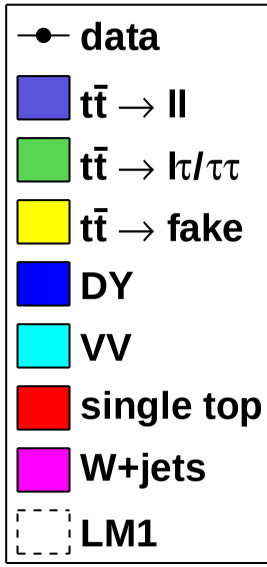
data
tt̄ → ll
tt̄ → lτ/ττ
tt̄ → fake
DY
VV
single top
W+jets
LM1

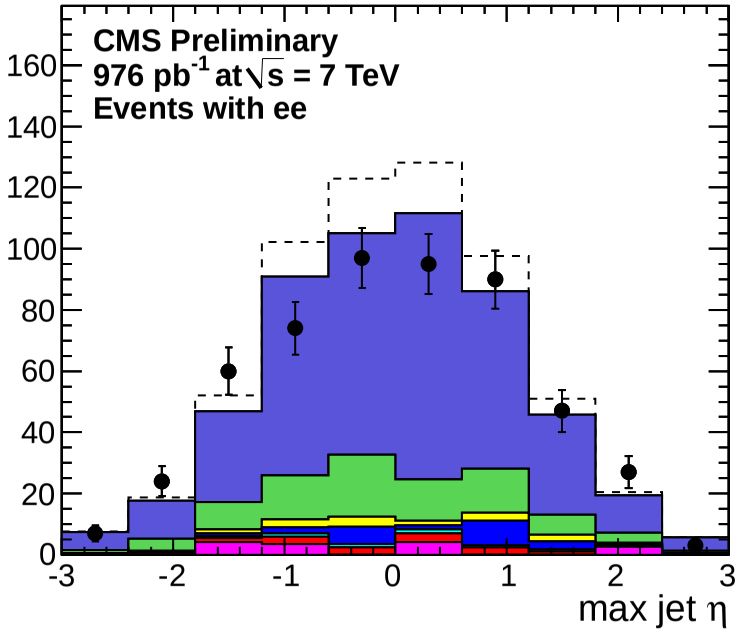
CMS Preliminary
976 pb-1 at √s = 7 TeV
Events with ee
max jet η

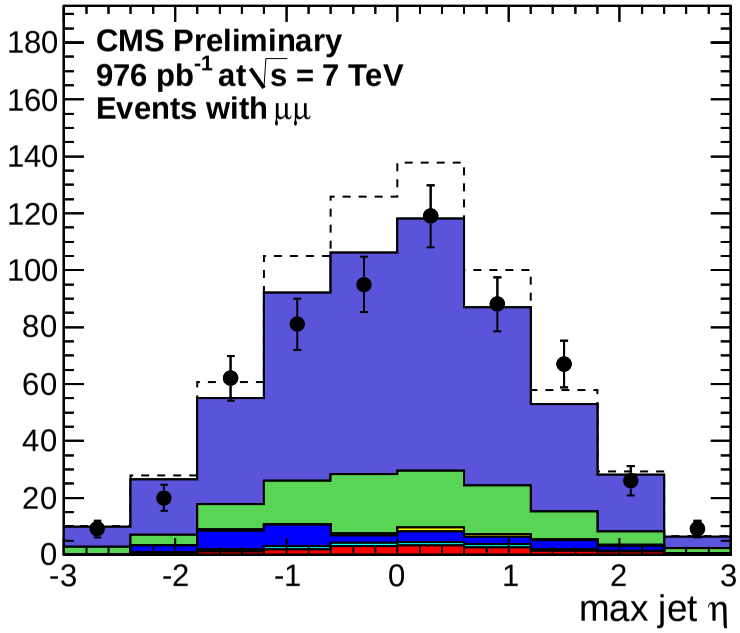
CMS Preliminary
976 pb-1 at √s = 7 TeV
Events with μμ
max jet η

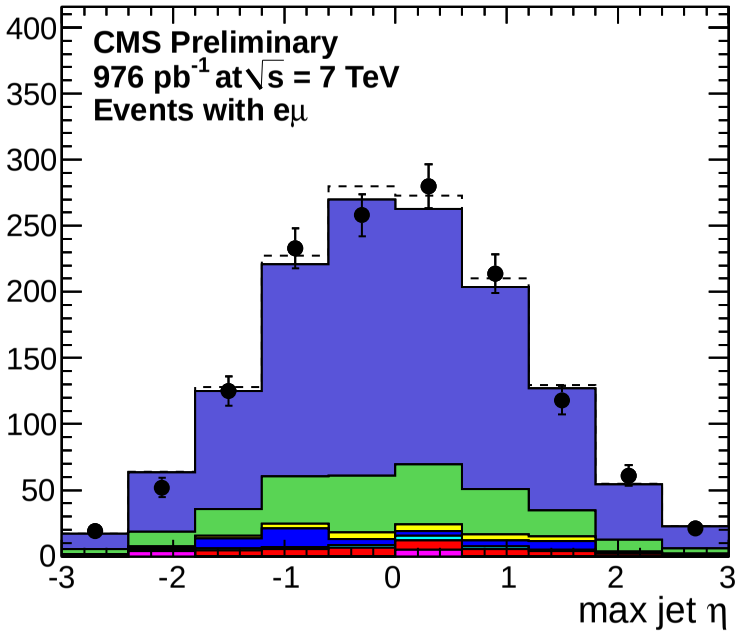
CMS Preliminary
976 pb-1 at √s = 7 TeV
Events with eμ
max jet η

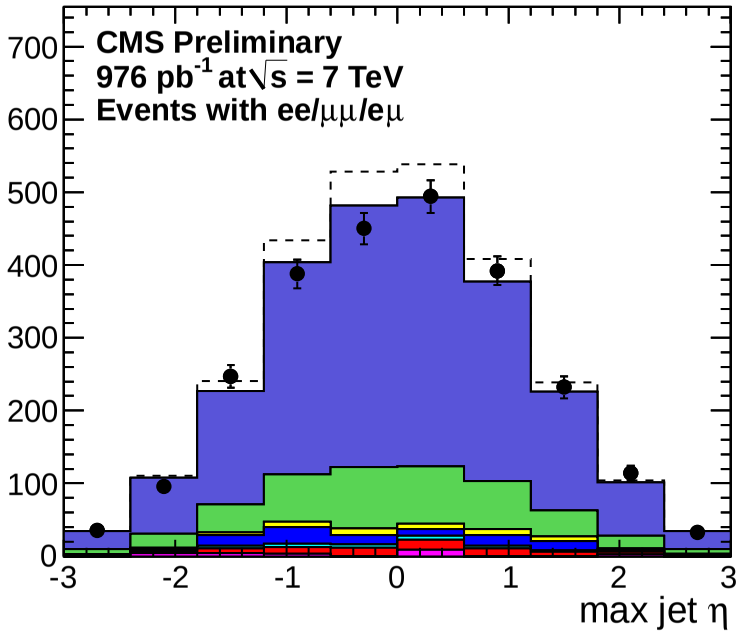
CMS Preliminary
976 pb-1 at √s = 7 TeV
Events with ee/μμ/eμ
max jet η

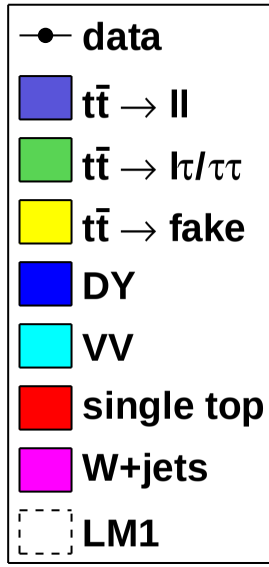
data
tt̄ → ll
tt̄ → lτ/ττ
tt̄ → fake
DY
VV
single top
W+jets
LM1

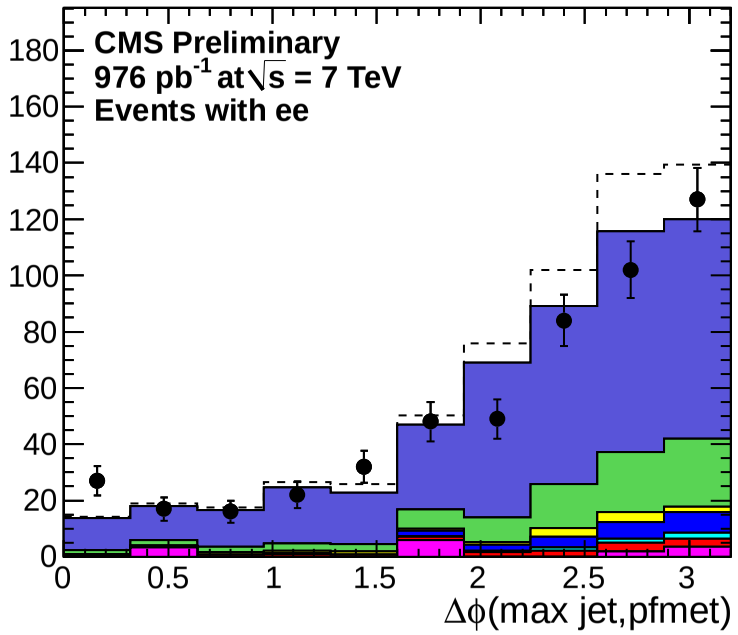
CMS Preliminary
976 pb-1 at √s = 7 TeV
Events with ee
Δφ(max jet,pfmet)

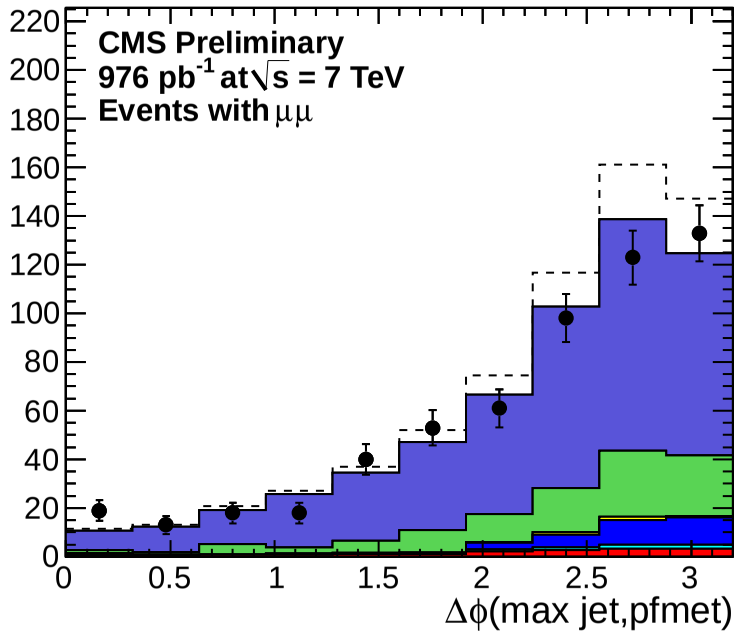
CMS Preliminary
976 pb-1 at √s = 7 TeV
Events with μμ
Δφ(max jet,pfmet)

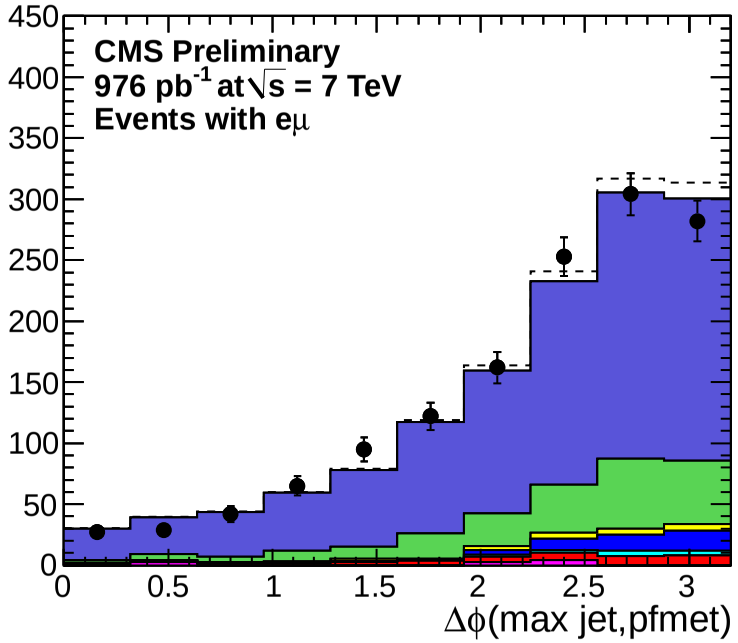
CMS Preliminary
976 pb-1 at √s = 7 TeV
Events with eμ
Δφ(max jet,pfmet)

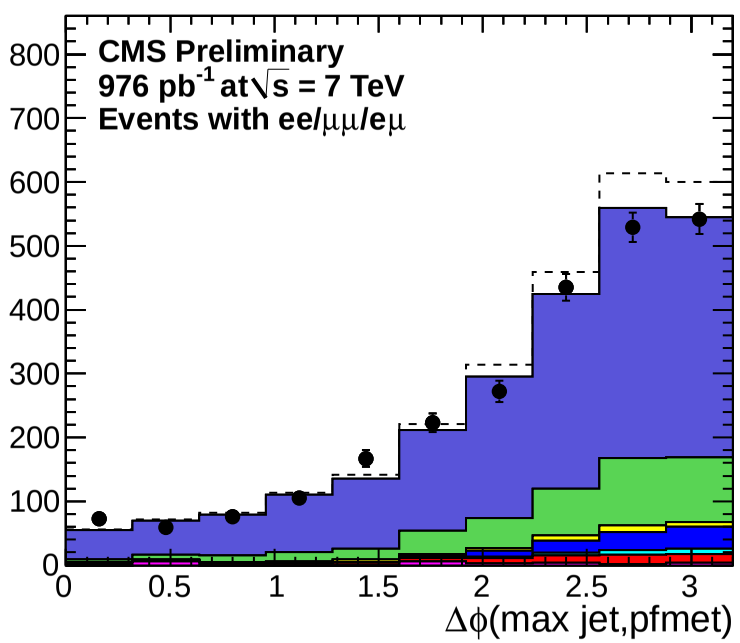
CMS Preliminary
976 pb-1 at √s = 7 TeV
Events with ee/μμ/eμ
Δφ(max jet,pfmet)

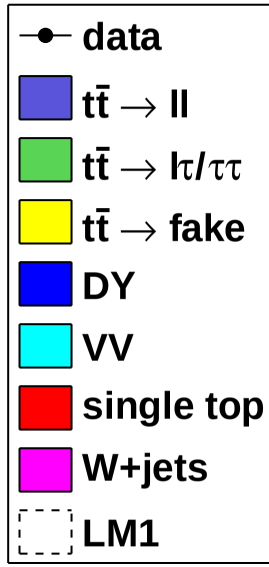
data
tt̄ → ll
tt̄ → lτ/ττ
tt̄ → fake
DY
VV
single top
W+jets
LM1

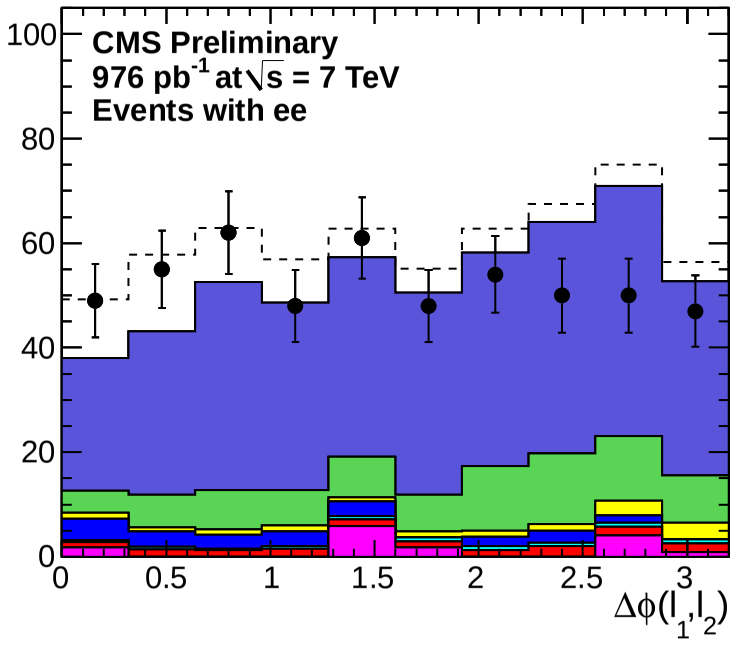
CMS Preliminary
976 pb-1 at √s = 7 TeV
Events with ee
Δφ(l1,l2)

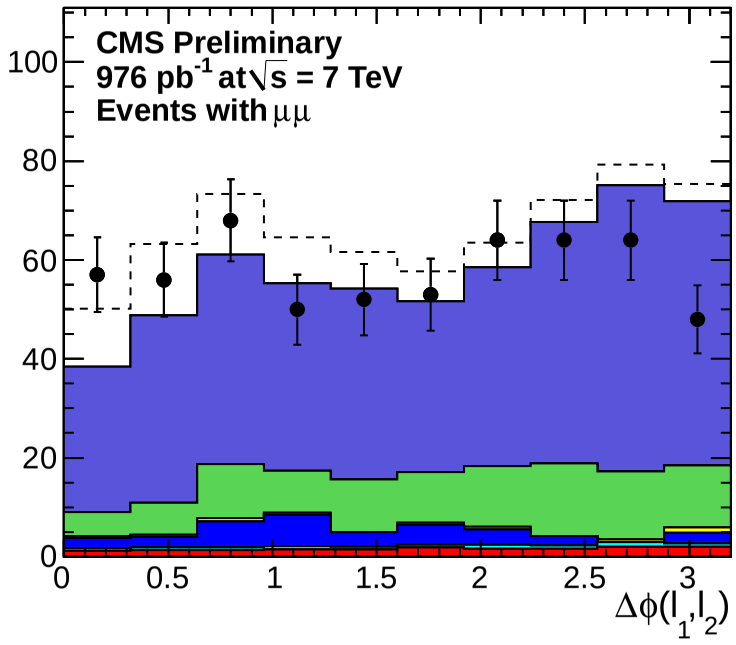
CMS Preliminary
976 pb-1 at √s = 7 TeV
Events with μμ
Δφ(l1,l2)

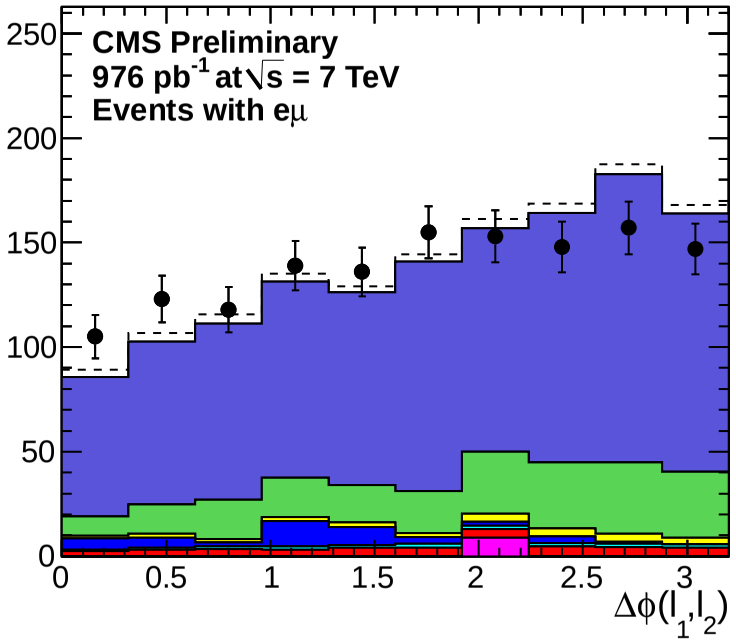
CMS Preliminary
976 pb-1 at √s = 7 TeV
Events with eμ
Δφ(l1,l2)

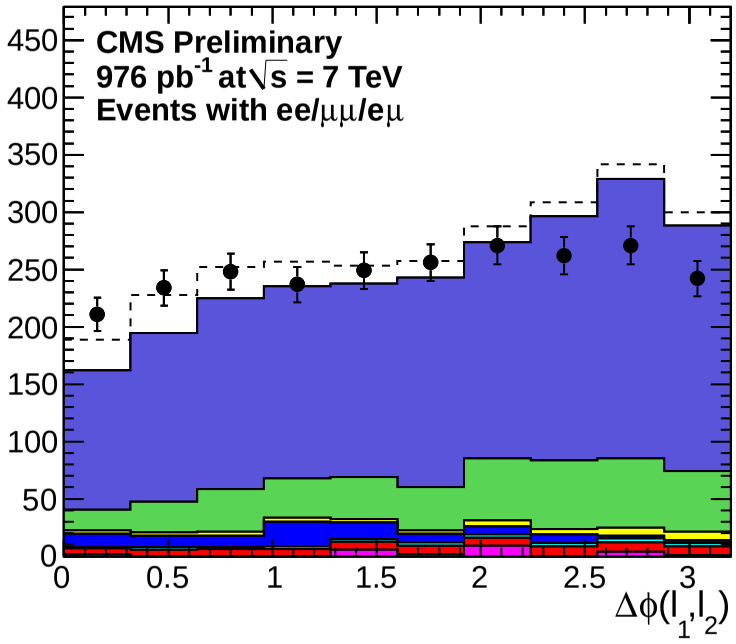
CMS Preliminary
976 pb-1 at √s = 7 TeV
Events with ee/μμ/eμ
Δφ(l1,l2)

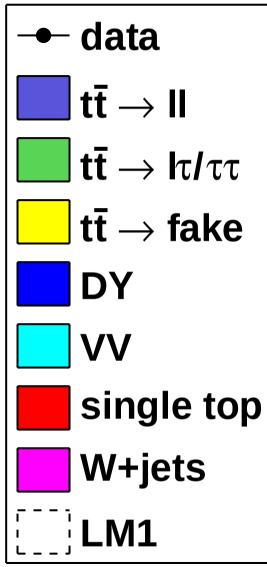
data
tt̄ → ll
tt̄ → lτ/ττ
tt̄ → fake
DY
VV
single top
W+jets
LM1

659

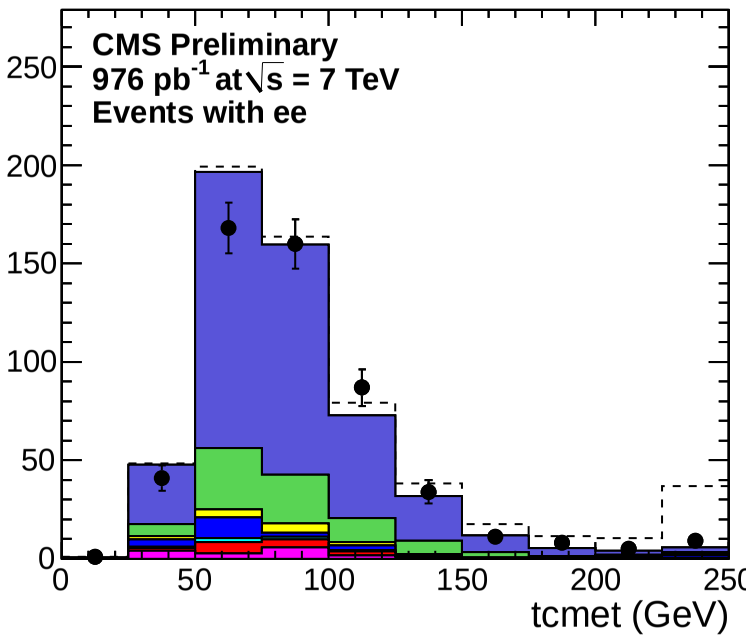
CMS Preliminary
976 pb-1 at √s = 7 TeV
Events with ee
tcmet (GeV)

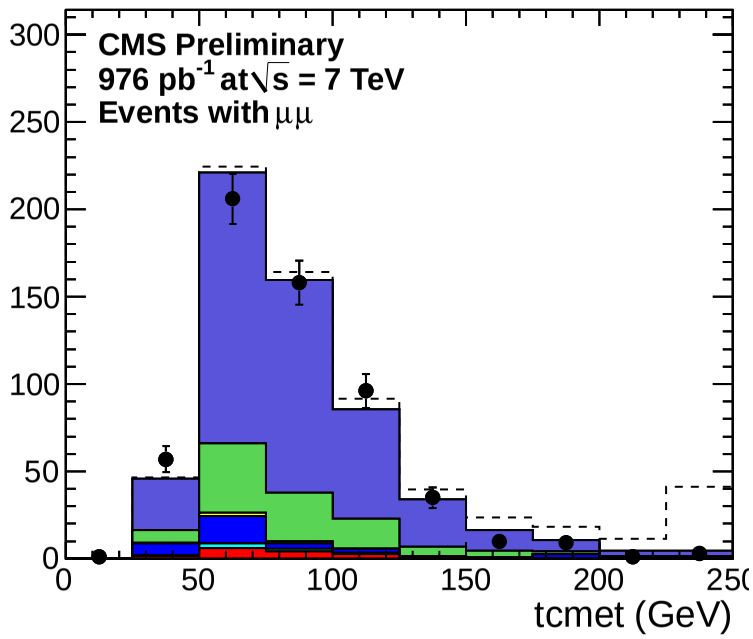
CMS Preliminary
976 pb-1 at √s = 7 TeV
Events with μμ
tcmet (GeV)

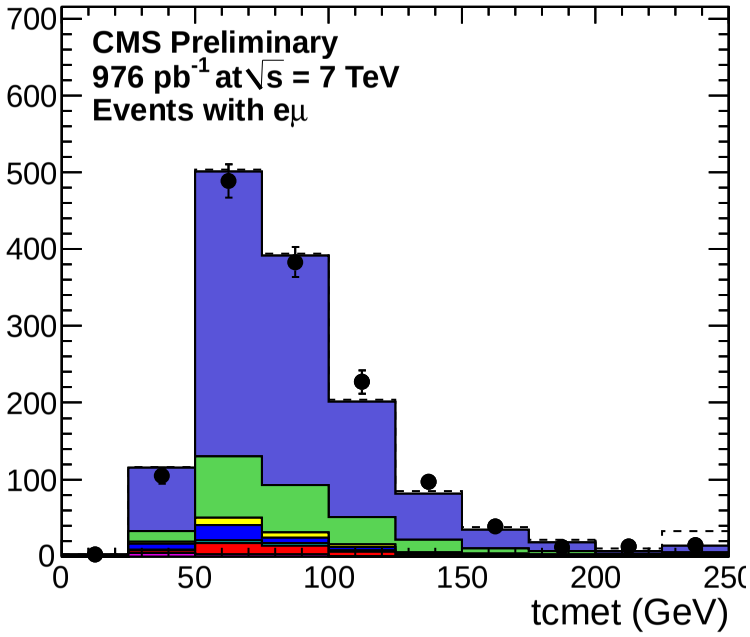
CMS Preliminary
976 pb-1 at √s = 7 TeV
Events with eμ
tcmet (GeV)

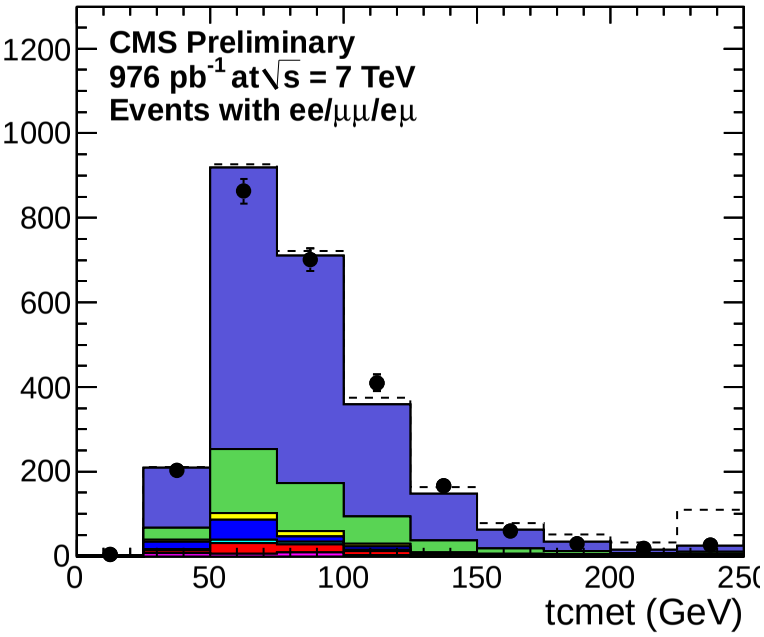
CMS Preliminary
976 pb-1 at √s = 7 TeV
Events with ee/μμ/eμ
tcmet (GeV)

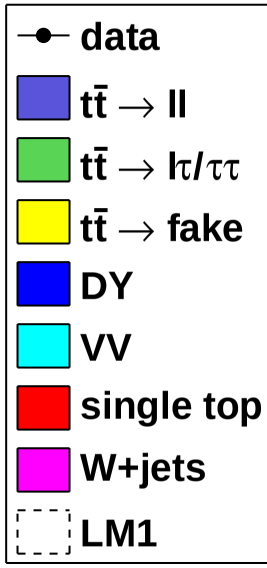
data
tt̄ → ll
tt̄ → lτ/ττ
tt̄ → fake
DY
VV
single top
W+jets
LM1

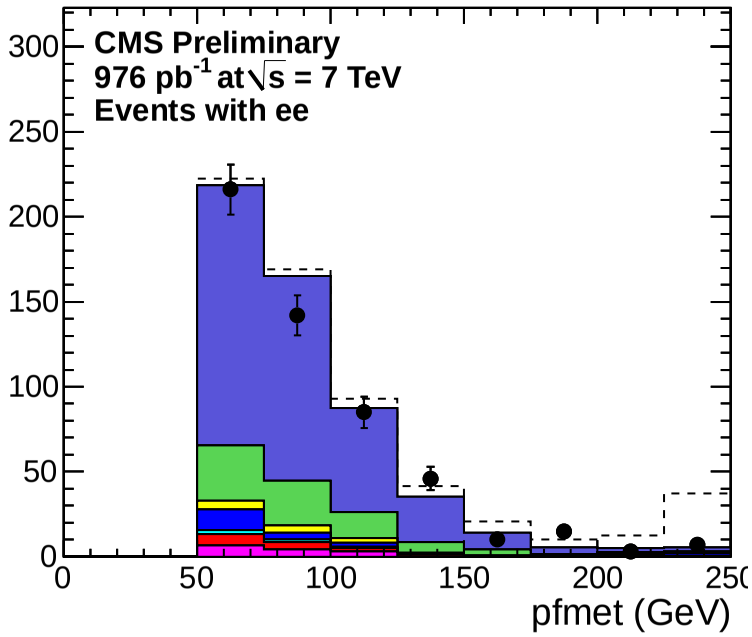
CMS Preliminary
976 pb-1 at √s = 7 TeV
Events with ee
pfmet (GeV)

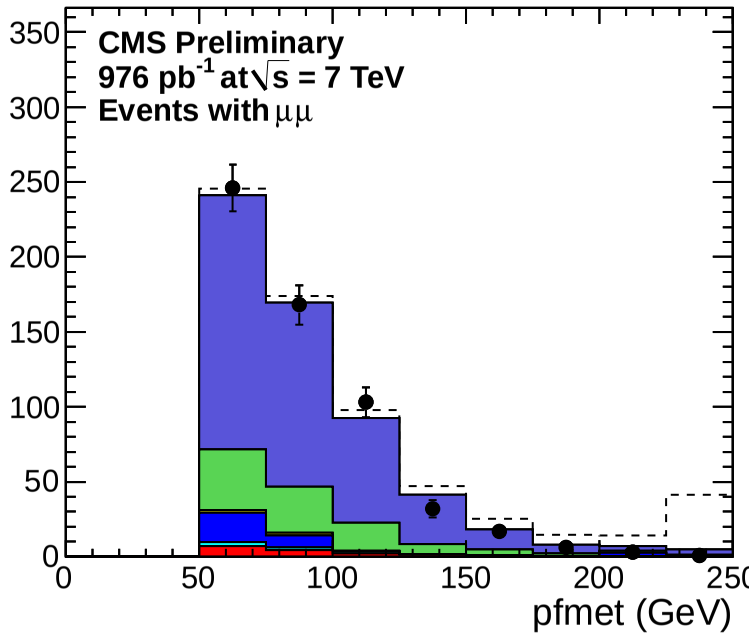
CMS Preliminary
976 pb-1 at √s = 7 TeV
Events with μμ
pfmet (GeV)

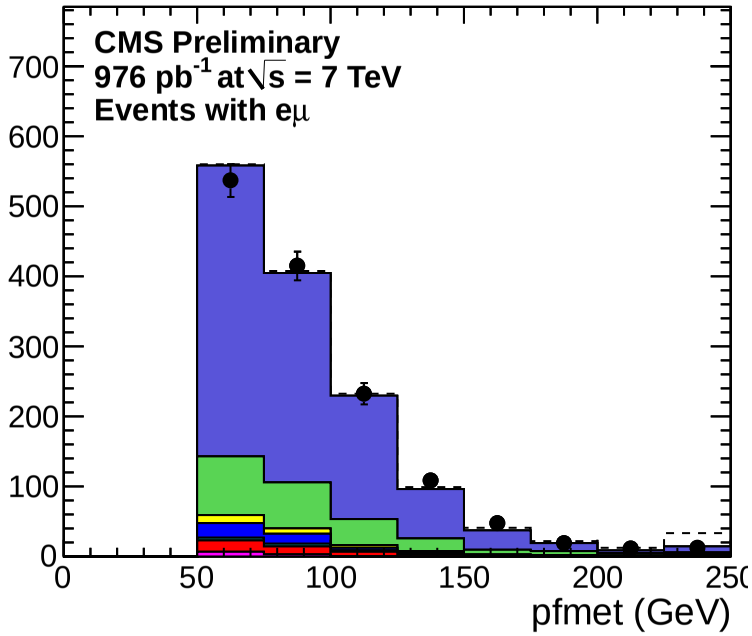
CMS Preliminary
976 pb-1 at √s = 7 TeV
Events with eμ
pfmet (GeV)

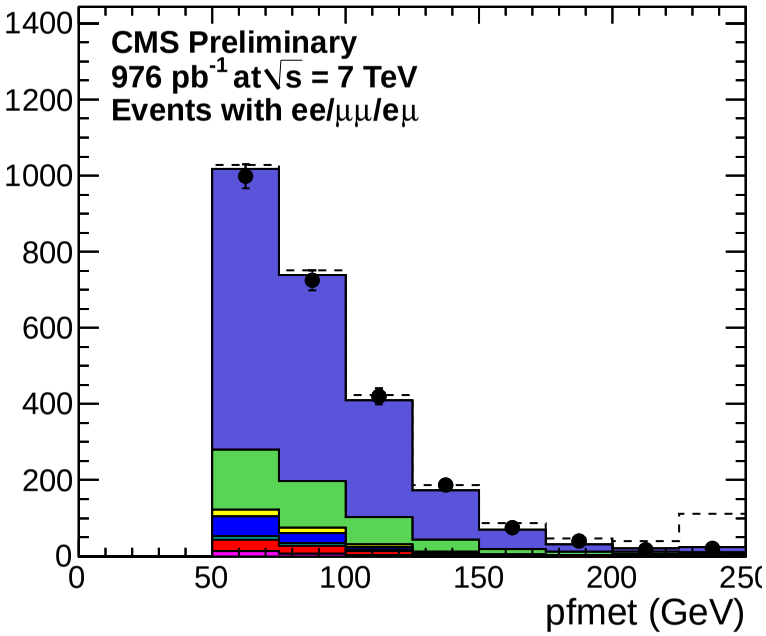
CMS Preliminary
976 pb-1 at √s = 7 TeV
Events with ee/μμ/eμ
pfmet (GeV)

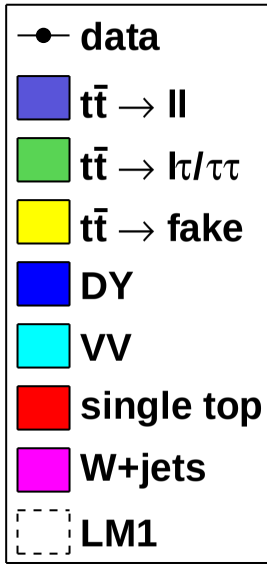
data
tt̄ → ll
tt̄ → lτ/ττ
tt̄ → fake
DY
VV
single top
W+jets
LM1

661

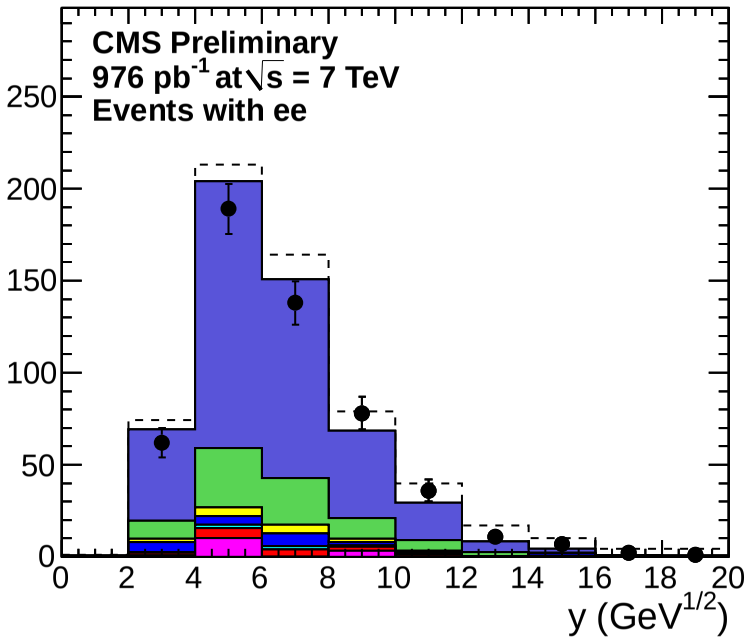
CMS Preliminary
976 pb-1 at √s = 7 TeV
Events with ee
y (GeV1/2)

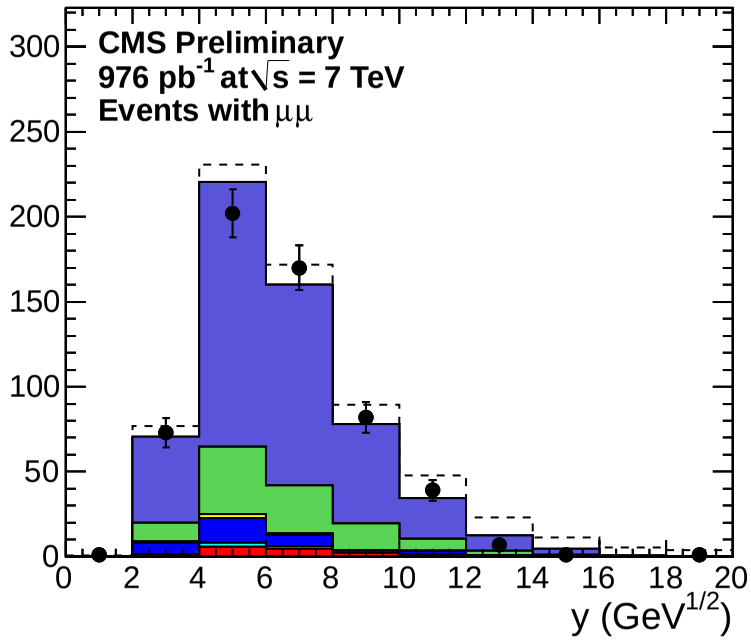
CMS Preliminary
976 pb-1 at √s = 7 TeV
Events with μμ
y (GeV1/2)

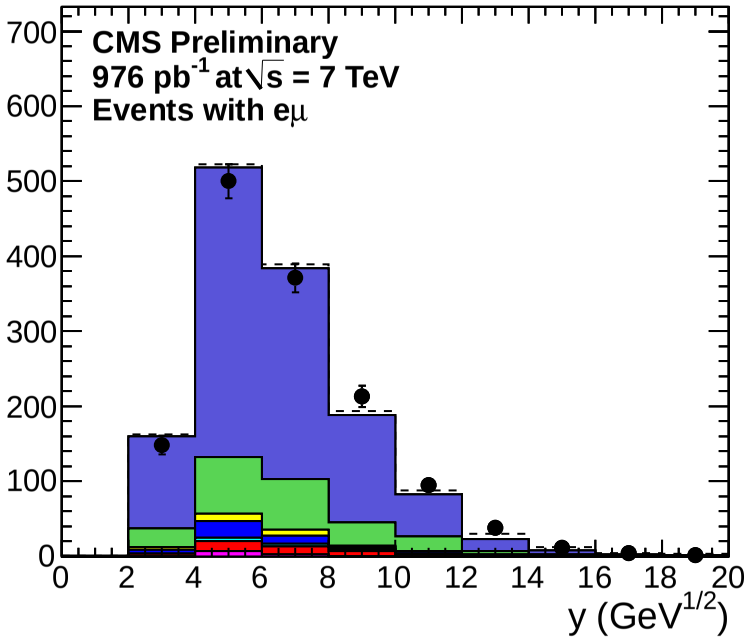
CMS Preliminary
976 pb-1 at √s = 7 TeV
Events with eμ
y (GeV1/2)

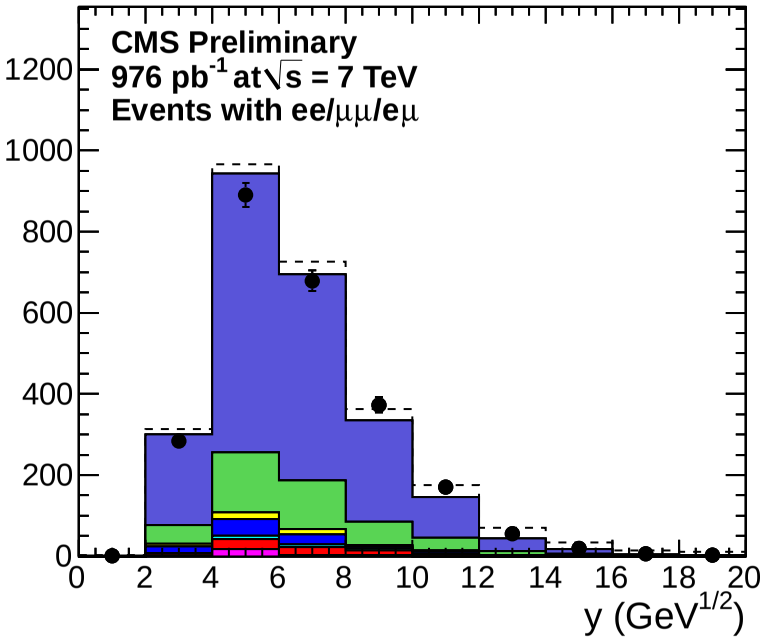
CMS Preliminary
976 pb-1 at √s = 7 TeV
Events with ee/μμ/eμ
y (GeV1/2)

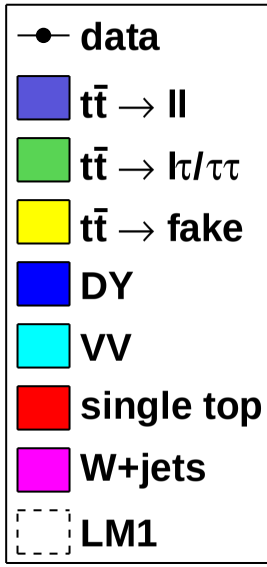
data
tt̄ → ll
tt̄ → lτ/ττ
tt̄ → fake
DY
VV
single top
W+jets
LM1

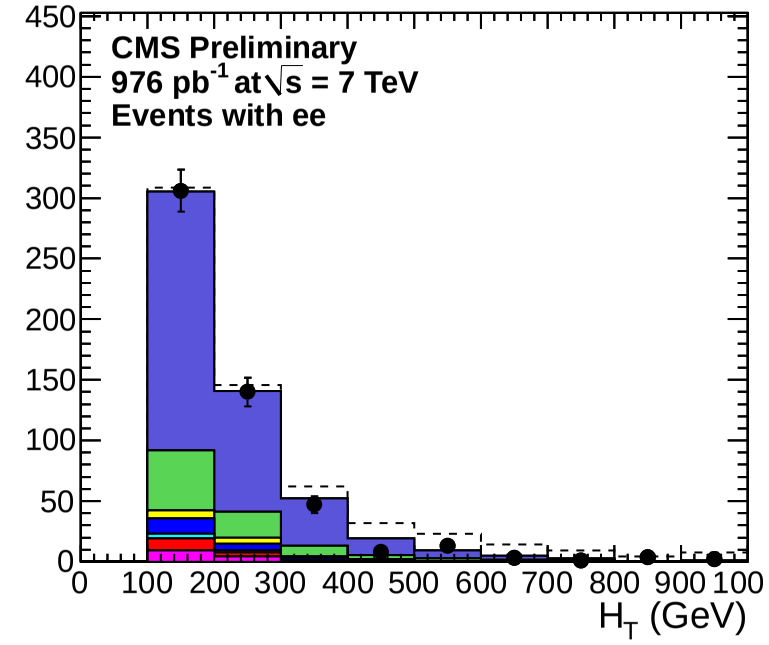
CMS Preliminary
976 pb-1 at √s = 7 TeV
Events with ee
HT (GeV)

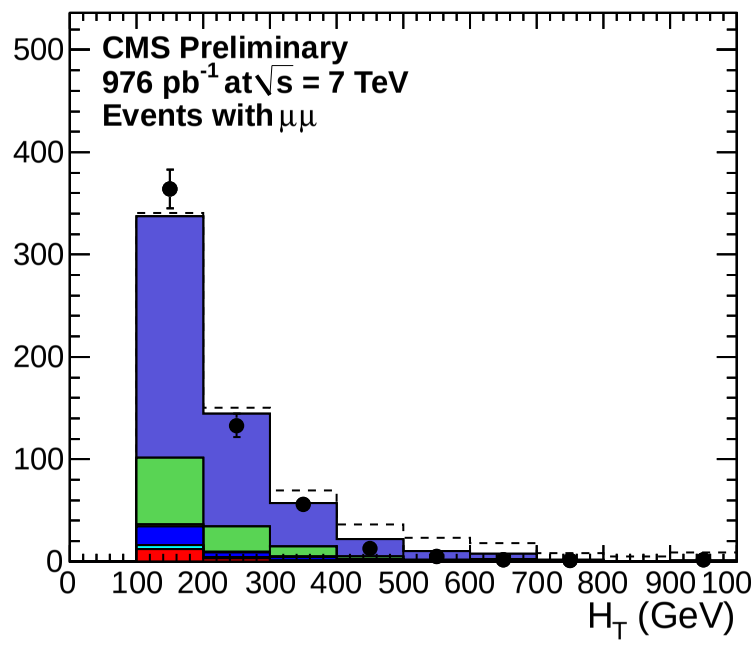
CMS Preliminary
976 pb-1 at √s = 7 TeV
Events with μμ
HT (GeV)

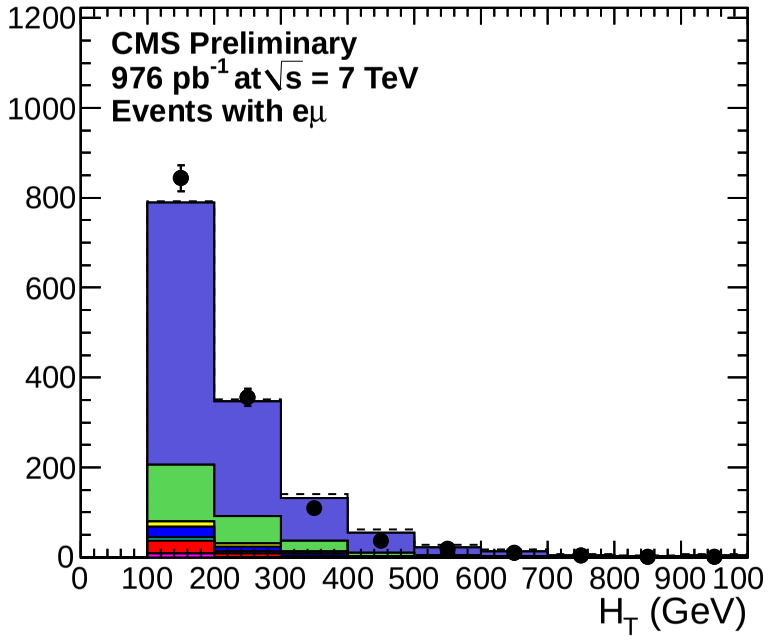
CMS Preliminary
976 pb-1 at √s = 7 TeV
Events with eμ
HT (GeV)

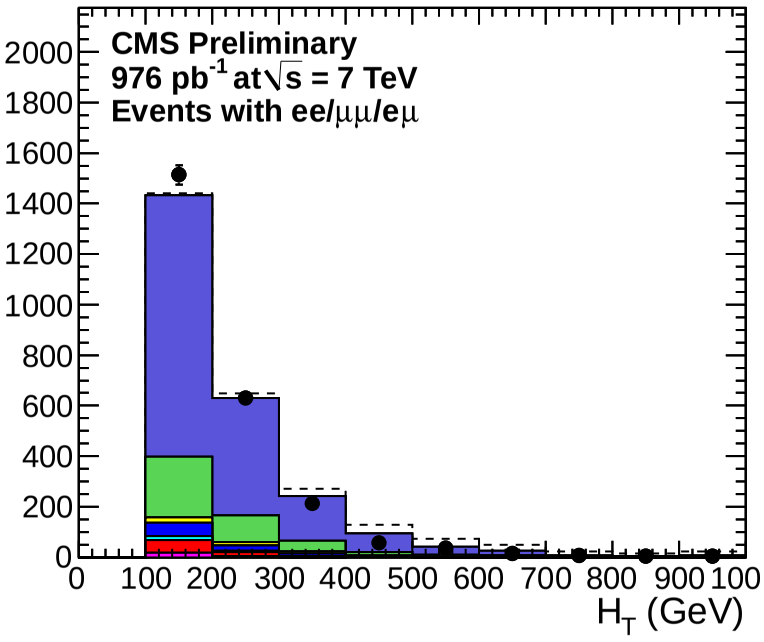
CMS Preliminary
976 pb-1 at √s = 7 TeV
Events with ee/μμ/eμ
HT (GeV)

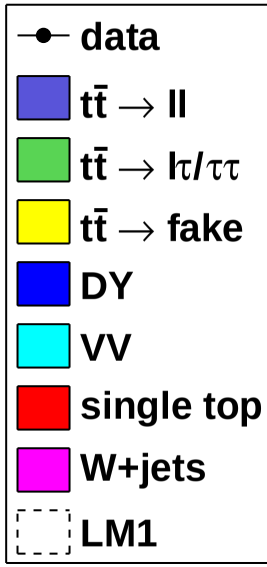
data
tt̄ → ll
tt̄ → lτ/ττ
tt̄ → fake
DY
VV
single top
W+jets
LM1

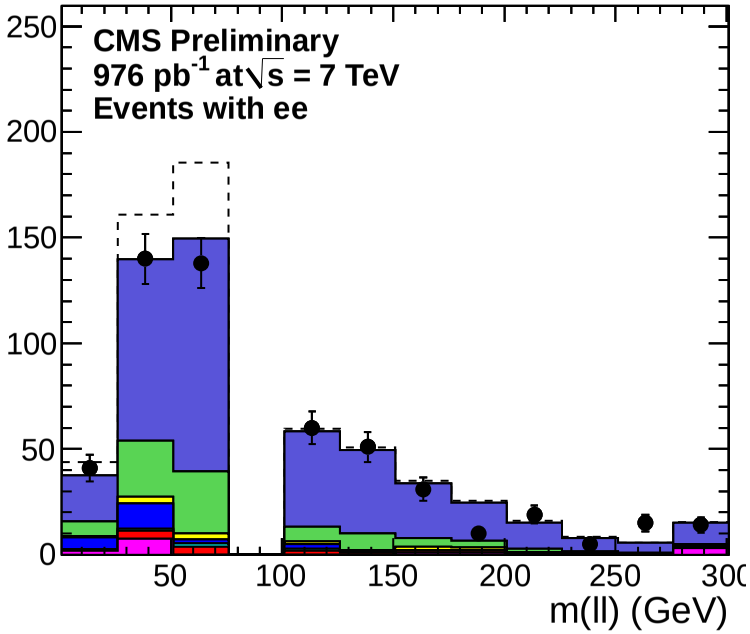
CMS Preliminary
976 pb-1 at √s = 7 TeV
Events with ee
m(ll) (GeV)

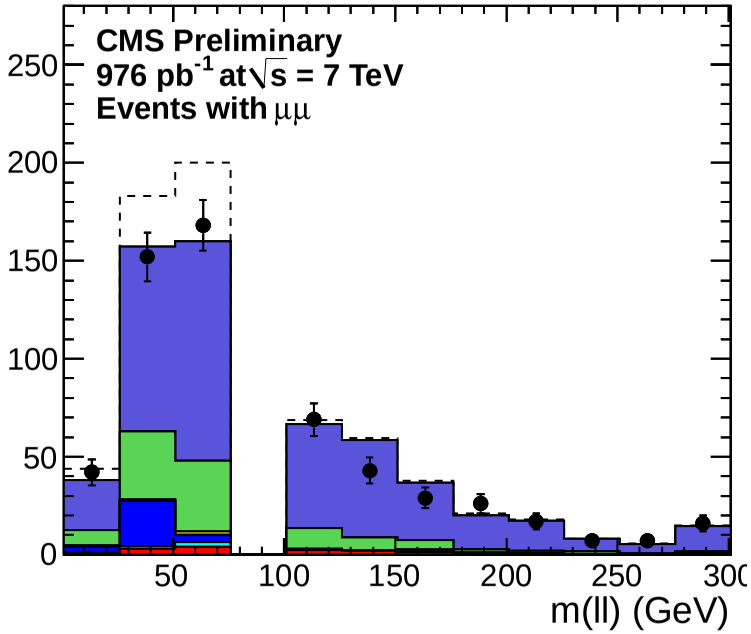
CMS Preliminary
976 pb-1 at √s = 7 TeV
Events with μμ
m(ll) (GeV)

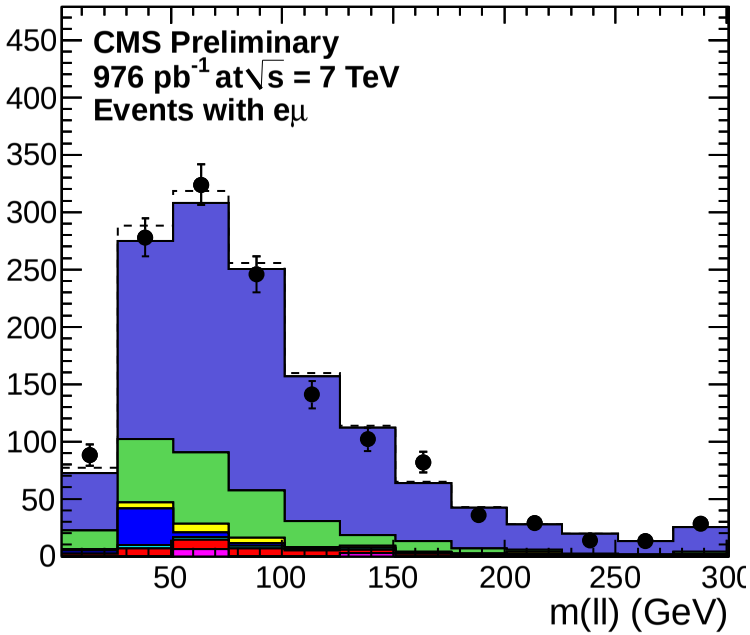
CMS Preliminary
976 pb-1 at √s = 7 TeV
Events with eμ
m(ll) (GeV)

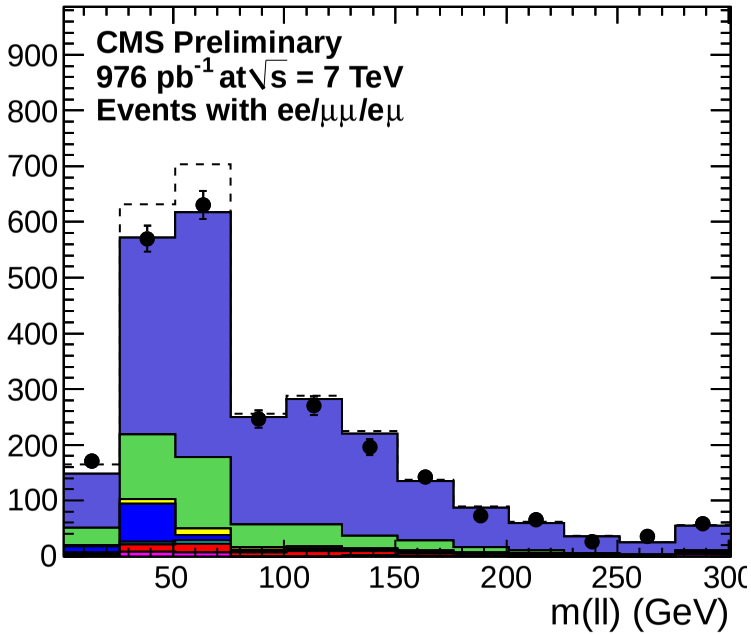
CMS Preliminary
976 pb-1 at √s = 7 TeV
Events with ee/μμ/eμ
m(ll) (GeV)

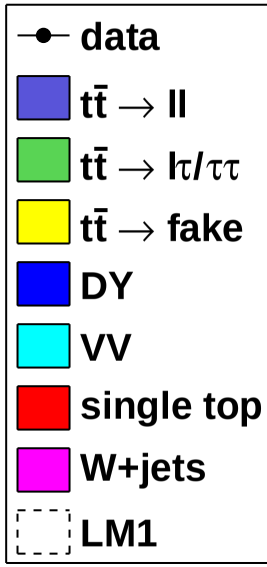
data
tt̄ → ll
tt̄ → lτ/ττ
tt̄ → fake
DY
VV
single top
W+jets
LM1

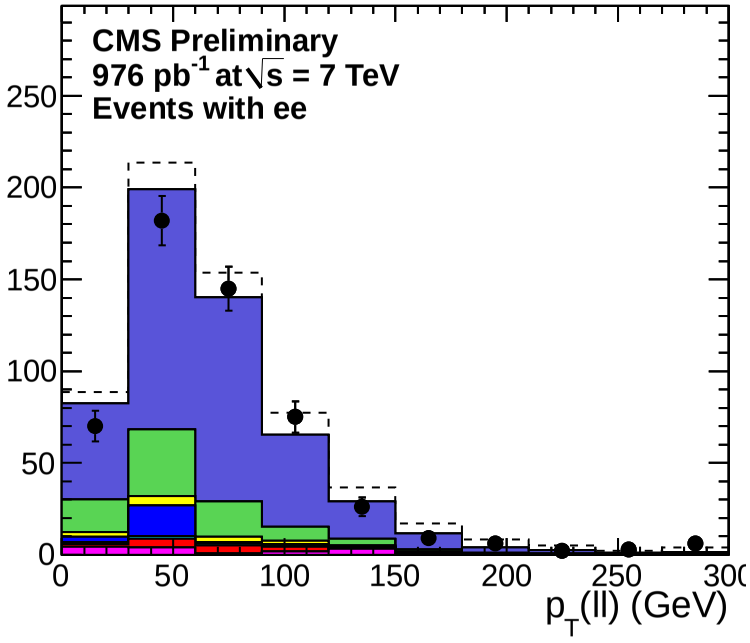
CMS Preliminary
976 pb-1 at √s = 7 TeV
Events with ee
pT(ll) (GeV)

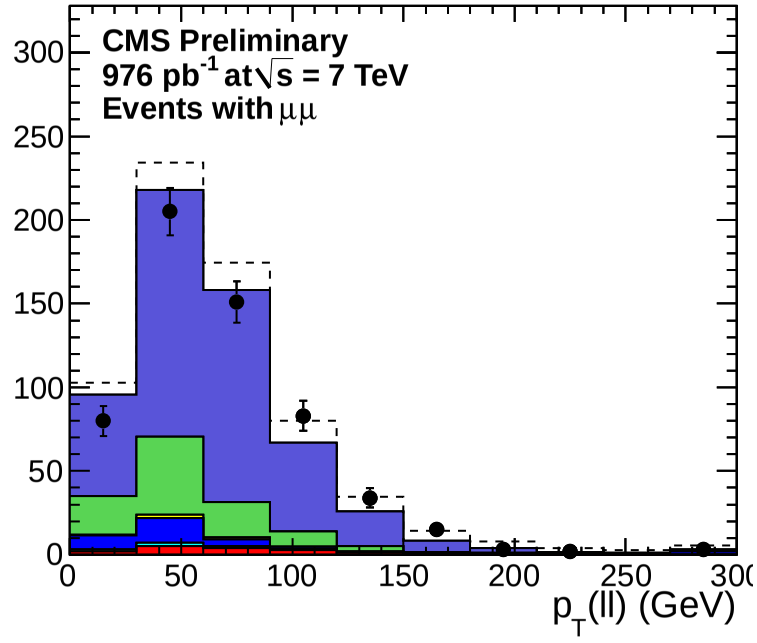
CMS Preliminary
976 pb-1 at √s = 7 TeV
Events with μμ
pT(ll) (GeV)

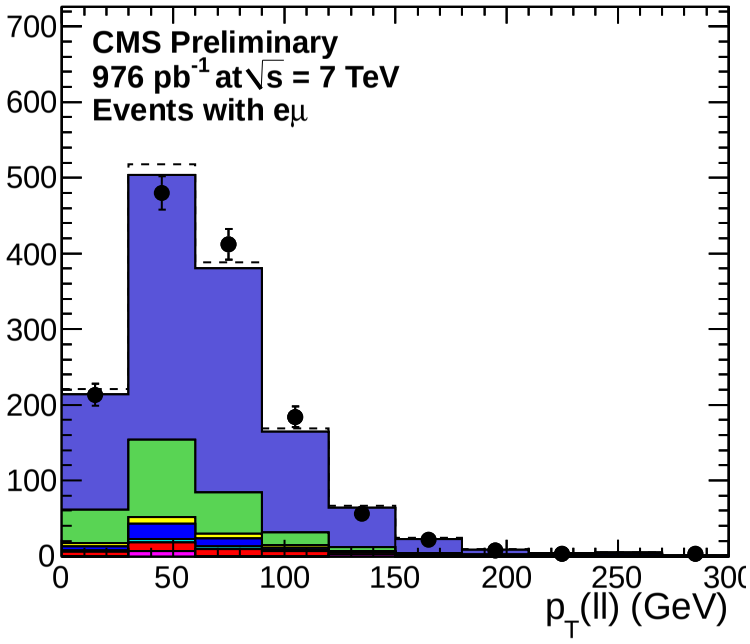
CMS Preliminary
976 pb-1 at √s = 7 TeV
Events with eμ
pT(ll) (GeV)

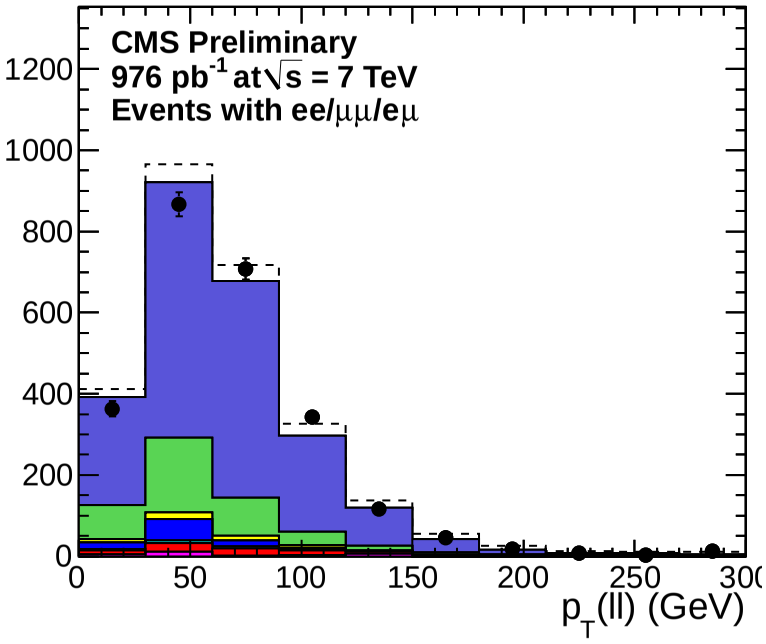
CMS Preliminary
976 pb-1 at √s = 7 TeV
Events with ee/μμ/eμ
pT(ll) (GeV)

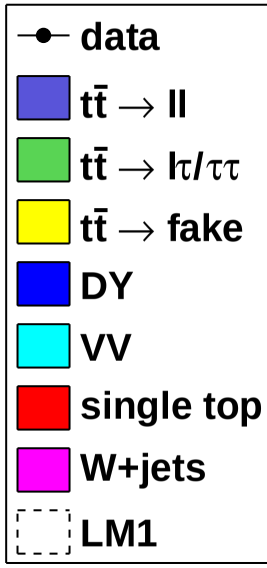
data
tt̄ → ll
tt̄ → lτ/ττ
tt̄ → fake
DY
VV
single top
W+jets
LM1

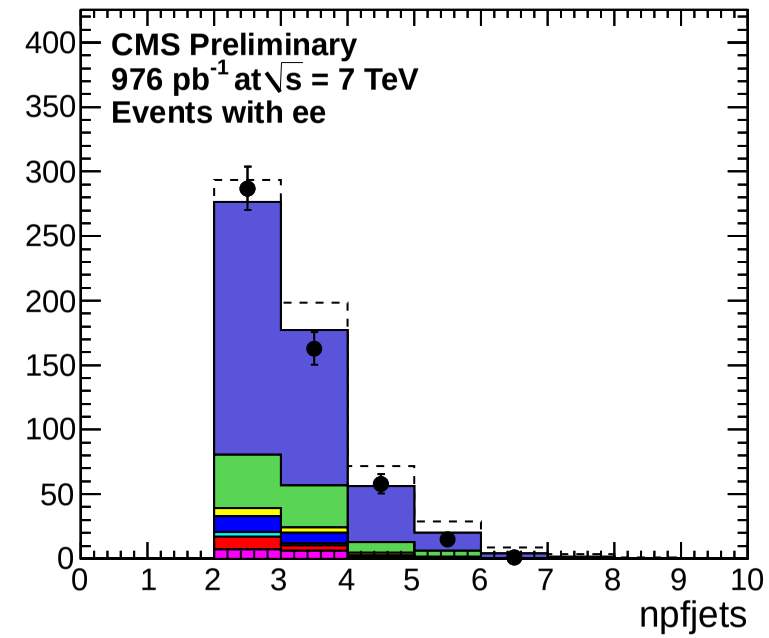
CMS Preliminary
976 pb-1 at √s = 7 TeV
Events with ee
npfjets

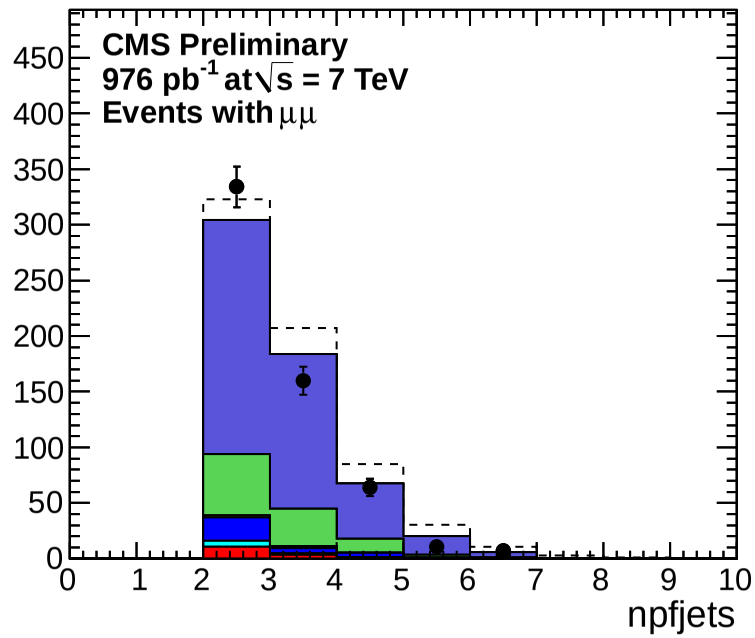
CMS Preliminary
976 pb-1 at √s = 7 TeV
Events with μμ
npfjets

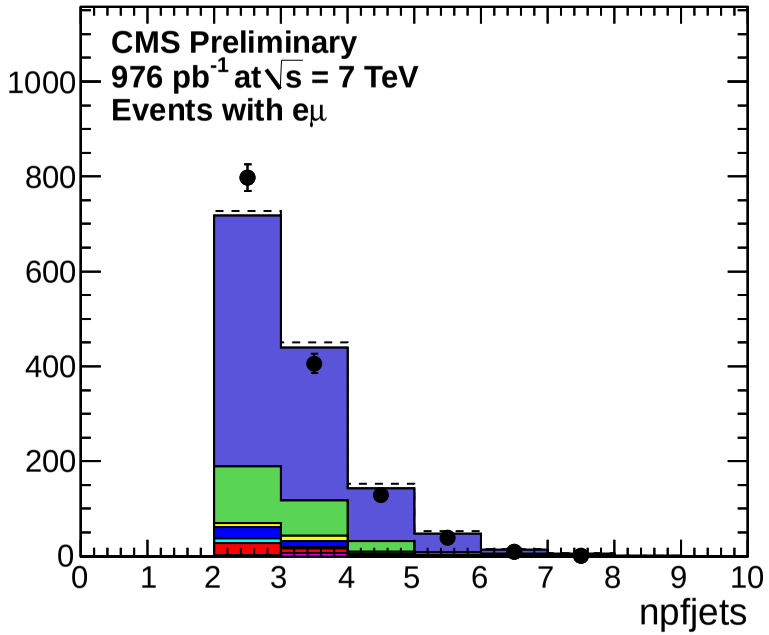
CMS Preliminary
976 pb-1 at √s = 7 TeV
Events with eμ
npfjets

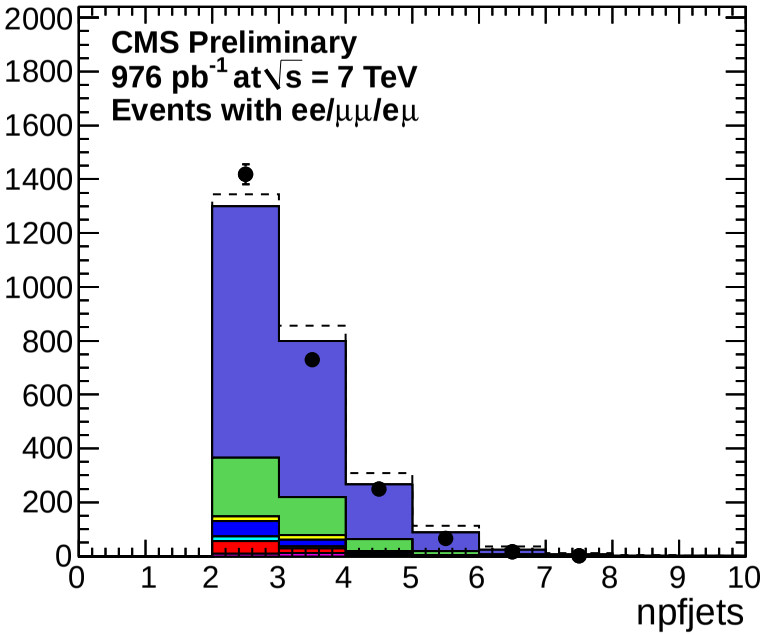
CMS Preliminary
976 pb-1 at √s = 7 TeV
Events with ee/μμ/eμ
npfjets

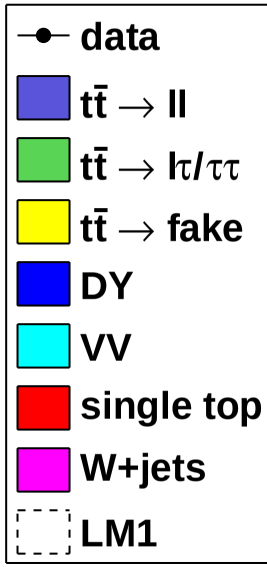
data
tt̄ → ll
tt̄ → lτ/ττ
tt̄ → fake
DY
VV
single top
W+jets
LM1

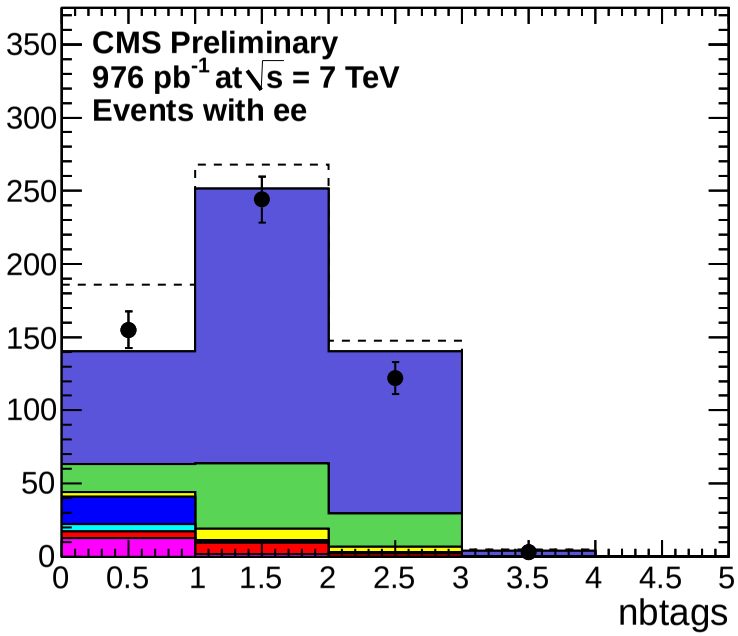
CMS Preliminary
976 pb-1 at √s = 7 TeV
Events with ee
nbtags

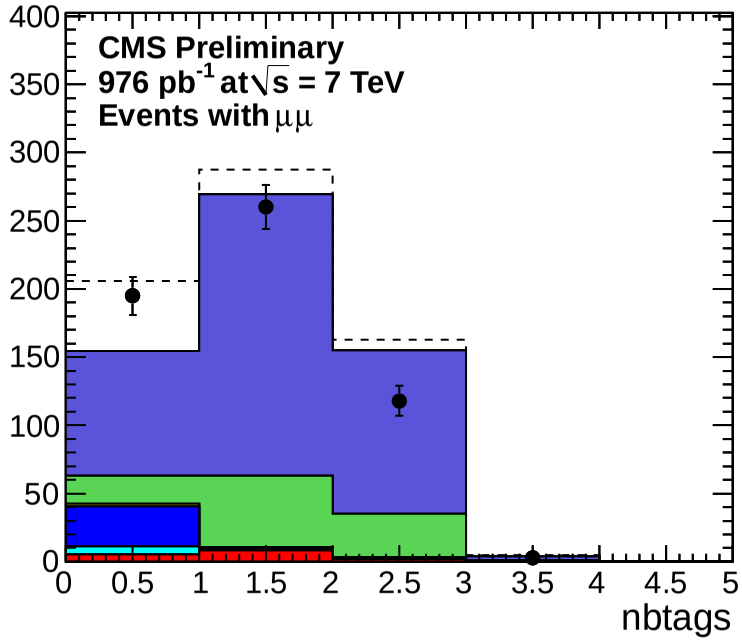
CMS Preliminary
976 pb-1 at √s = 7 TeV
Events with μμ
nbtags

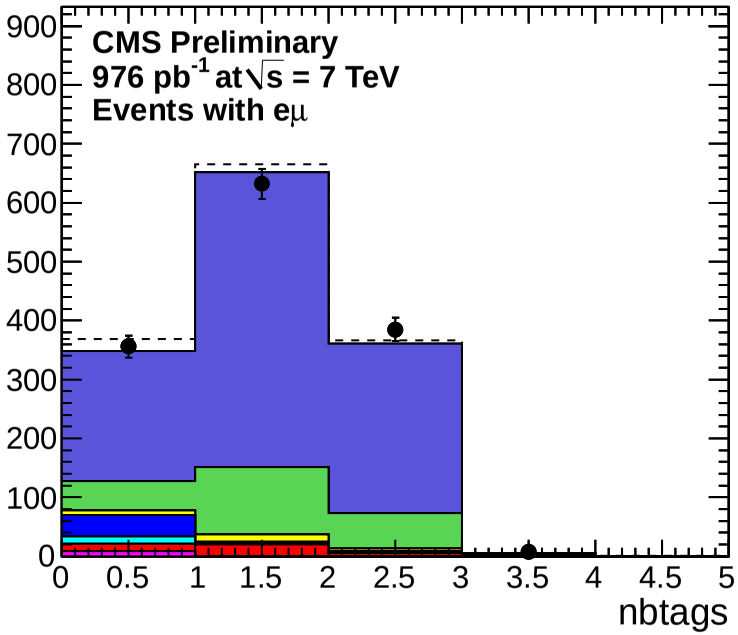
CMS Preliminary
976 pb-1 at √s = 7 TeV
Events with eμ
nbtags

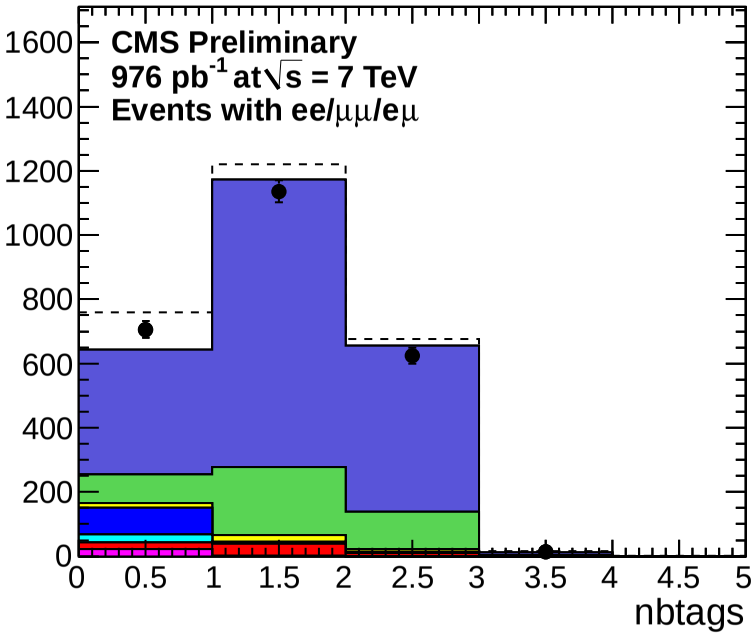
CMS Preliminary
976 pb-1 at √s = 7 TeV
Events with ee/μμ/eμ
nbtags

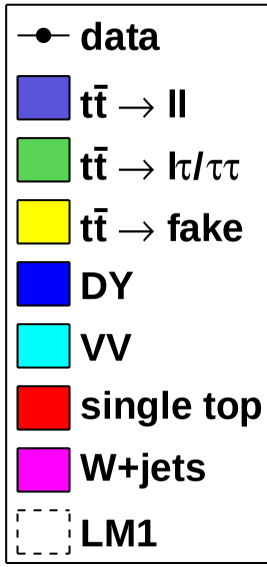
data
tt̄ → ll
tt̄ → lτ/ττ
tt̄ → fake
DY
VV
single top
W+jets
LM1

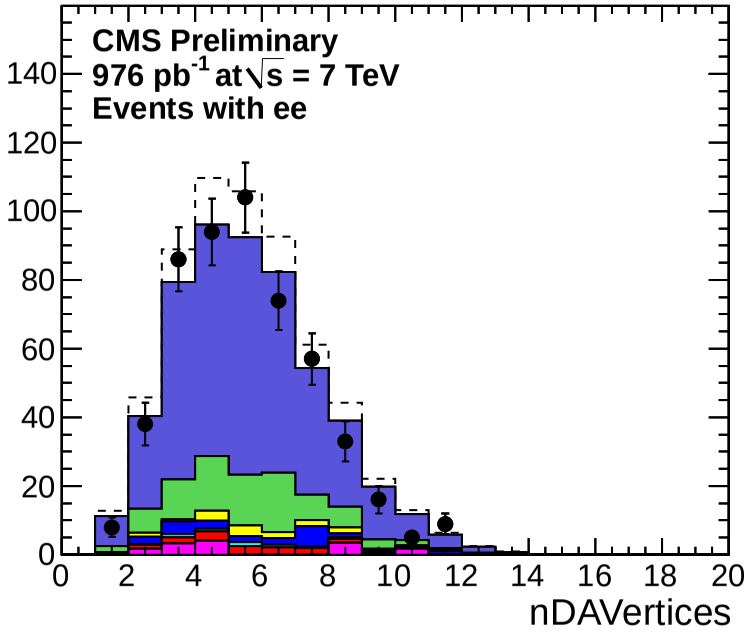
CMS Preliminary
976 pb-1 at √s = 7 TeV
Events with ee
nDAVertices

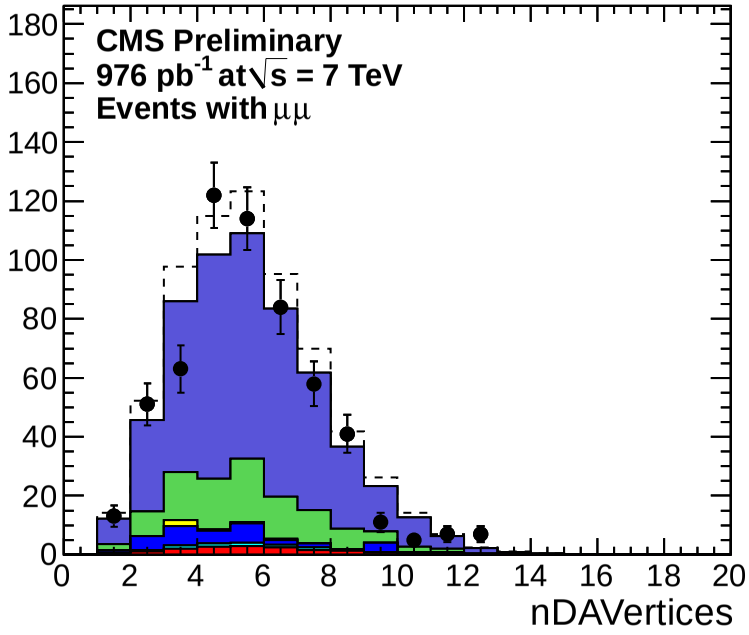
CMS Preliminary
976 pb-1 at √s = 7 TeV
Events with μμ
nDAVertices

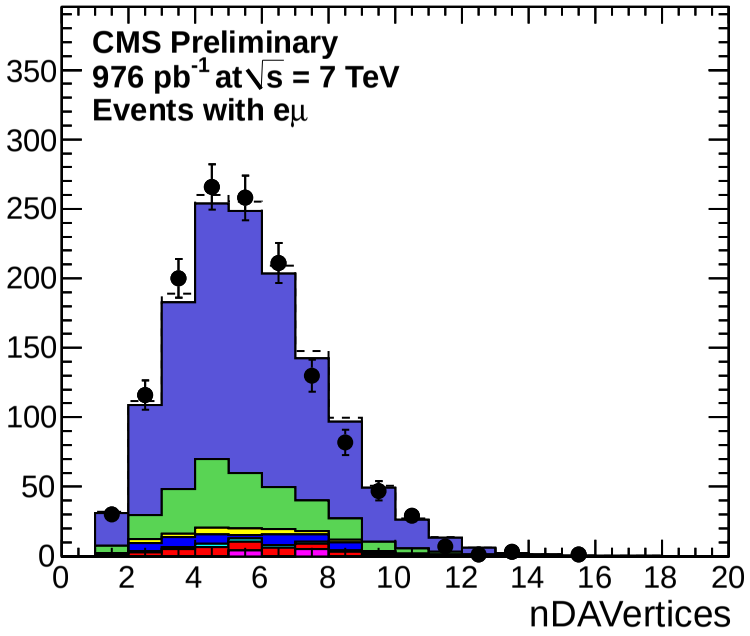
CMS Preliminary
976 pb-1 at √s = 7 TeV
Events with eμ
nDAVertices

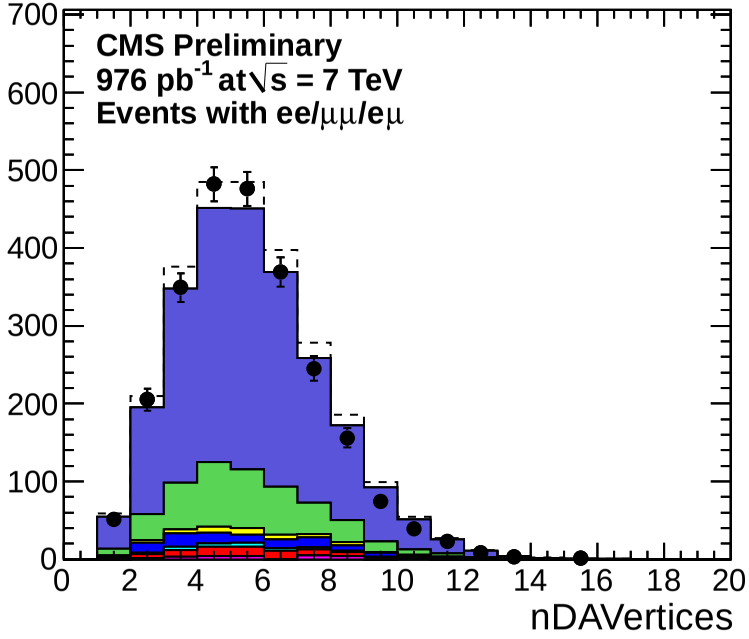
CMS Preliminary
976 pb-1 at √s = 7 TeV
Events with ee/μμ/eμ
nDAVertices

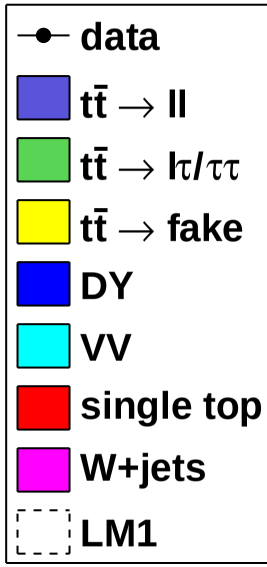
data
tt̄ → ll
tt̄ → lτ/ττ
tt̄ → fake
DY
VV
single top
W+jets
LM1

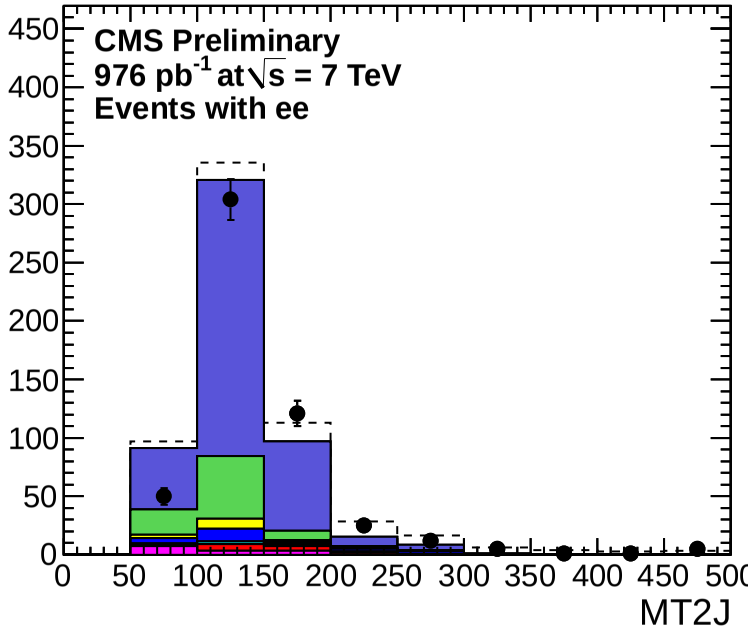
CMS Preliminary
976 pb-1 at √s = 7 TeV
Events with ee
MT2J

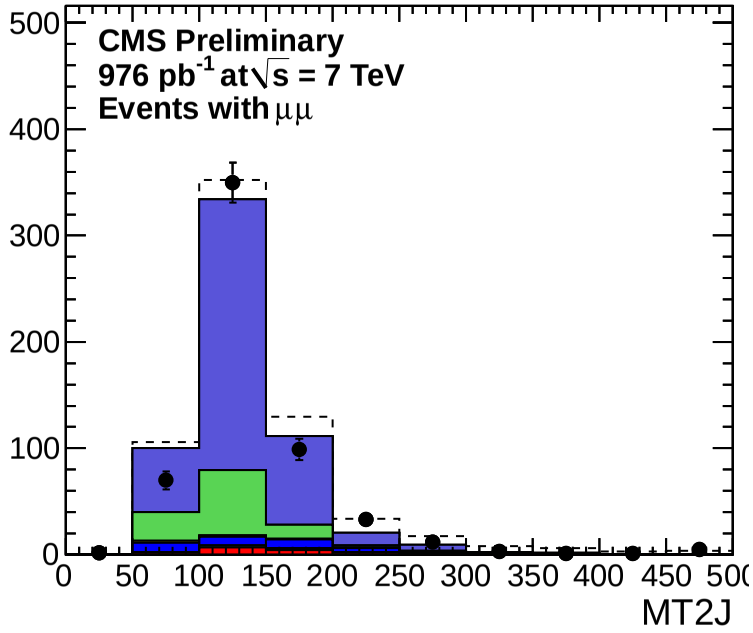
CMS Preliminary
976 pb-1 at √s = 7 TeV
Events with μμ
MT2J

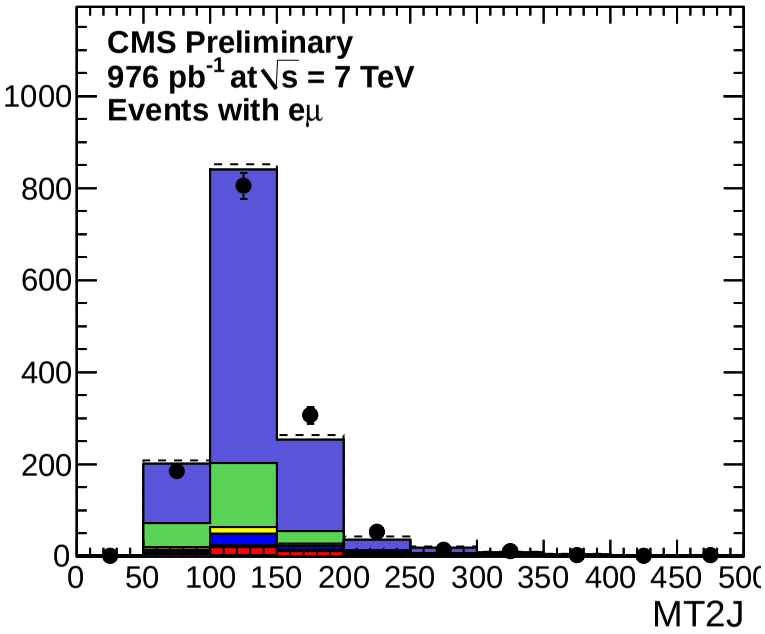
CMS Preliminary
976 pb-1 at √s = 7 TeV
Events with eμ
MT2J

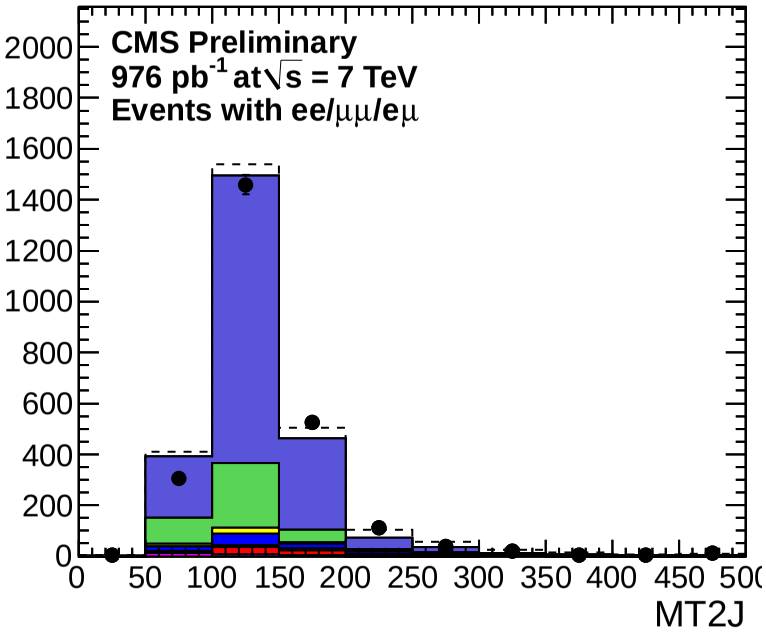
CMS Preliminary
976 pb-1 at √s = 7 TeV
Events with ee/μμ/eμ
MT2J

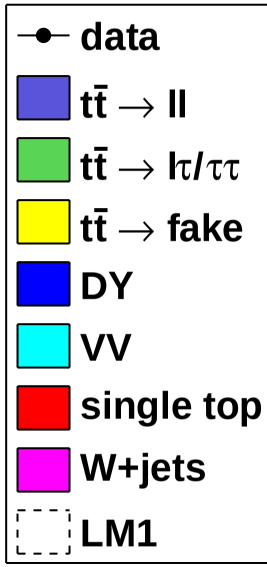
data
tt̄ → ll
tt̄ → lτ/ττ
tt̄ → fake
DY
VV
single top
W+jets
LM1

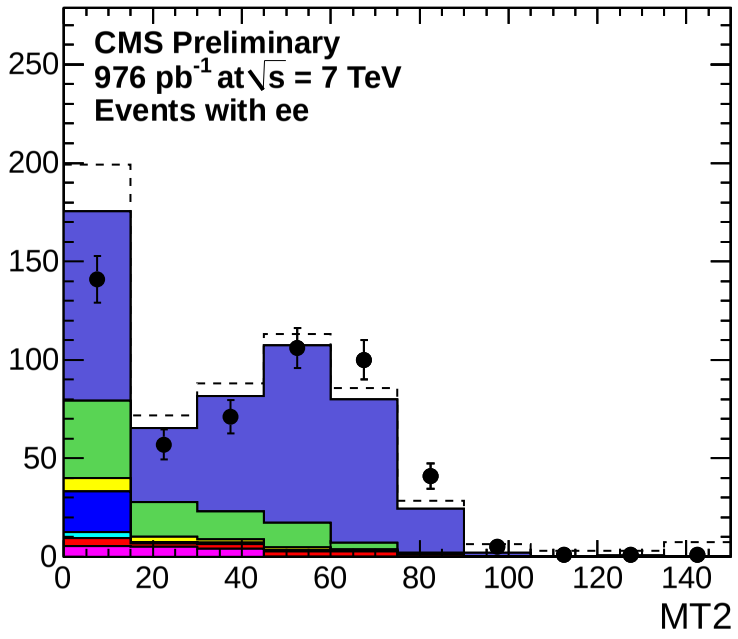
CMS Preliminary
976 pb-1 at √s = 7 TeV
Events with ee
MT2

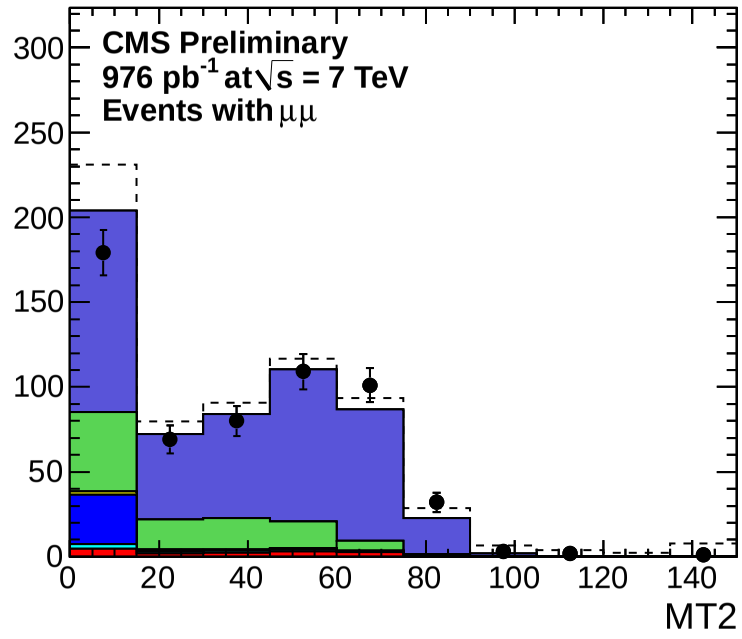
CMS Preliminary
976 pb-1 at √s = 7 TeV
Events with μμ
MT2

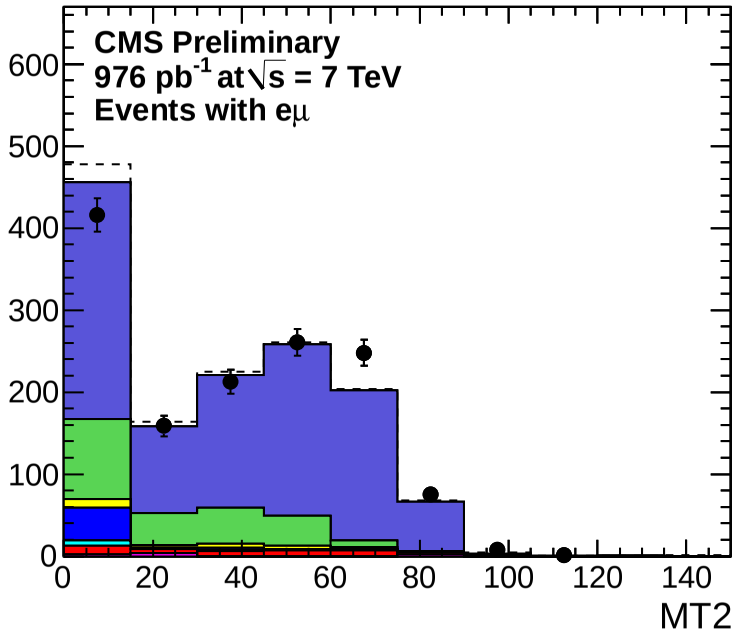
CMS Preliminary
976 pb-1 at √s = 7 TeV
Events with eμ
MT2

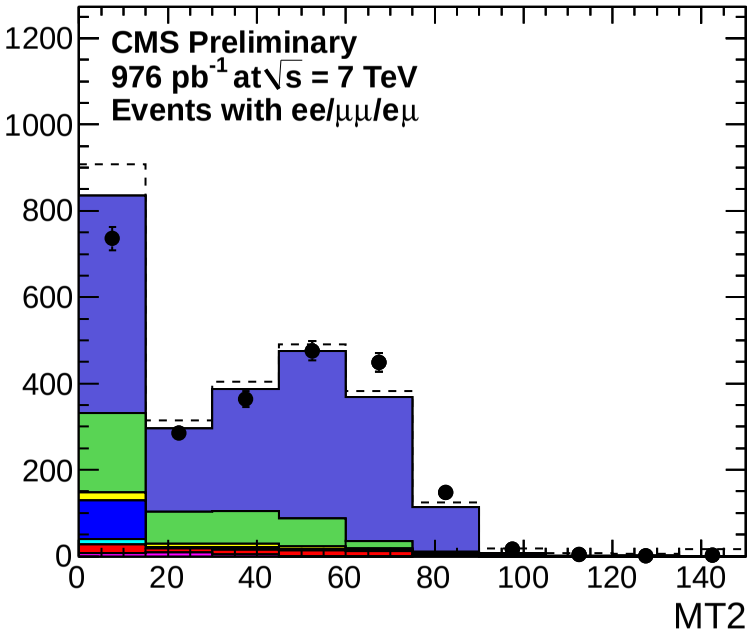
CMS Preliminary
976 pb-1 at √s = 7 TeV
Events with ee/μμ/eμ
MT2

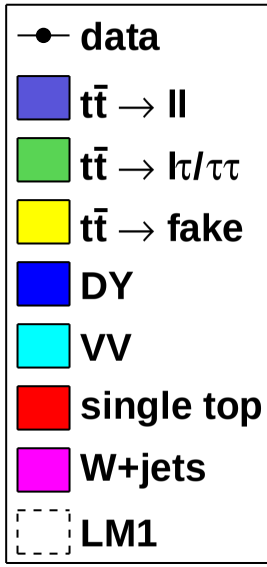
data
tt̄ → ll
tt̄ → lτ/ττ
tt̄ → fake
DY
VV
single top
W+jets
LM1

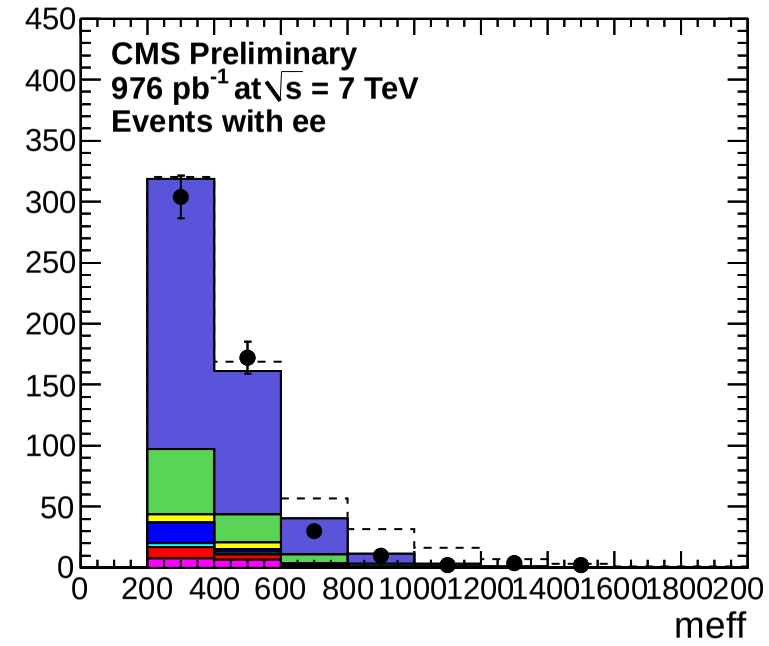
CMS Preliminary
976 pb-1 at √s = 7 TeV
Events with ee
meff

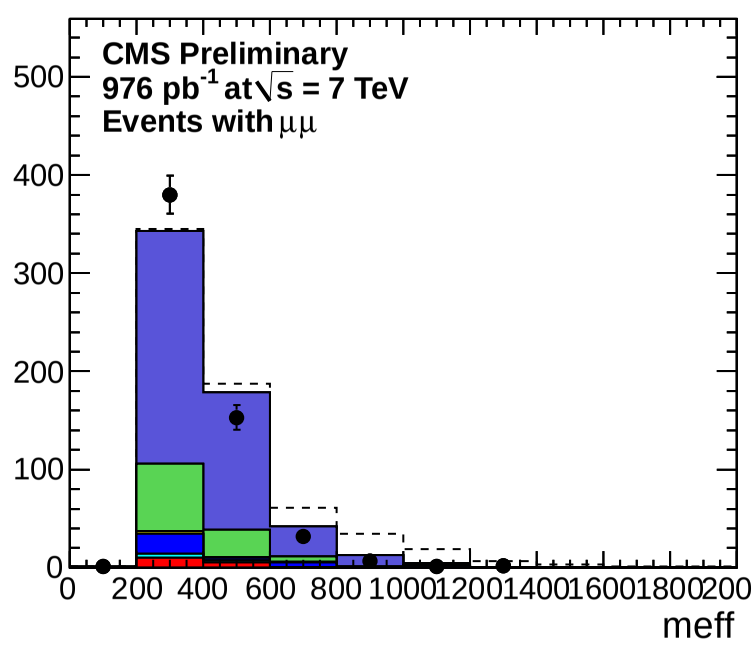
CMS Preliminary
976 pb-1 at √s = 7 TeV
Events with μμ
meff

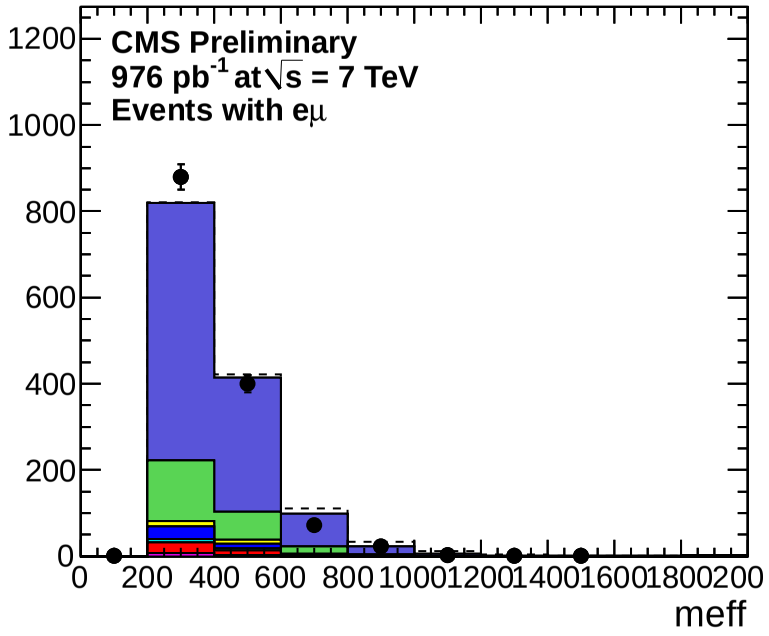
CMS Preliminary
976 pb-1 at √s = 7 TeV
Events with eμ
meff

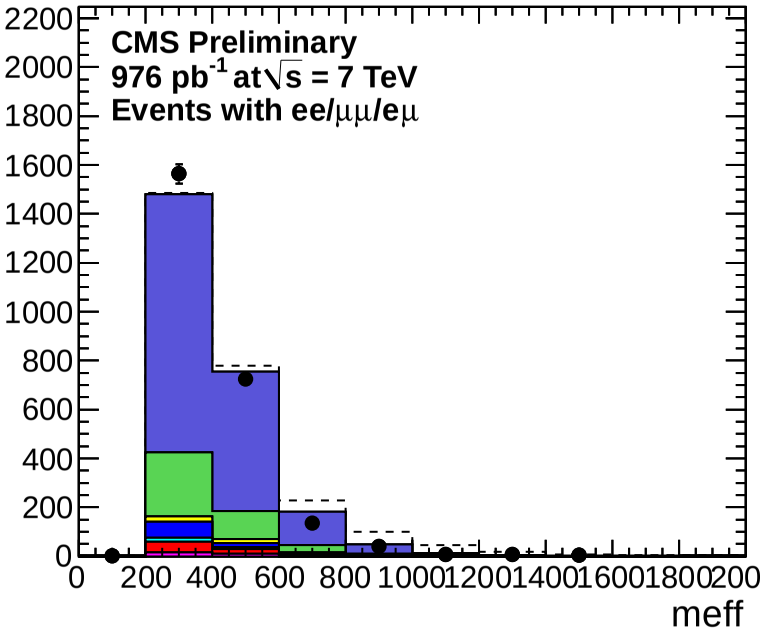
CMS Preliminary
976 pb-1 at √s = 7 TeV
Events with ee/μμ/eμ
meff

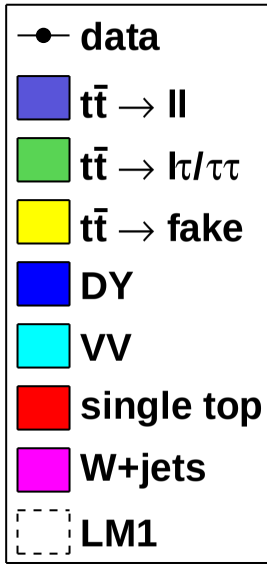
data
tt̄ → ll
tt̄ → lτ/ττ
tt̄ → fake
DY
VV
single top
W+jets
LM1

Appendix D Data/MC Comparison: 2010 Signal Region

Here we compare data and MC distributions for data passing the 2010 signal region requirements (preselection + $y > 8.5$ GeV$^{1/2}$ + $H_T > 300$ GeV. The high p_T dilepton trigger data is used. We observe 45 events in this region.

All MC samples are scaled by an overall factor 1.13, the ratio of the observed data yield in the preselection region to the prediction from MC. For illustration purposes, we overlay the distributions from the LM1 SUSY benchmakr point.

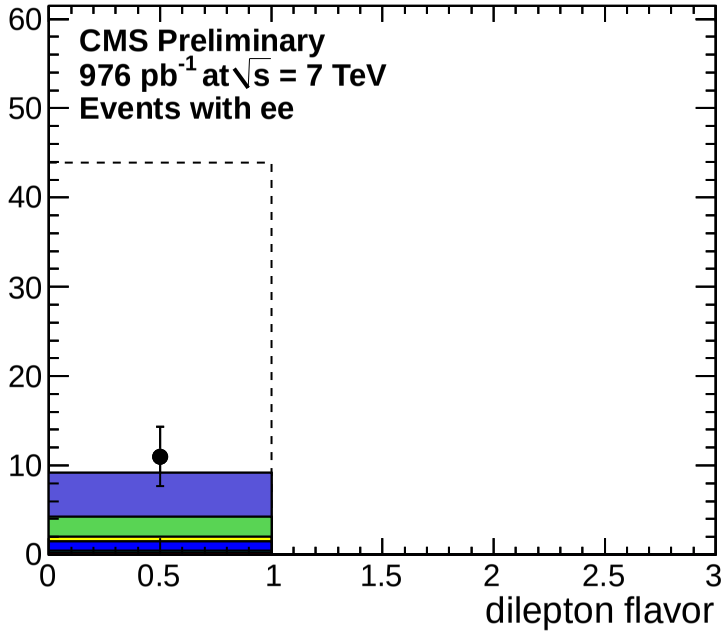
CMS Preliminary
976 pb-1 at √s = 7 TeV
Events with ee
dilepton flavor

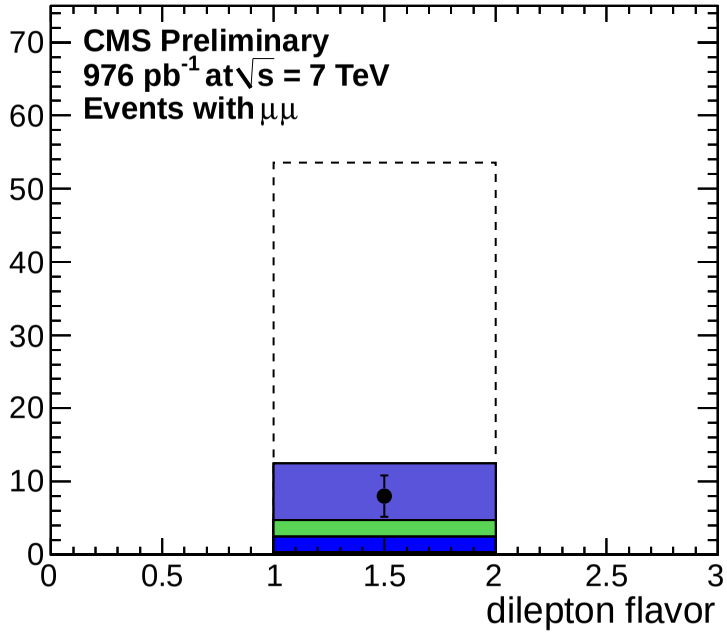
CMS Preliminary
976 pb-1 at √s = 7 TeV
Events with μμ
dilepton flavor

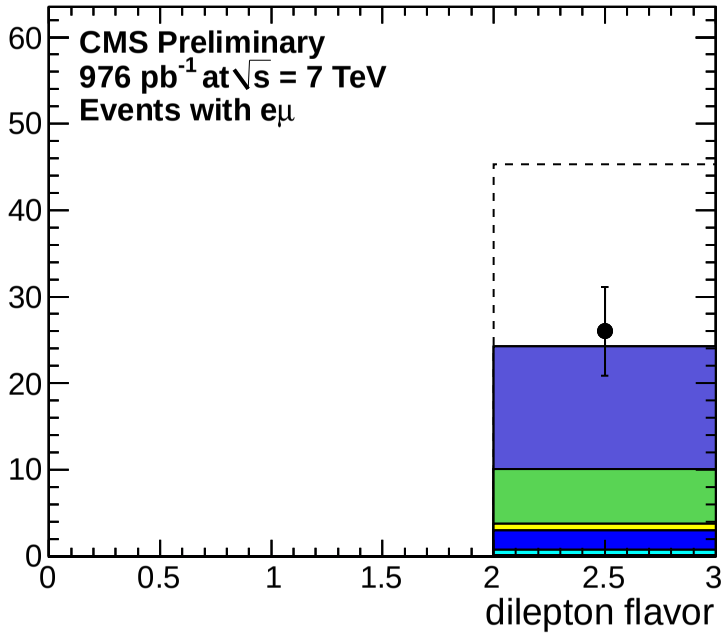
CMS Preliminary
976 pb-1 at √s = 7 TeV
Events with eμ
dilepton flavor

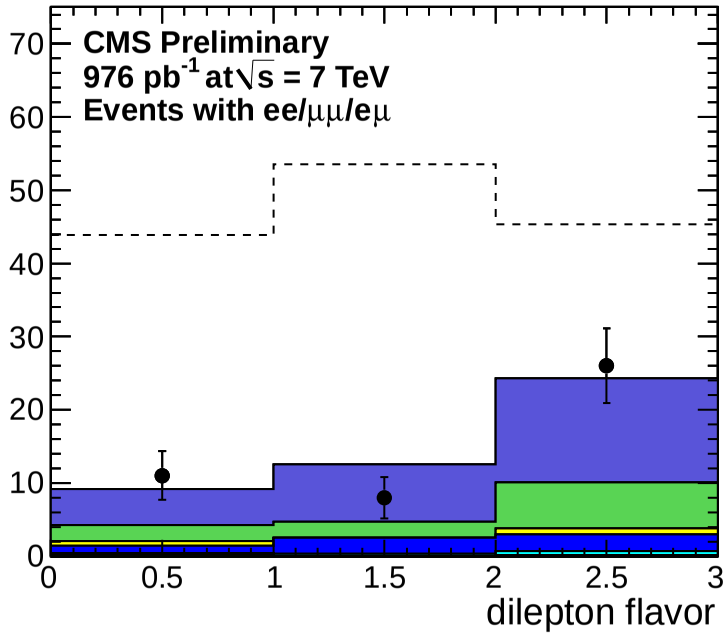
CMS Preliminary
976 pb-1 at √s = 7 TeV
Events with ee/μμ/eμ
dilepton flavor

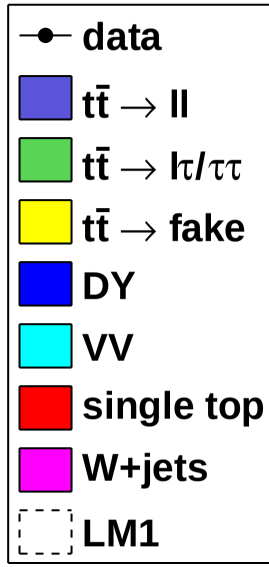
data
tt̄ → ll
tt̄ → lτ/ττ
tt̄ → fake
DY
VV
single top
W+jets
LM1

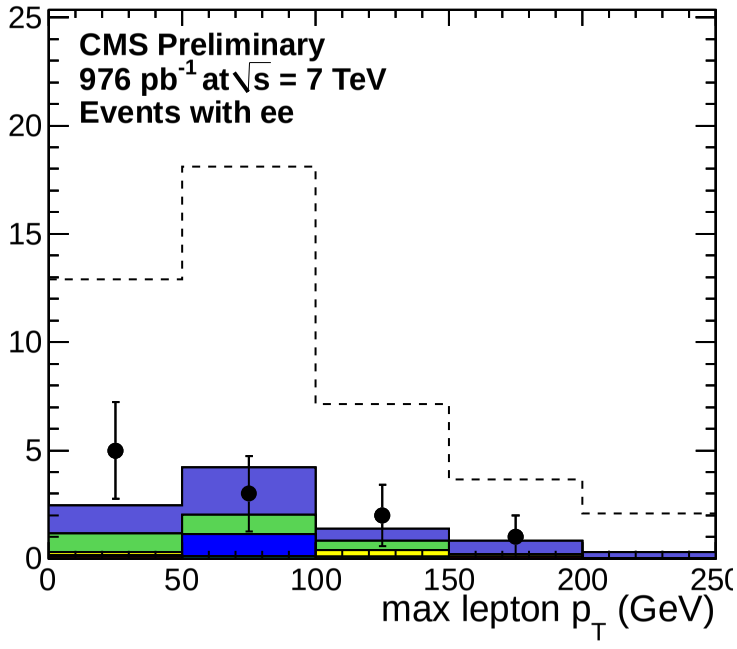
CMS Preliminary
976 pb-1 at √s = 7 TeV
Events with ee
max lepton pT (GeV)

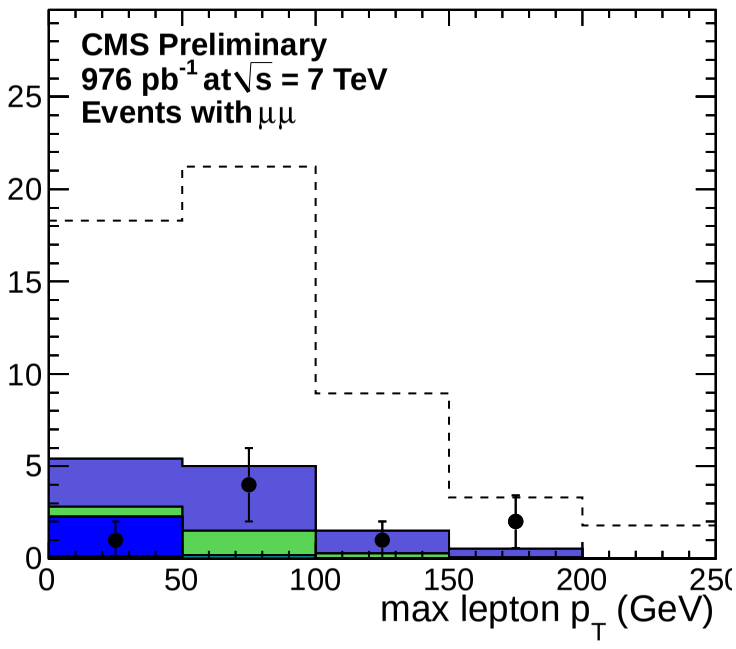
CMS Preliminary
976 pb-1 at √s = 7 TeV
Events with μμ
max lepton pT (GeV)

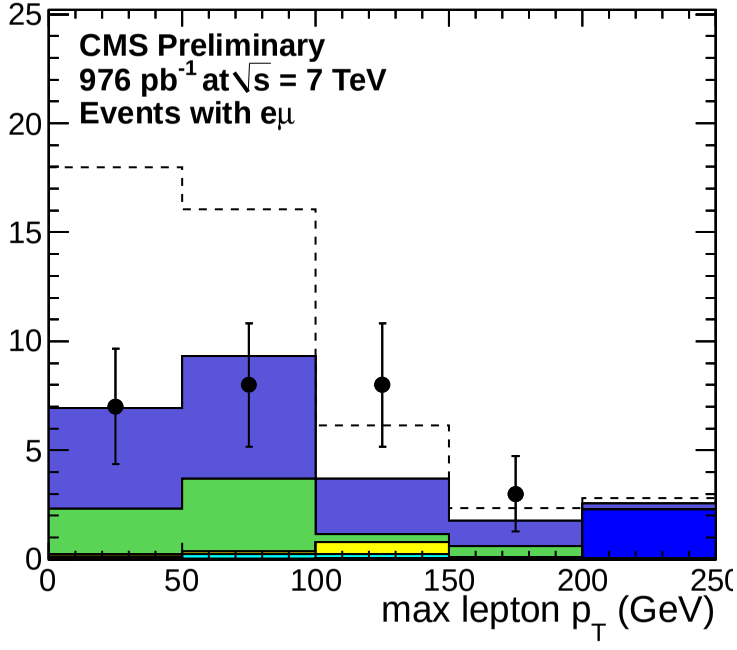
CMS Preliminary
976 pb-1 at √s = 7 TeV
Events with eμ
max lepton pT (GeV)

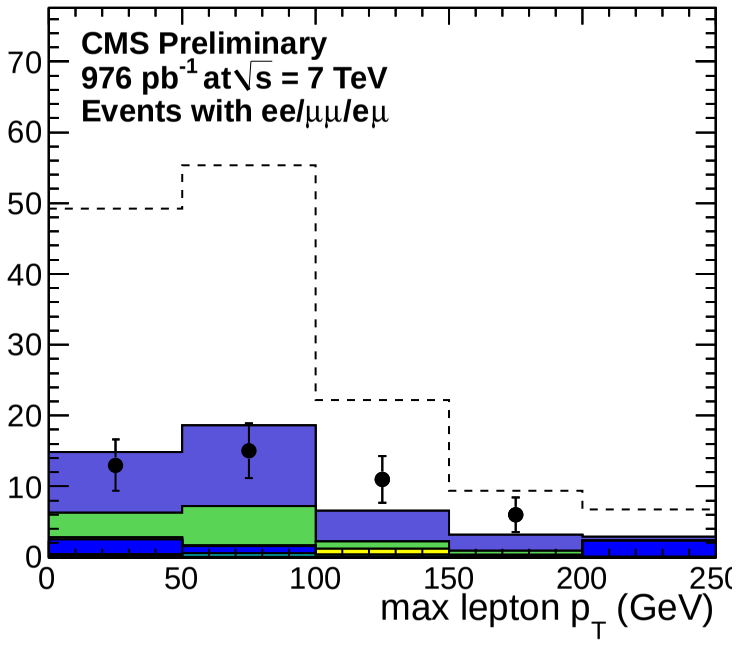
CMS Preliminary
976 pb-1 at √s = 7 TeV
Events with ee/μμ/eμ
max lepton pT (GeV)

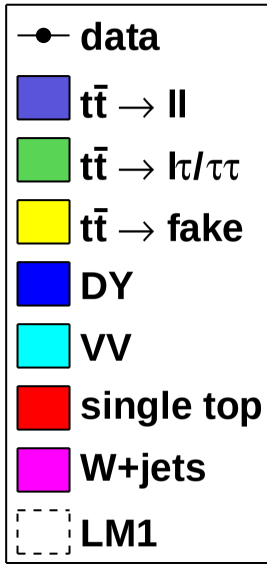
data
tt̄ → ll
tt̄ → lτ/ττ
tt̄ → fake
DY
VV
single top
W+jets
LM1

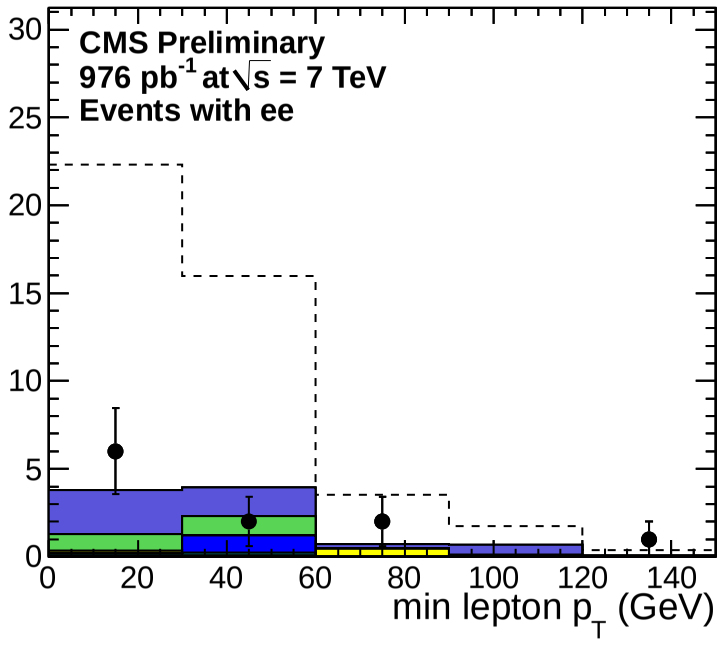
CMS Preliminary
976 pb-1 at √s = 7 TeV
Events with ee
min lepton pT (GeV)

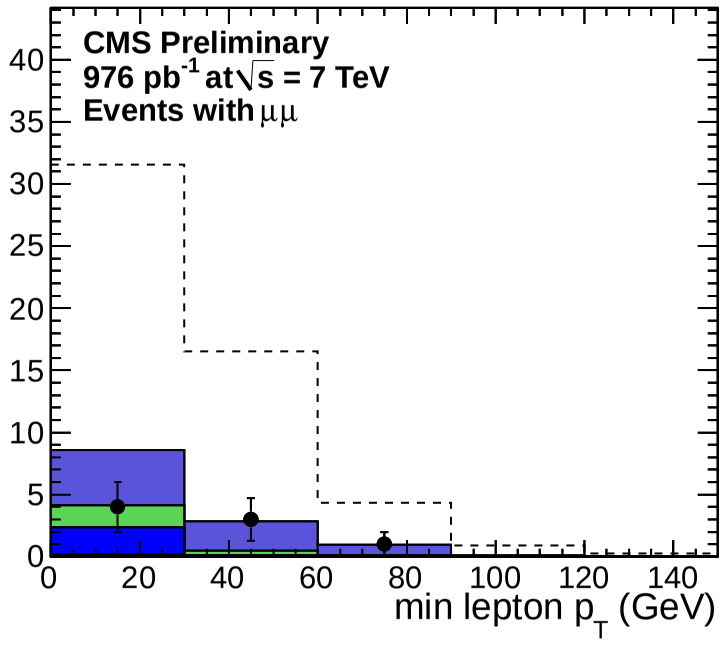
CMS Preliminary
976 pb-1 at √s = 7 TeV
Events with μμ
min lepton pT (GeV)

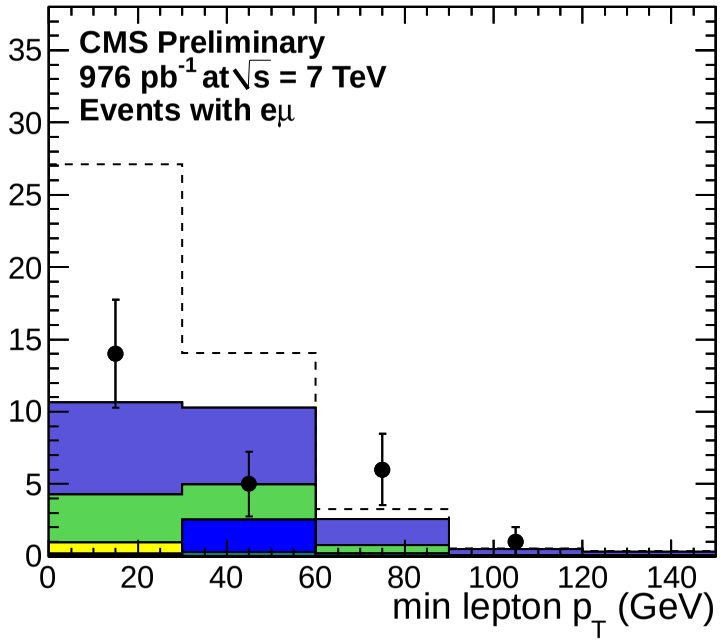
CMS Preliminary
976 pb-1 at √s = 7 TeV
Events with eμ
min lepton pT (GeV)

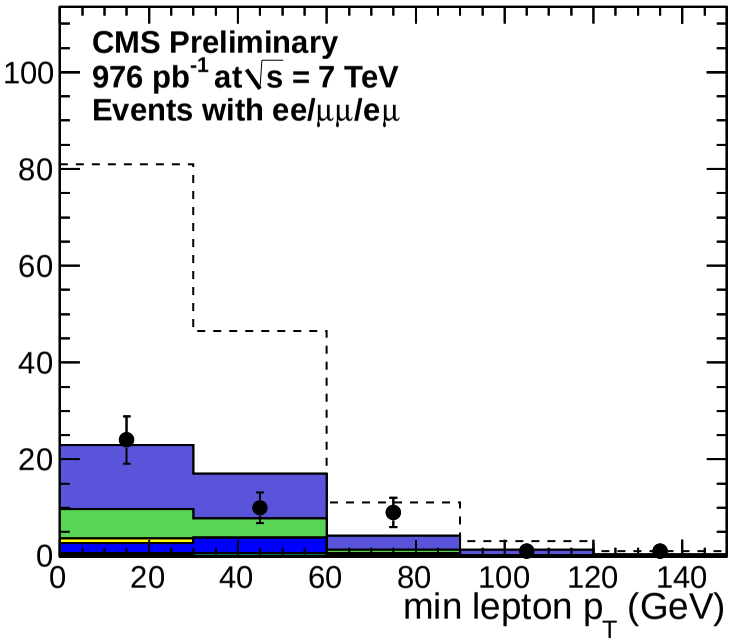
CMS Preliminary
976 pb-1 at √s = 7 TeV
Events with ee/μμ/eμ
min lepton pT (GeV)

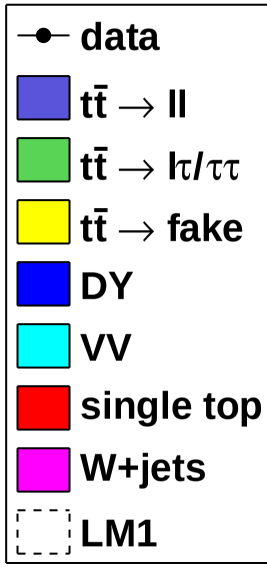
data
tt̄ → ll
tt̄ → lτ/ττ
tt̄ → fake
DY
VV
single top
W+jets
LM1

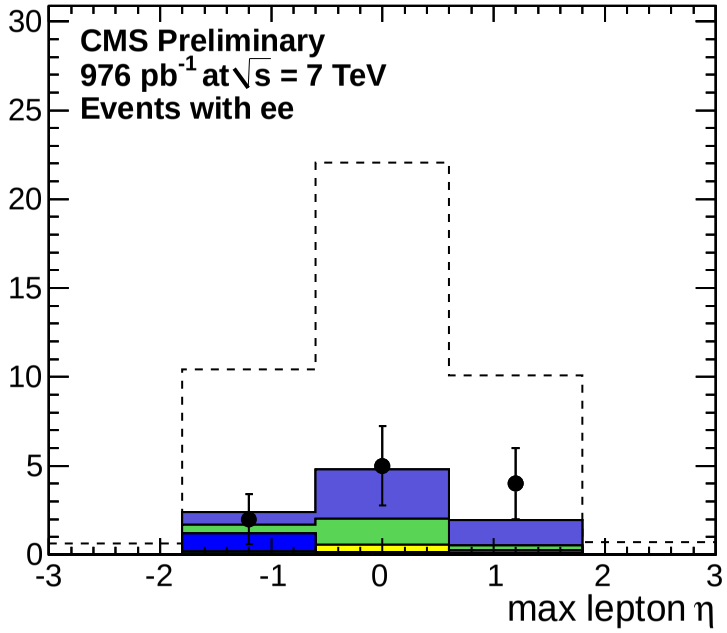
CMS Preliminary
976 pb-1 at √s = 7 TeV
Events with ee
max lepton η

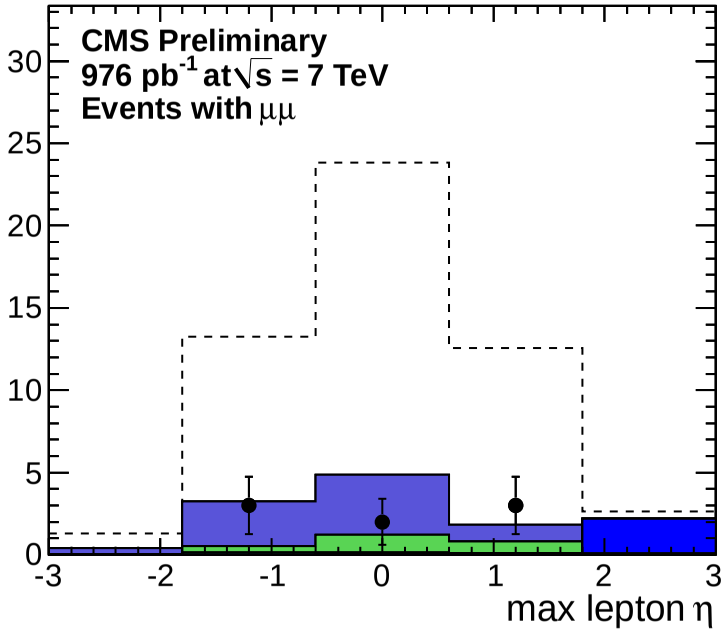
CMS Preliminary
976 pb-1 at √s = 7 TeV
Events with μμ
max lepton η

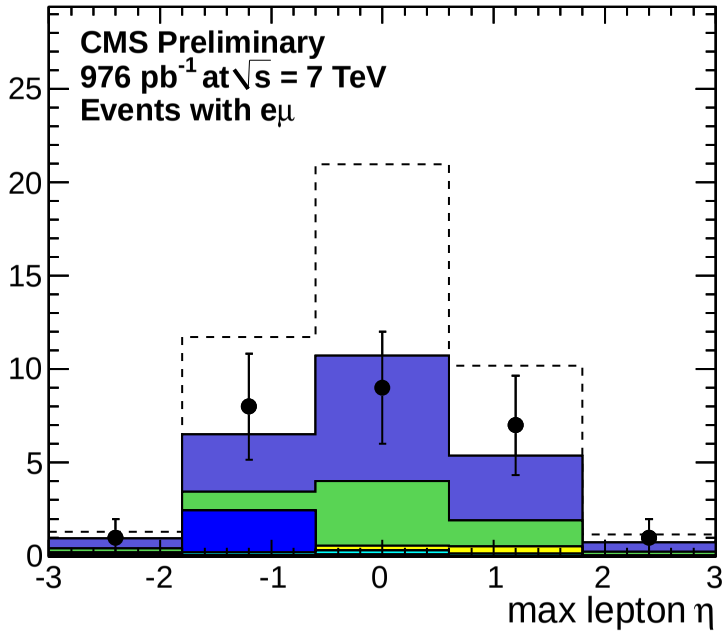
CMS Preliminary
976 pb-1 at √s = 7 TeV
Events with eμ
max lepton η

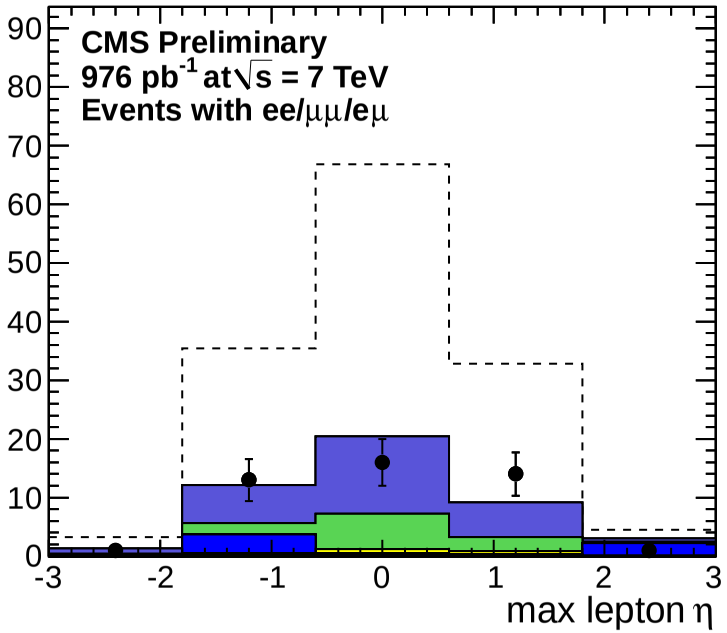
CMS Preliminary
976 pb-1 at √s = 7 TeV
Events with ee/μμ/eμ
max lepton η

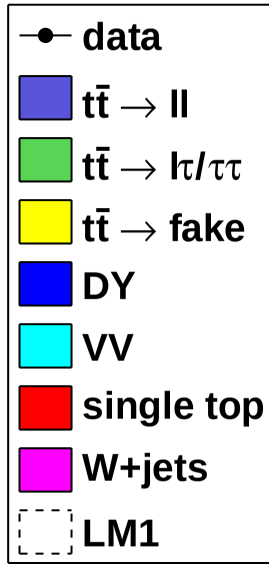
data
tt̄ → ll
tt̄ → lτ/ττ
tt̄ → fake
DY
VV
single top
W+jets
LM1

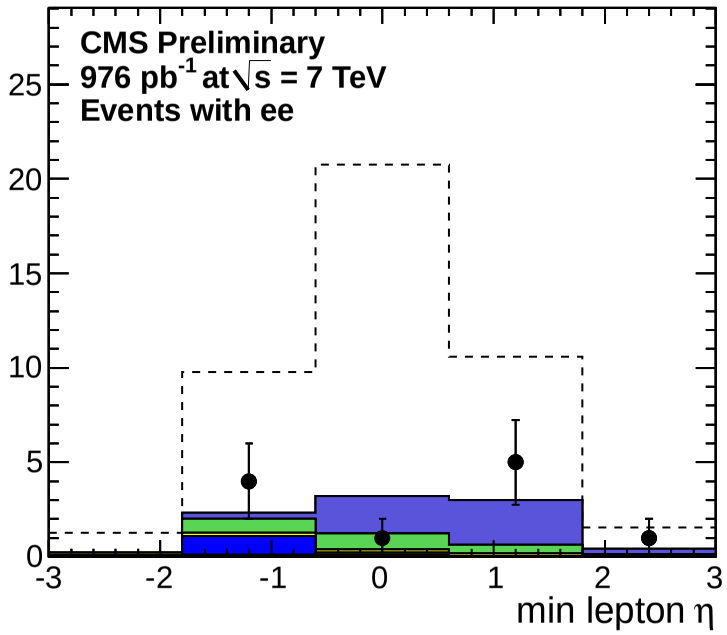
CMS Preliminary
976 pb-1 at √s = 7 TeV
Events with ee
min lepton η

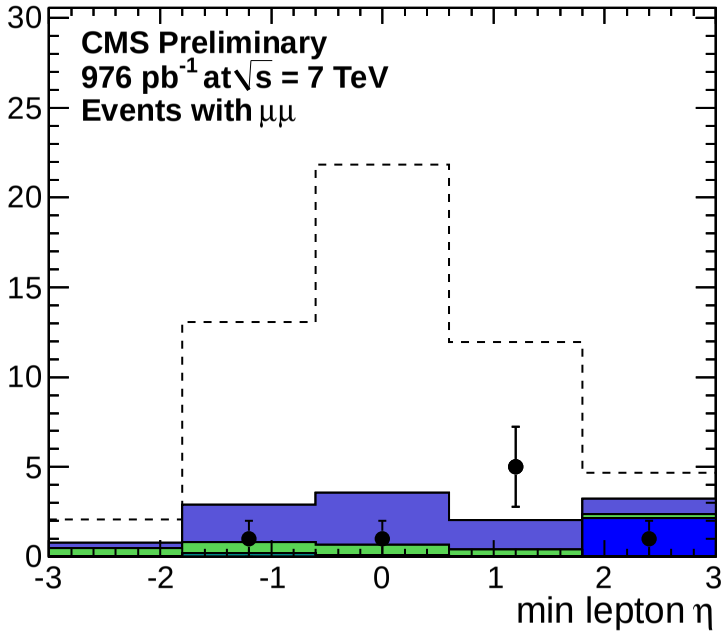
CMS Preliminary
976 pb-1 at √s = 7 TeV
Events with μμ
min lepton η

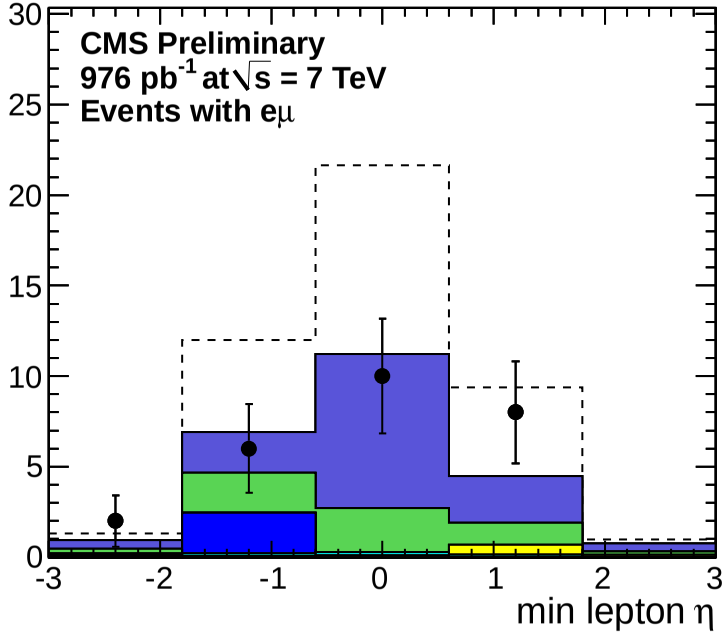
CMS Preliminary
976 pb-1 at √s = 7 TeV
Events with eμ
min lepton η

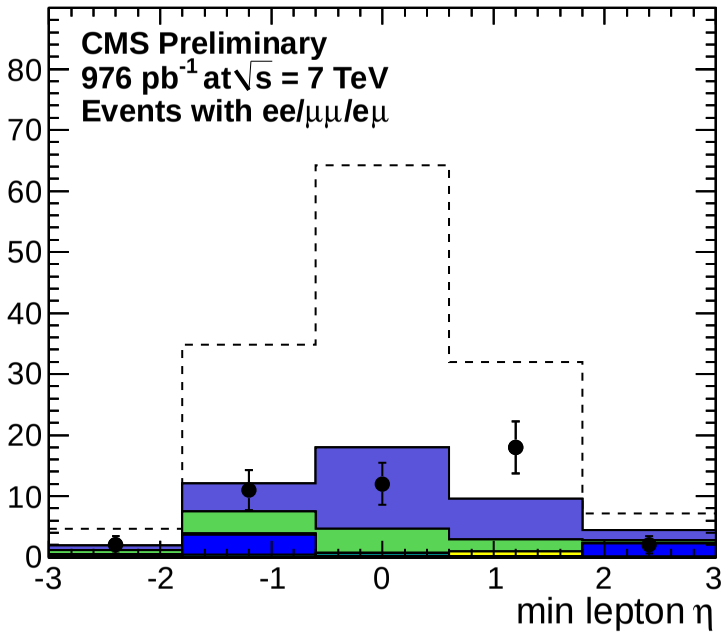
CMS Preliminary
976 pb-1 at √s = 7 TeV
Events with ee/μμ/eμ
min lepton η

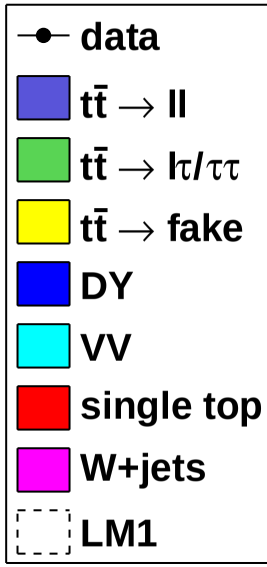
data
tt̄ → ll
tt̄ → lτ/ττ
tt̄ → fake
DY
VV
single top
W+jets
LM1

682

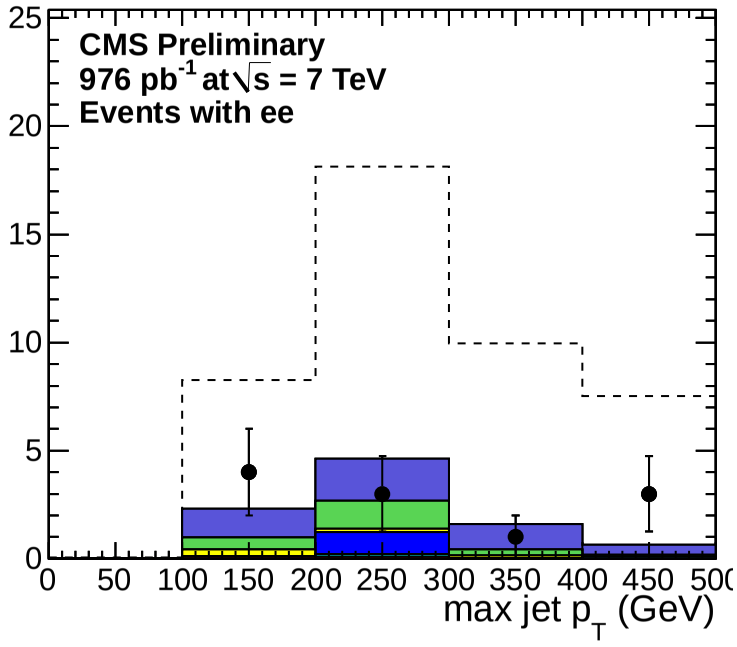
CMS Preliminary
976 pb-1 at √s = 7 TeV
Events with ee
max jet pT (GeV)

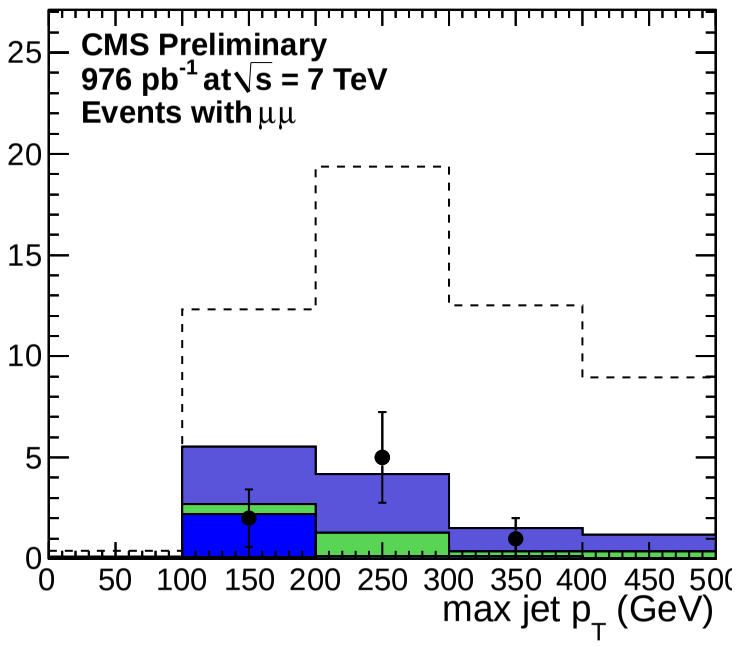
CMS Preliminary
976 pb-1 at √s = 7 TeV
Events with μμ
max jet pT (GeV)

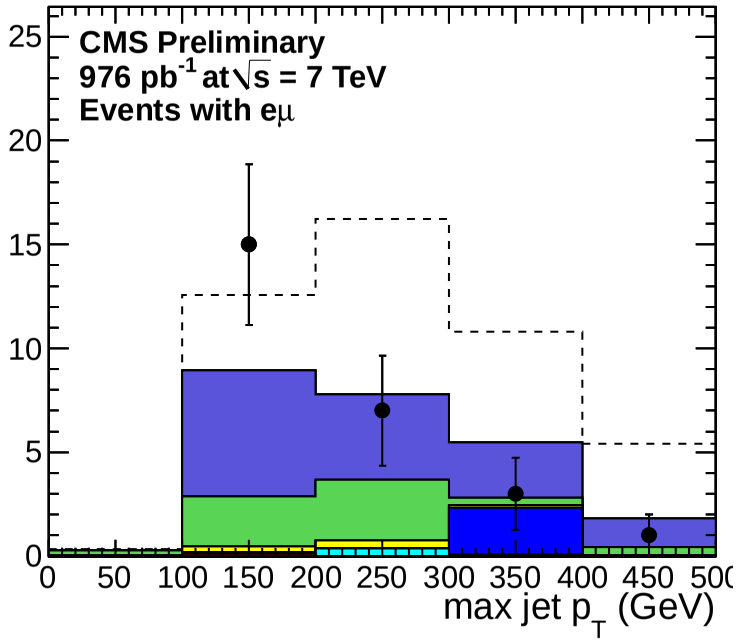
CMS Preliminary
976 pb-1 at √s = 7 TeV
Events with eμ
max jet pT (GeV)

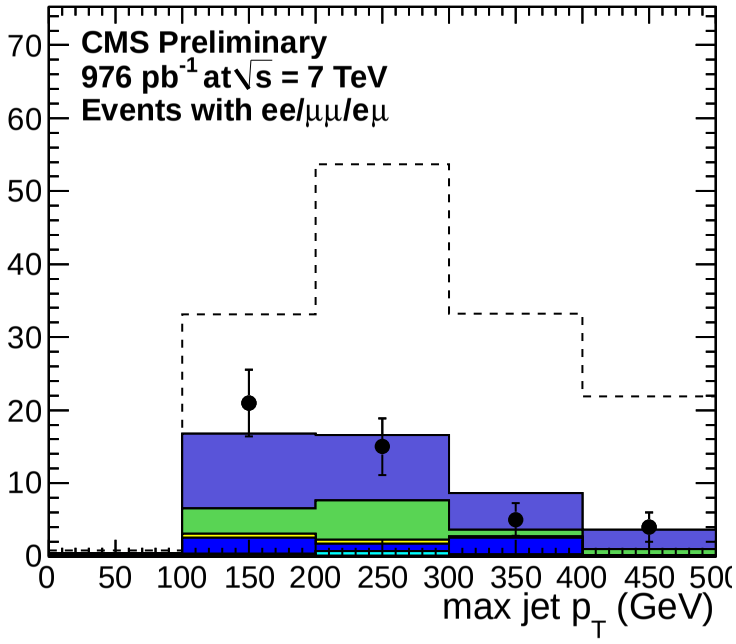
CMS Preliminary
976 pb-1 at √s = 7 TeV
Events with ee/μμ/eμ
max jet pT (GeV)

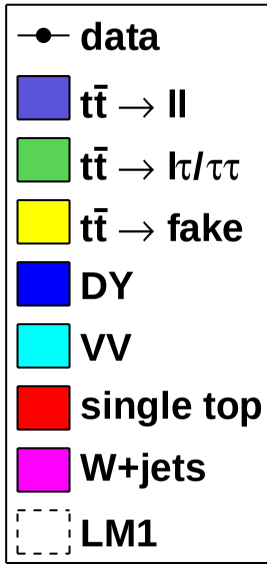
data
tt̄ → ll
tt̄ → lτ/ττ
tt̄ → fake
DY
VV
single top
W+jets
LM1

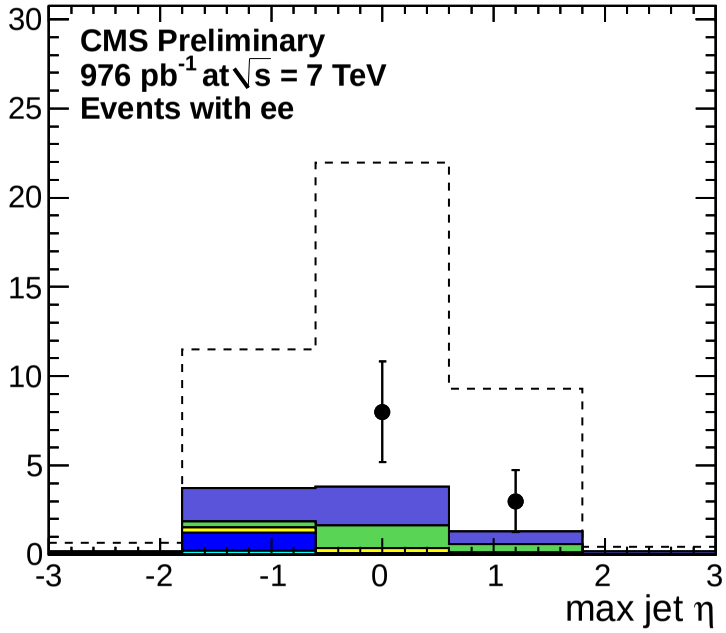
CMS Preliminary
976 pb-1 at √s = 7 TeV
Events with ee
max jet η

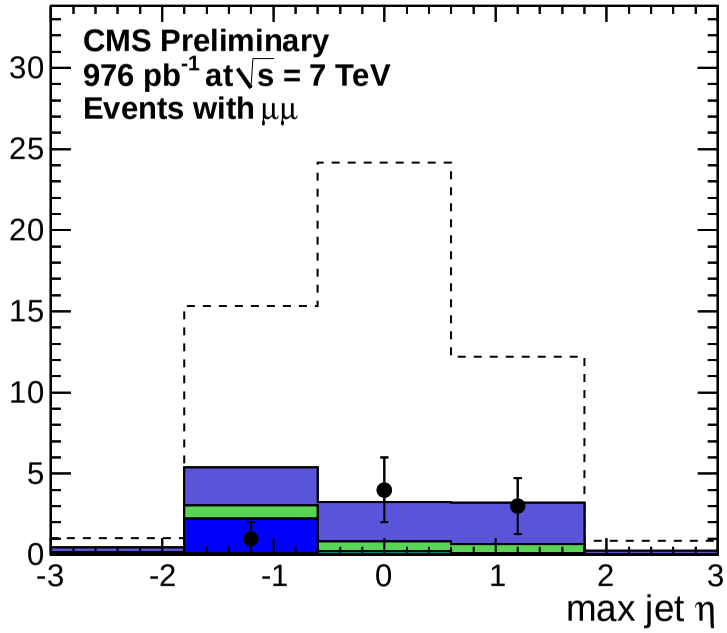
CMS Preliminary
976 pb-1 at √s = 7 TeV
Events with μμ
max jet η

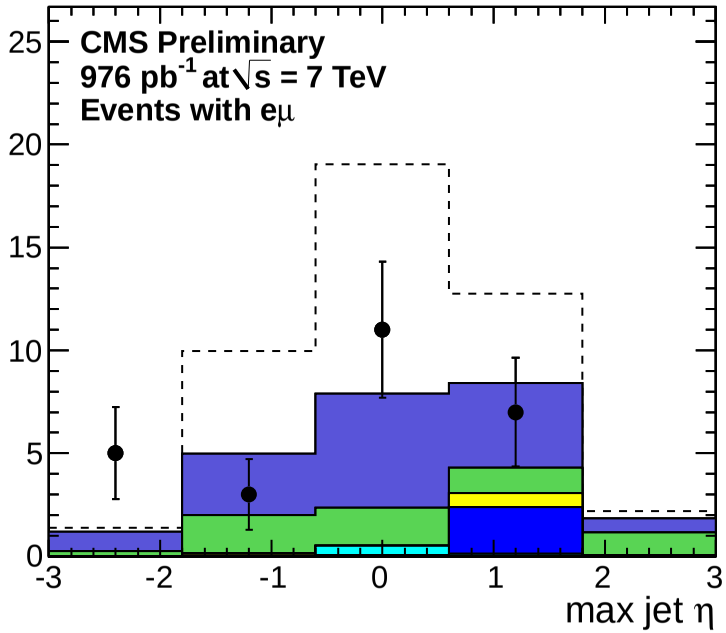
CMS Preliminary
976 pb-1 at √s = 7 TeV
Events with eμ
max jet η

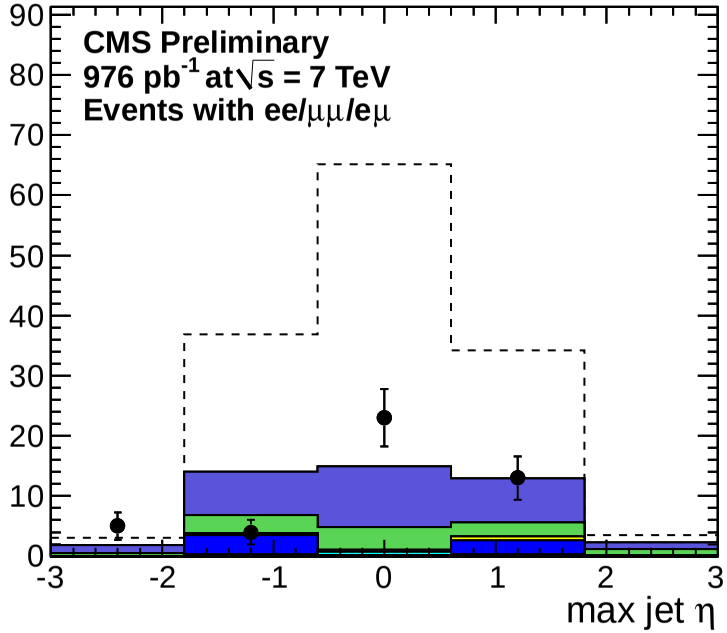
CMS Preliminary
976 pb-1 at √s = 7 TeV
Events with ee/μμ/eμ
max jet η

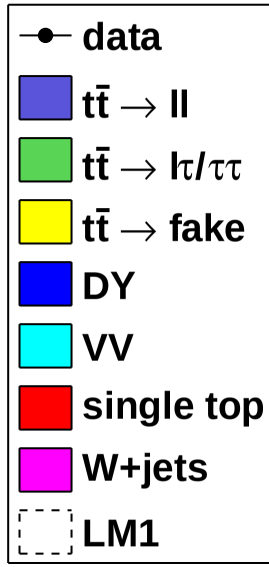
data
tt̄ → ll
tt̄ → lτ/ττ
tt̄ → fake
DY
VV
single top
W+jets
LM1

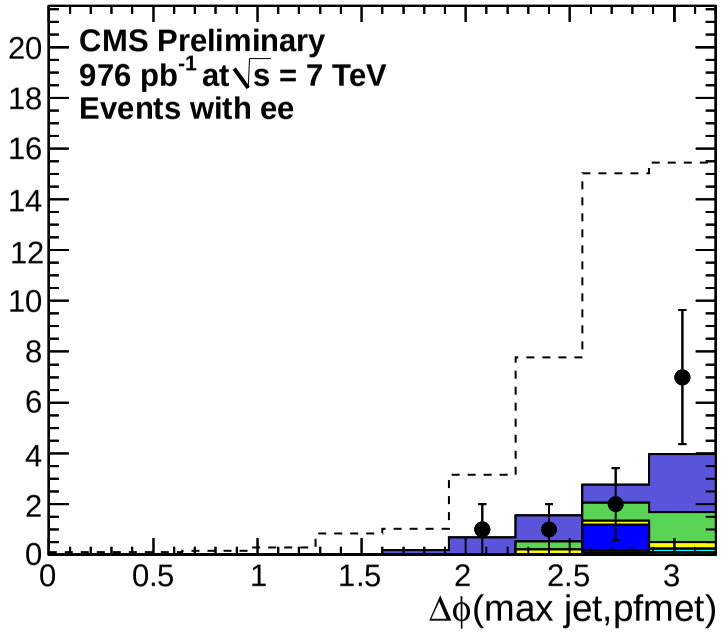
CMS Preliminary
976 pb-1 at √s = 7 TeV
Events with ee
Δφ(max jet,pfmet)

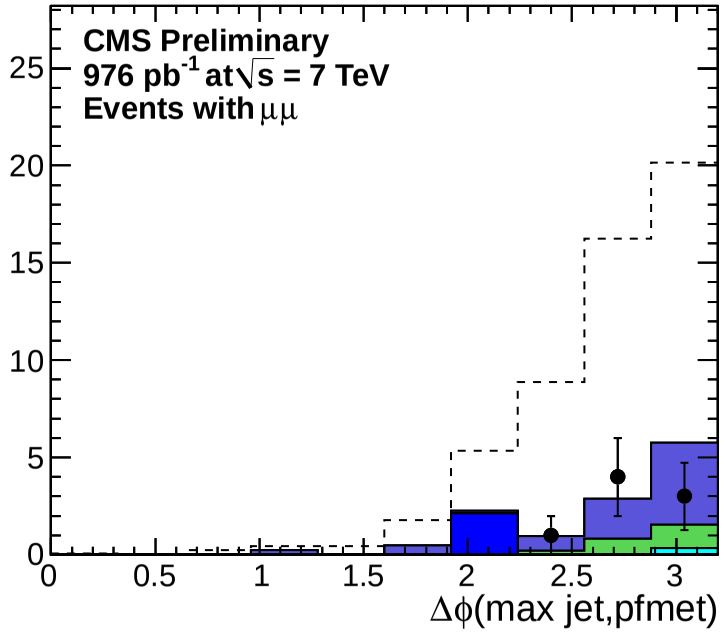
CMS Preliminary
976 pb-1 at √s = 7 TeV
Events with μμ
Δφ(max jet,pfmet)

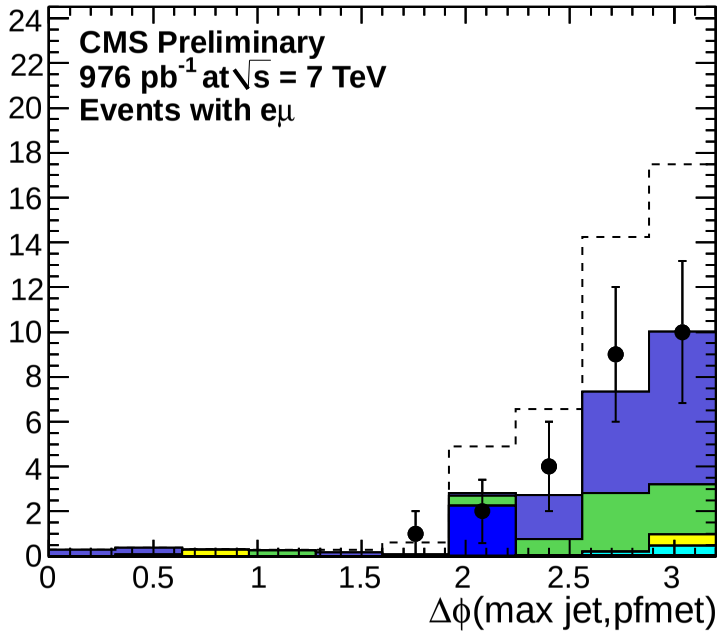
CMS Preliminary
976 pb-1 at √s = 7 TeV
Events with eμ
Δφ(max jet,pfmet)

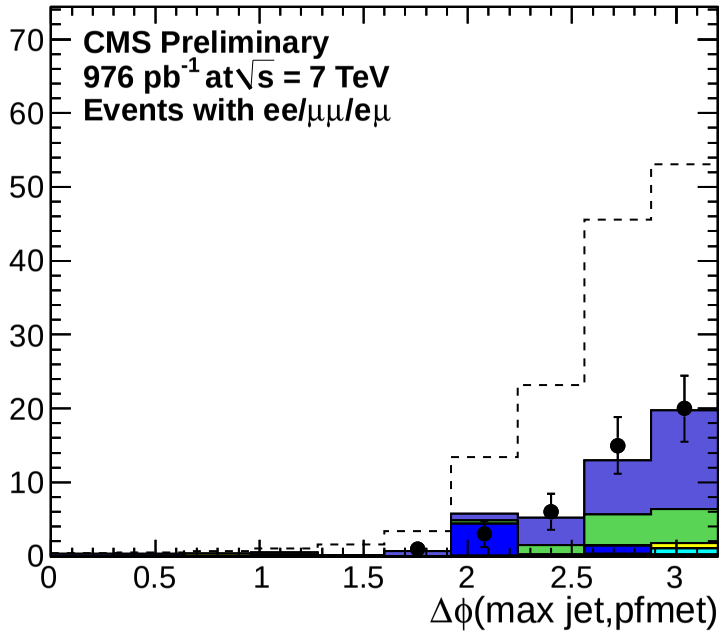
CMS Preliminary
976 pb-1 at √s = 7 TeV
Events with ee/μμ/eμ
Δφ(max jet,pfmet)

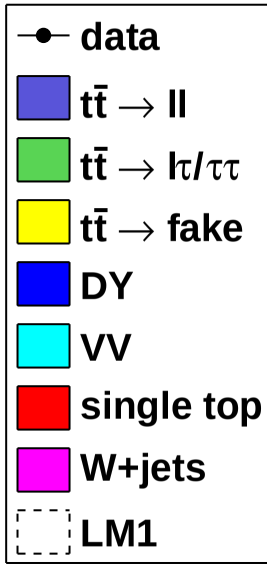
data
tt̄ → ll
tt̄ → lτ/ττ
tt̄ → fake
DY
VV
single top
W+jets
LM1

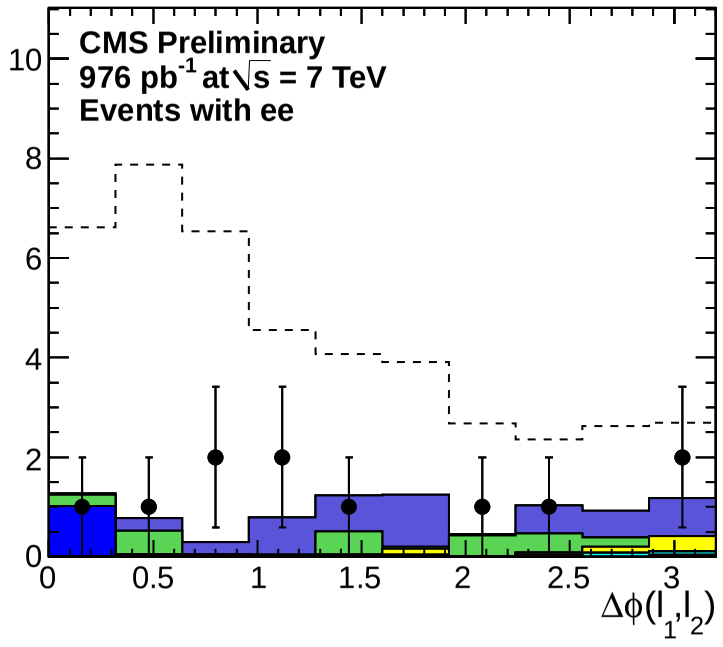
CMS Preliminary
976 pb-1 at √s = 7 TeV
Events with ee
Δφ(l1,l2)

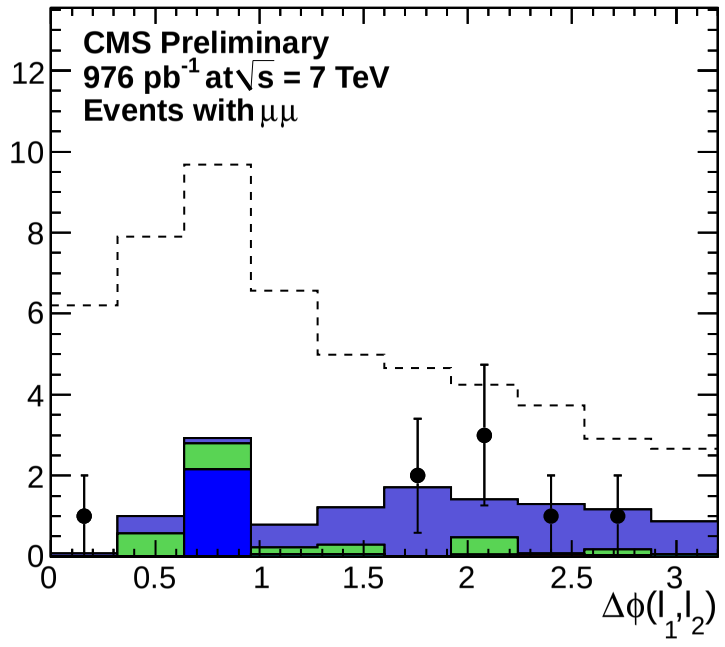
CMS Preliminary
976 pb-1 at √s = 7 TeV
Events with μμ
Δφ(l1,l2)

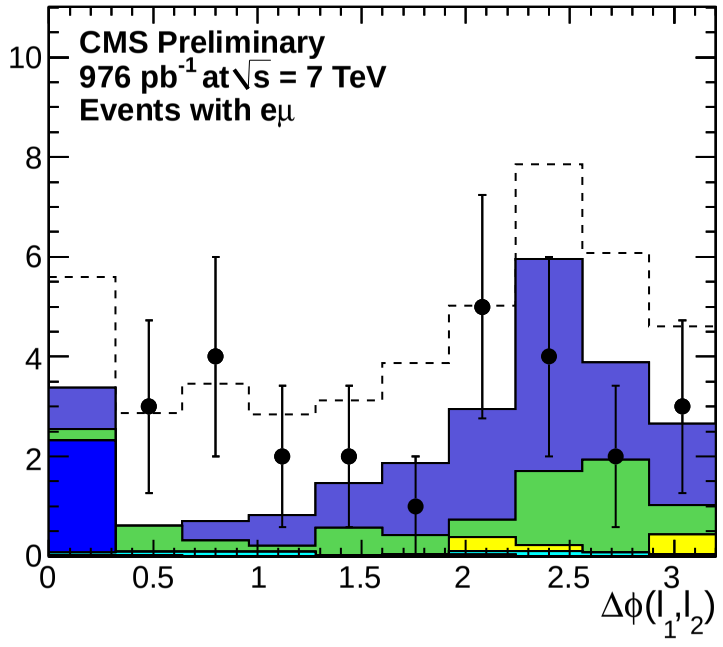
CMS Preliminary
976 pb-1 at √s = 7 TeV
Events with eμ
Δφ(l1,l2)

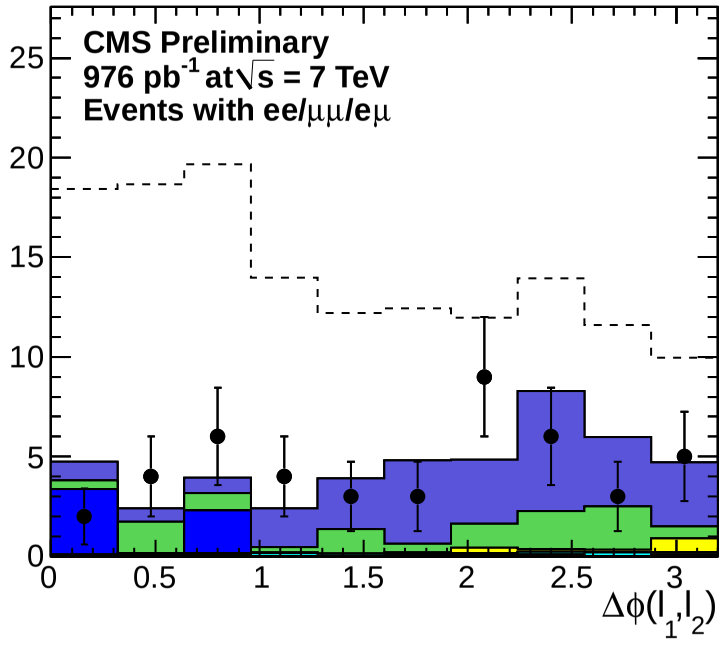
CMS Preliminary
976 pb-1 at √s = 7 TeV
Events with ee/μμ/eμ
Δφ(l1,l2)

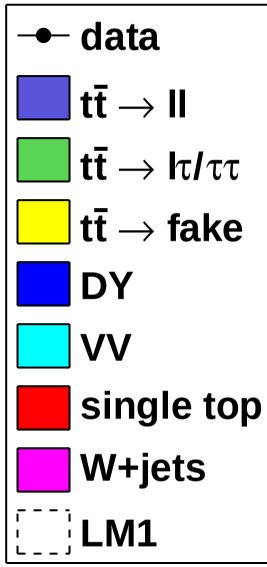
data
tt̄ → ll
tt̄ → lτ/ττ
tt̄ → fake
DY
VV
single top
W+jets
LM1

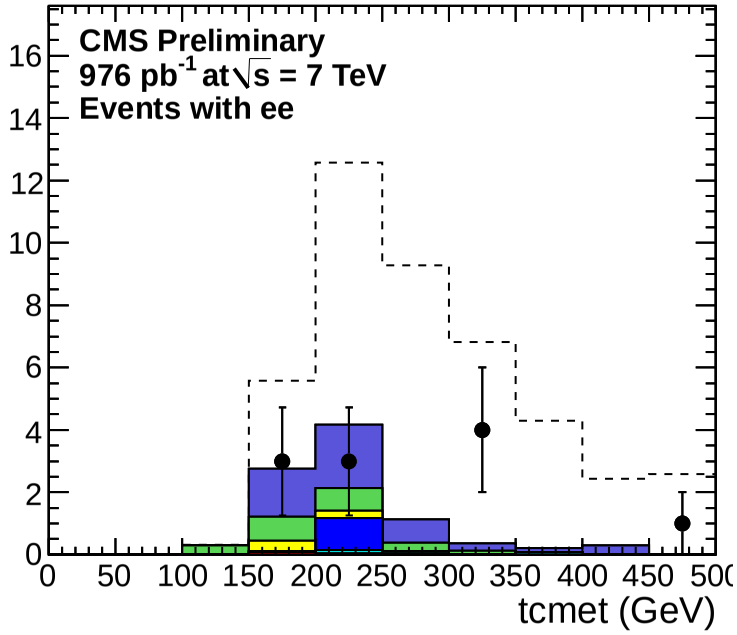
CMS Preliminary
976 pb-1 at √s = 7 TeV
Events with ee
tcmet (GeV)

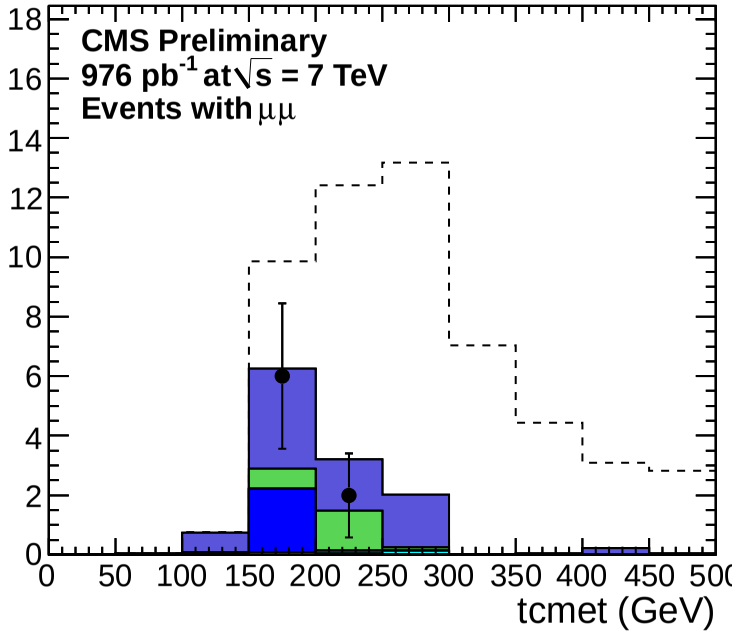
CMS Preliminary
976 pb-1 at √s = 7 TeV
Events with μμ
tcmet (GeV)

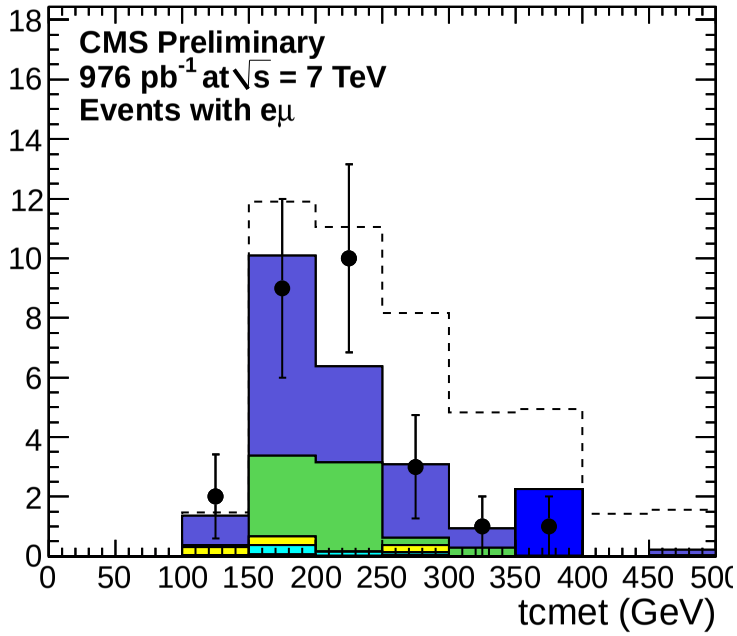
CMS Preliminary
976 pb-1 at √s = 7 TeV
Events with eμ
tcmet (GeV)

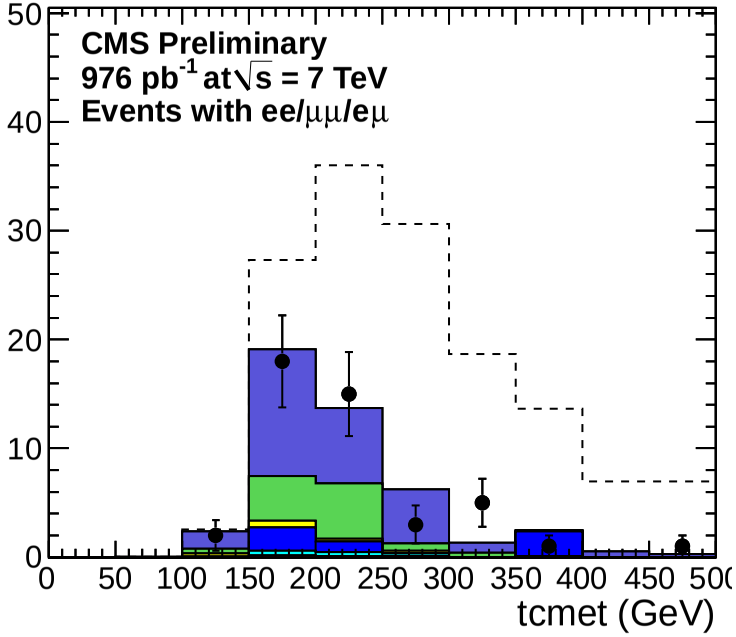
CMS Preliminary
976 pb-1 at √s = 7 TeV
Events with ee/μμ/eμ
tcmet (GeV)

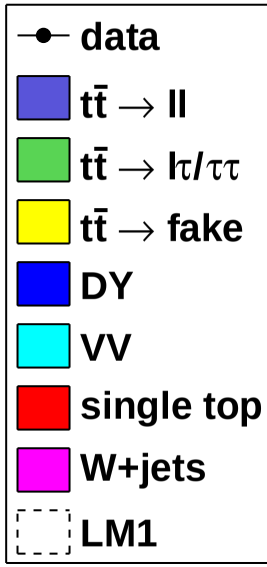
data
tt̄ → ll
tt̄ → lτ/ττ
tt̄ → fake
DY
VV
single top
W+jets
LM1

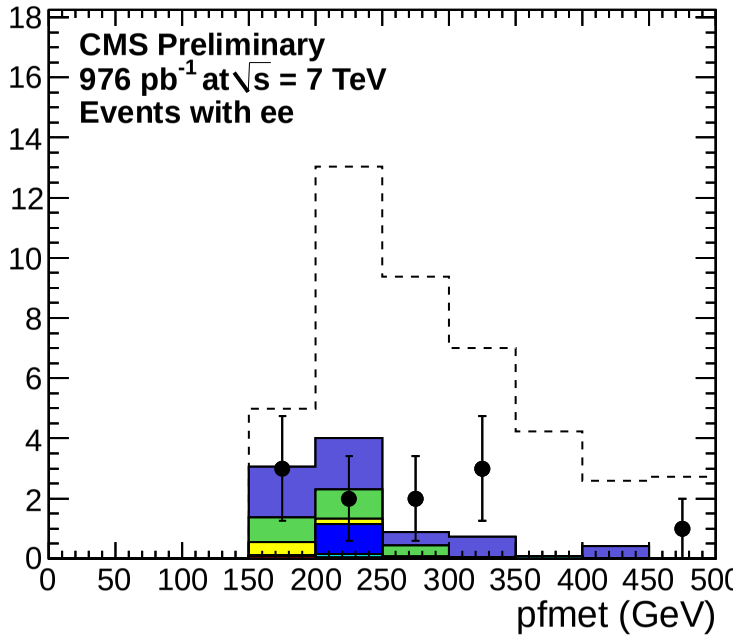
CMS Preliminary
976 pb-1 at √s = 7 TeV
Events with ee
pfmet (GeV)

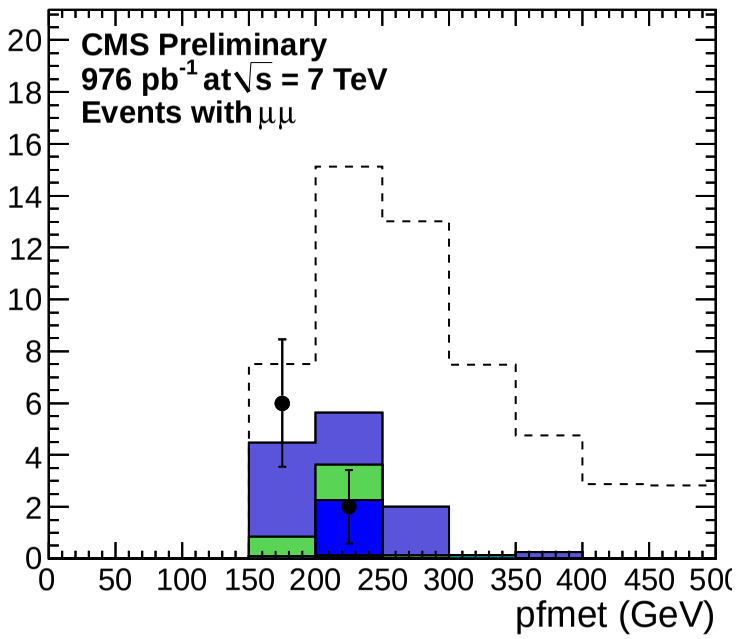
CMS Preliminary
976 pb-1 at √s = 7 TeV
Events with μμ
pfmet (GeV)

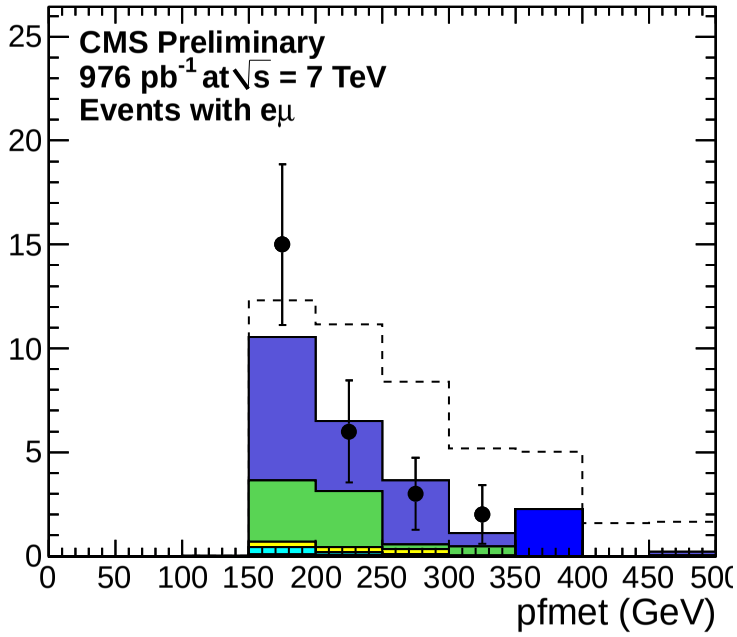
CMS Preliminary
976 pb-1 at √s = 7 TeV
Events with eμ
pfmet (GeV)

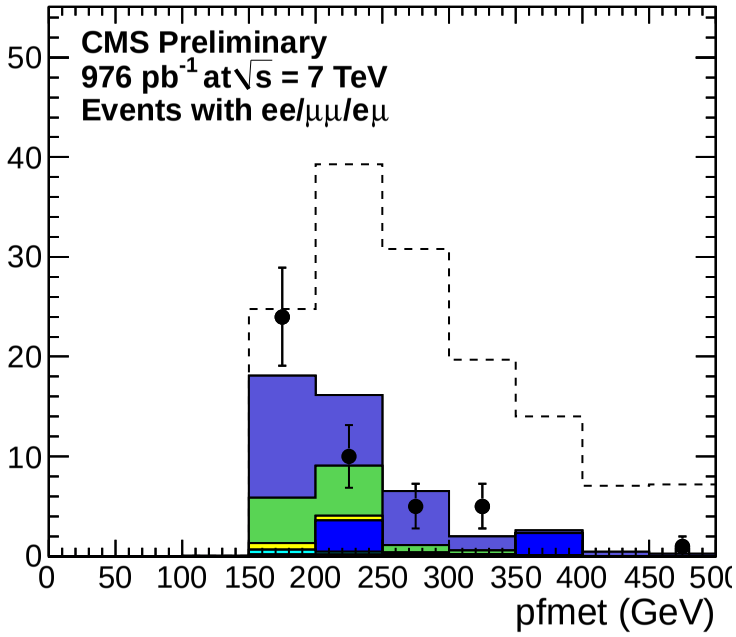
CMS Preliminary
976 pb-1 at √s = 7 TeV
Events with ee/μμ/eμ
pfmet (GeV)

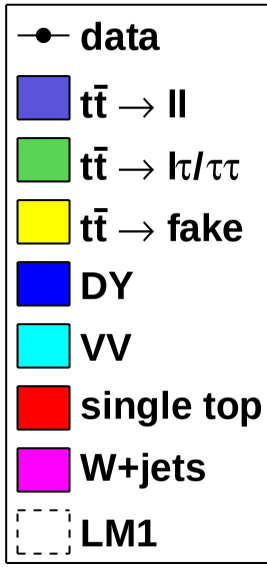
data
tt̄ → ll
tt̄ → lτ/ττ
tt̄ → fake
DY
VV
single top
W+jets
LM1

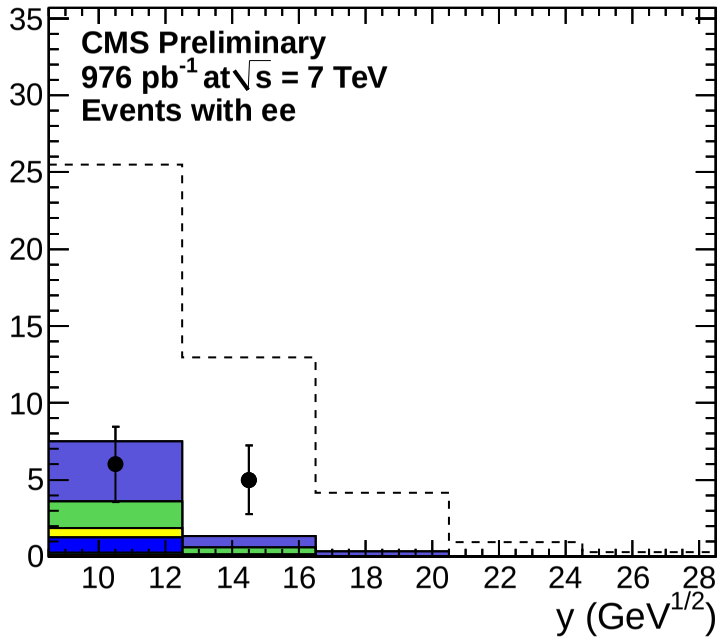
CMS Preliminary
976 pb-1 at √s = 7 TeV
Events with ee
y (GeV1/2)

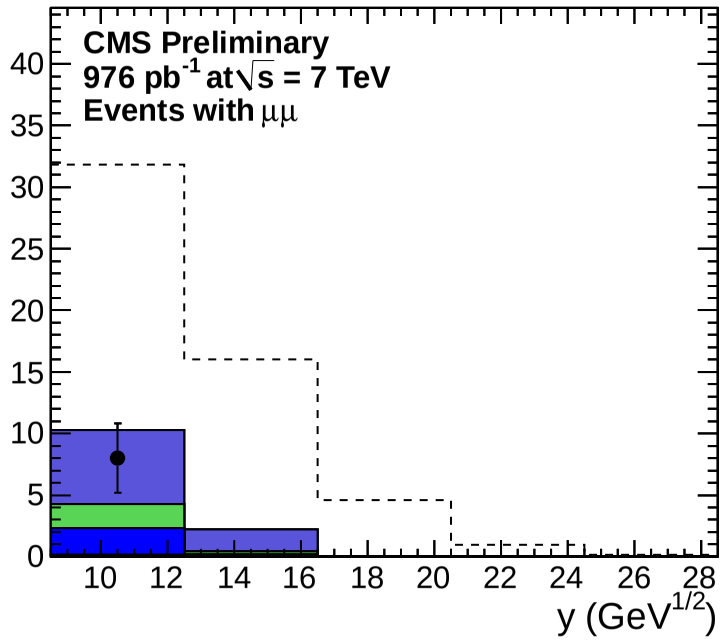
CMS Preliminary
976 pb-1 at √s = 7 TeV
Events with μμ
y (GeV1/2)

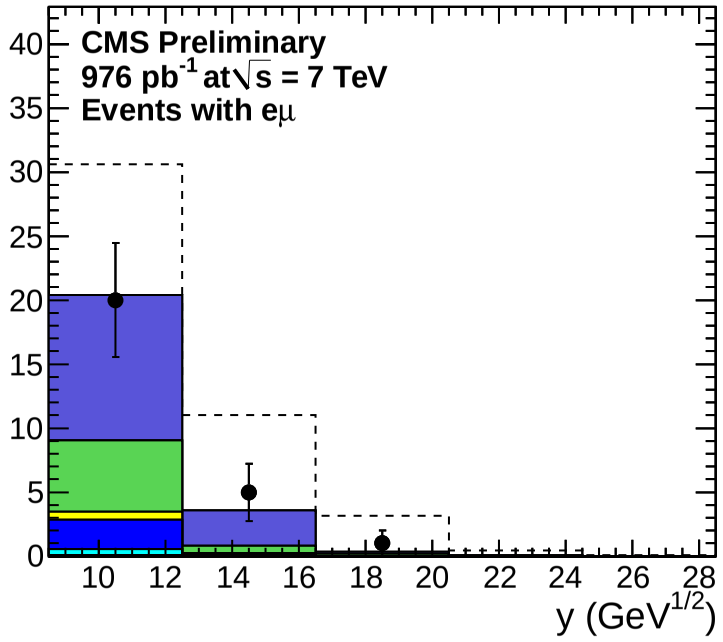
CMS Preliminary
976 pb-1 at √s = 7 TeV
Events with eμ
y (GeV1/2)

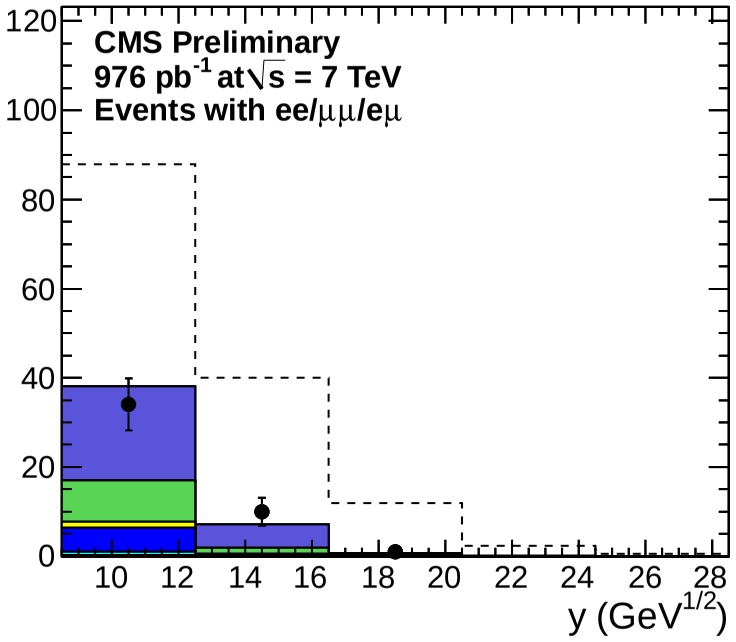
CMS Preliminary
976 pb-1 at √s = 7 TeV
Events with ee/μμ/eμ
y (GeV1/2)

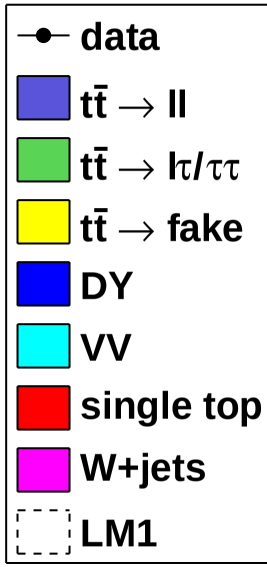
data
tt̄ → ll
tt̄ → lτ/ττ
tt̄ → fake
DY
VV
single top
W+jets
LM1

689

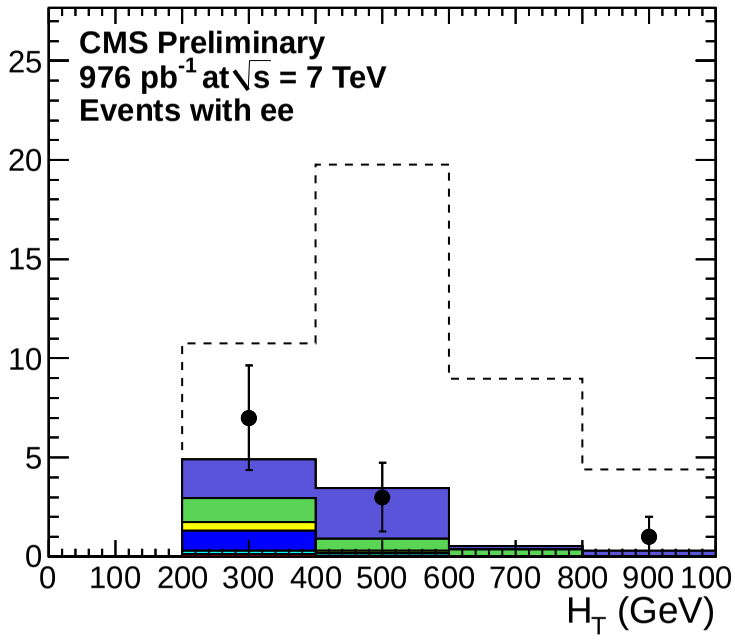
CMS Preliminary
976 pb-1 at √s = 7 TeV
Events with ee
HT (GeV)

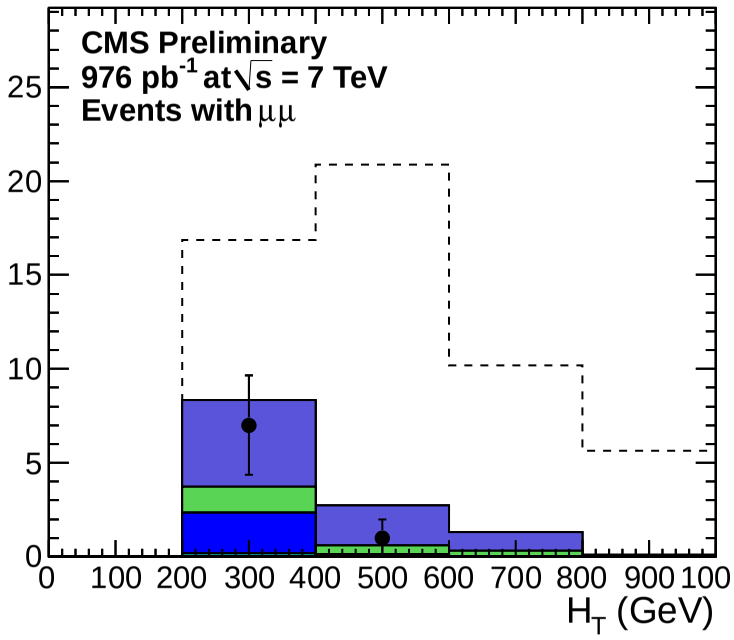
CMS Preliminary
976 pb-1 at √s = 7 TeV
Events with μμ
HT (GeV)

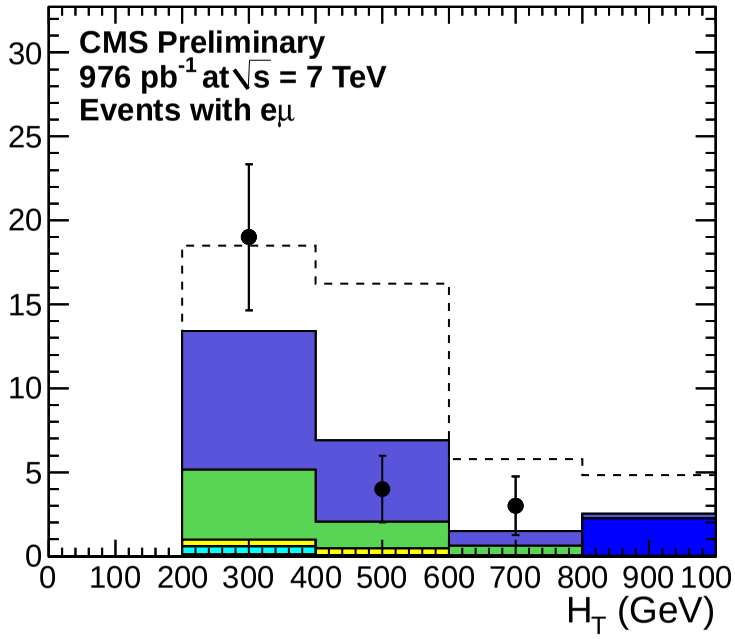
CMS Preliminary
976 pb-1 at √s = 7 TeV
Events with eμ
HT (GeV)

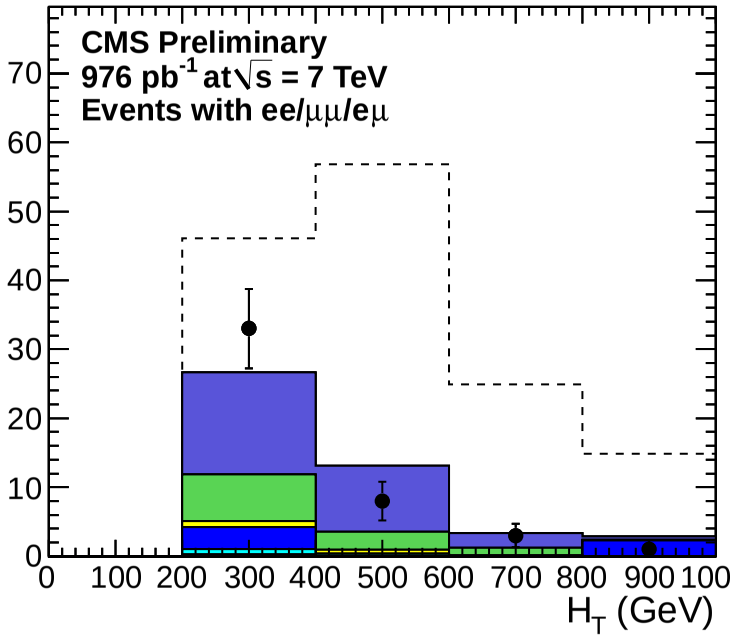
CMS Preliminary
976 pb-1 at √s = 7 TeV
Events with ee/μμ/eμ
HT (GeV)

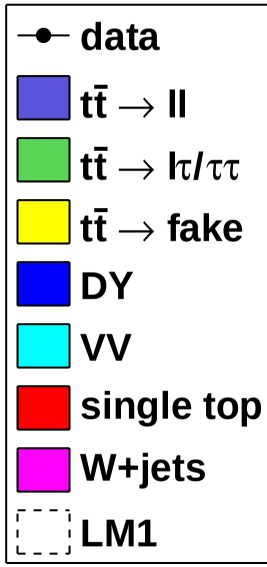
data
tt̄ → ll
tt̄ → lτ/ττ
tt̄ → fake
DY
VV
single top
W+jets
LM1

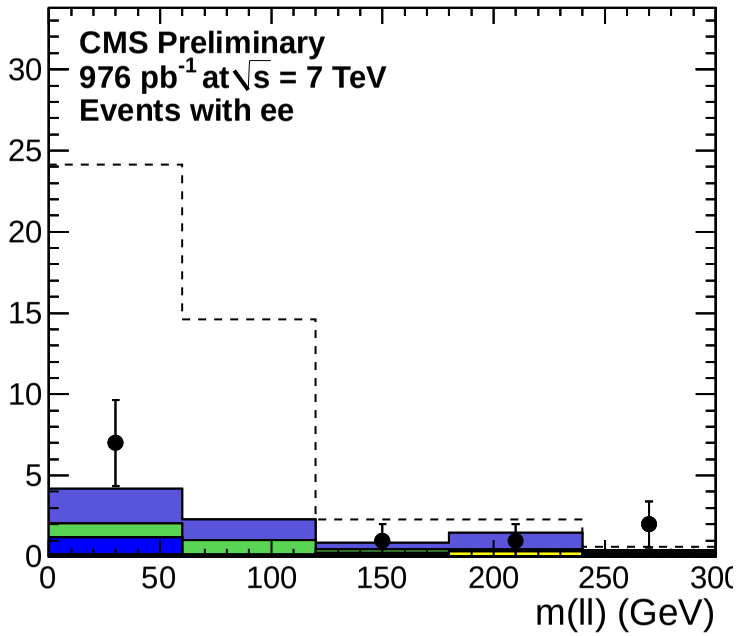
CMS Preliminary
976 pb-1 at √s = 7 TeV
Events with ee
m(ll) (GeV)

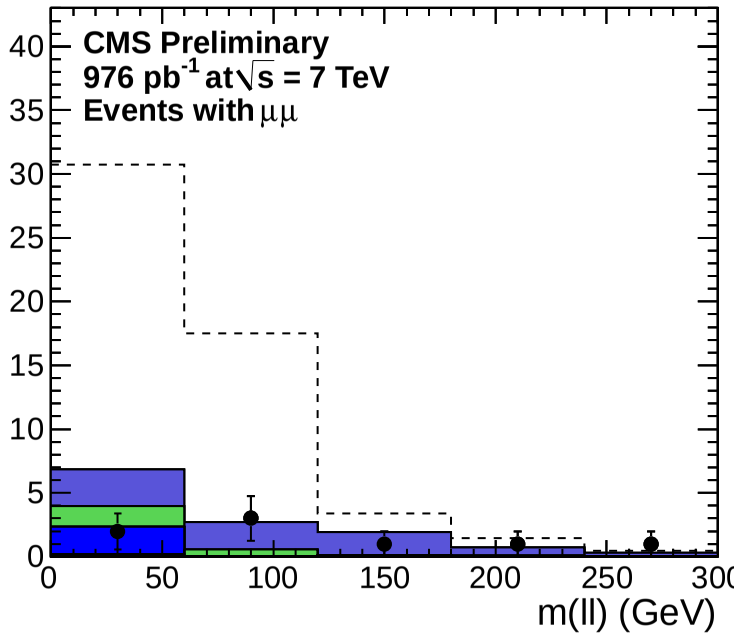
CMS Preliminary
976 pb-1 at √s = 7 TeV
Events with μμ
m(ll) (GeV)

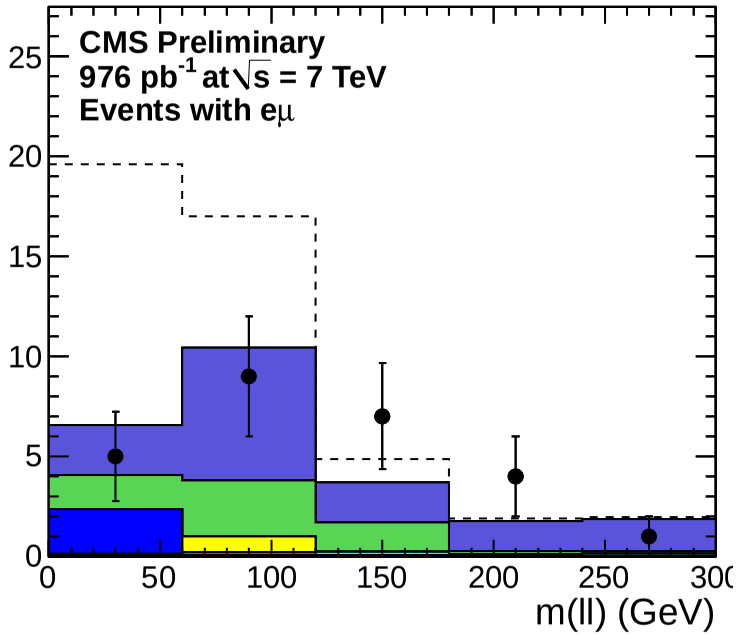
CMS Preliminary
976 pb-1 at √s = 7 TeV
Events with eμ
m(ll) (GeV)

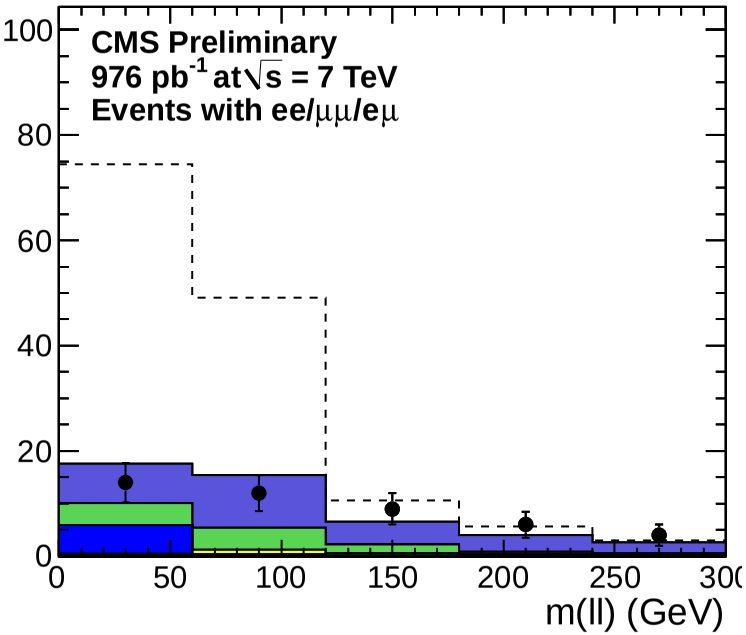
CMS Preliminary
976 pb-1 at √s = 7 TeV
Events with ee/μμ/eμ
m(ll) (GeV)

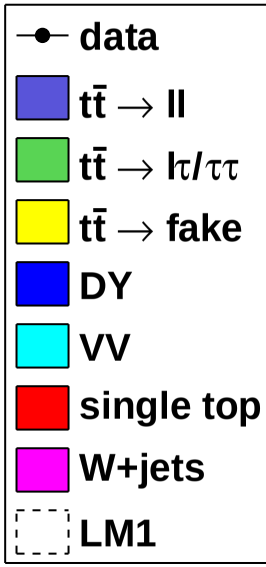
data
tt̄ → ll
tt̄ → lτ/ττ
tt̄ → fake
DY
VV
single top
W+jets
LM1

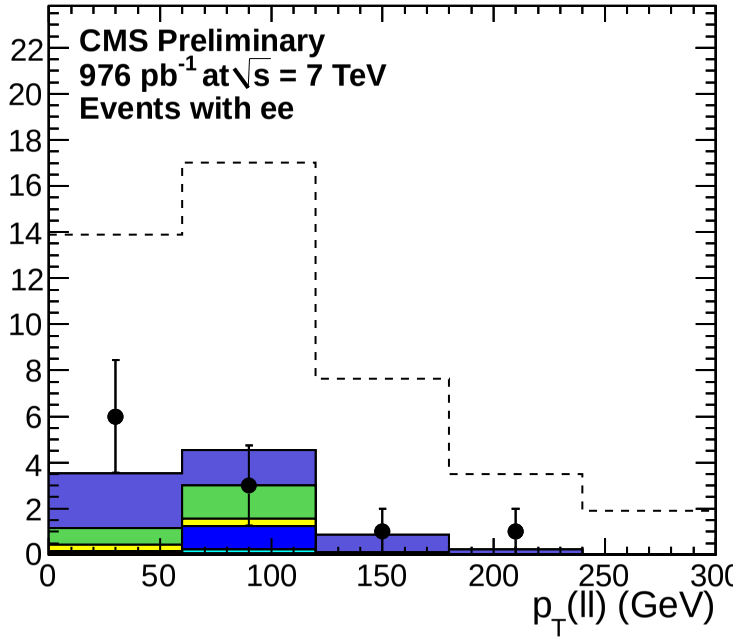
CMS Preliminary
976 pb-1 at √s = 7 TeV
Events with ee
pT(ll) (GeV)

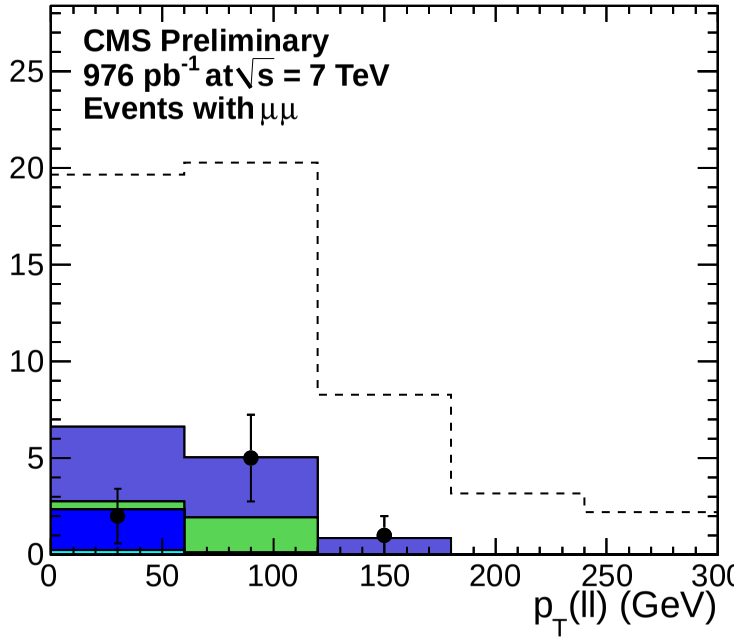
CMS Preliminary
976 pb-1 at √s = 7 TeV
Events with μμ
pT(ll) (GeV)

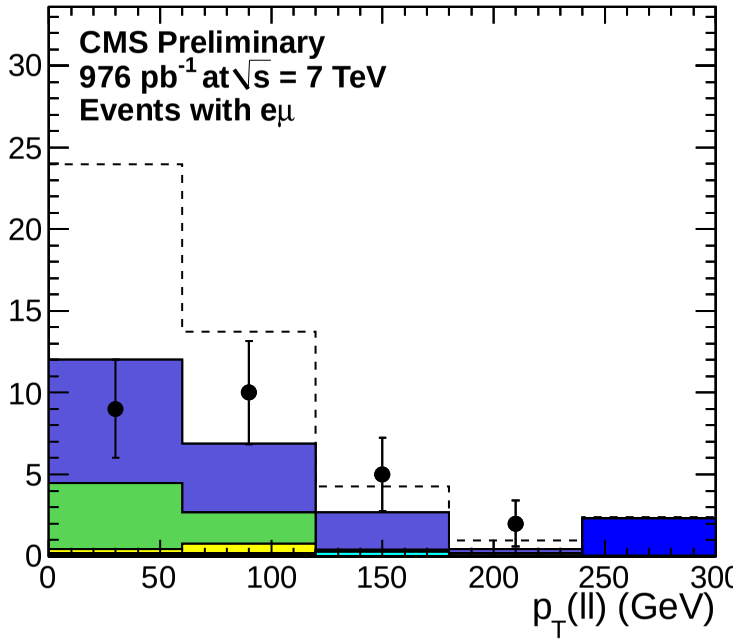
CMS Preliminary
976 pb-1 at √s = 7 TeV
Events with eμ
pT(ll) (GeV)

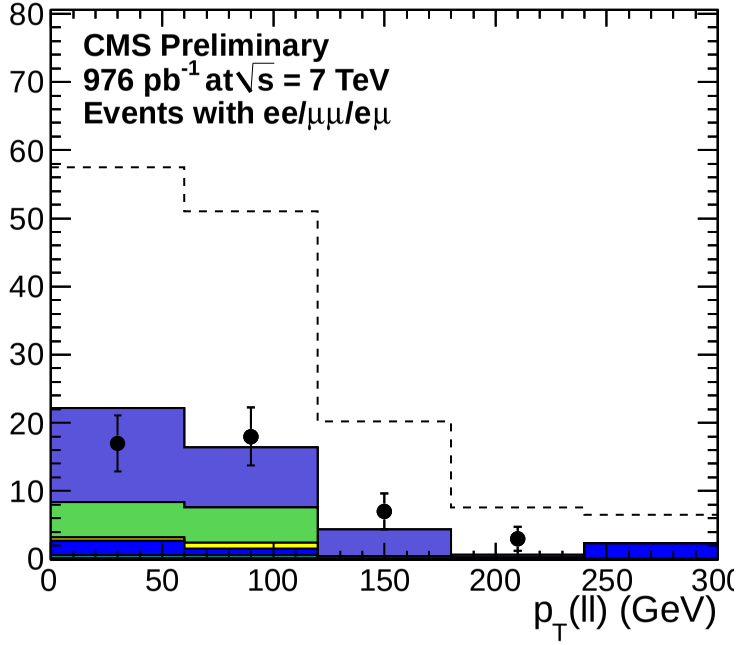
CMS Preliminary
976 pb-1 at √s = 7 TeV
Events with ee/μμ/eμ
pT(ll) (GeV)

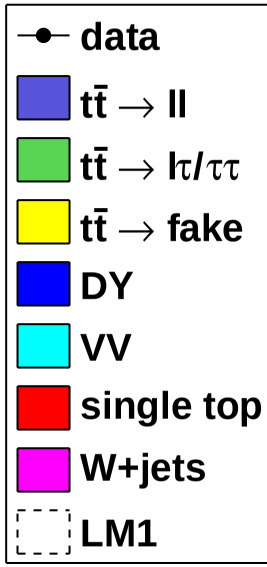
data
tt̄ → ll
tt̄ → lτ/ττ
tt̄ → fake
DY
VV
single top
W+jets
LM1

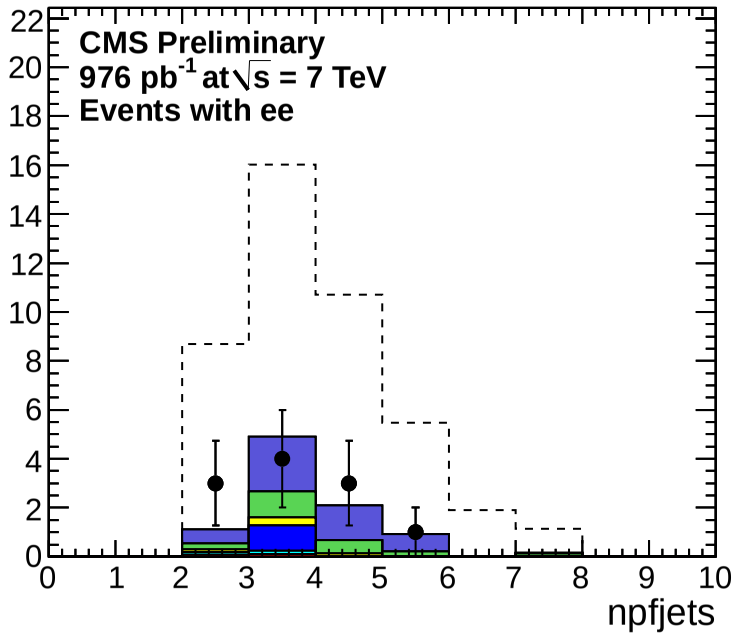
CMS Preliminary
976 pb-1 at √s = 7 TeV
Events with ee
npfjets

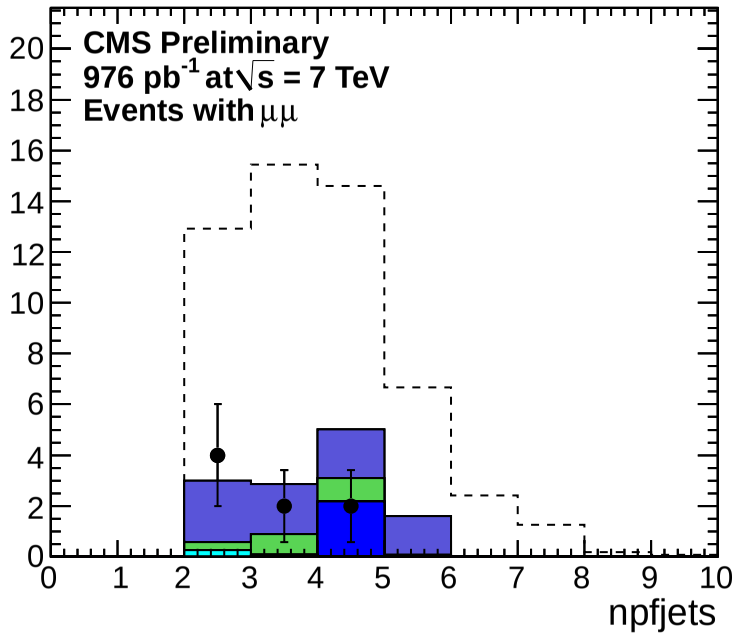
CMS Preliminary
976 pb-1 at √s = 7 TeV
Events with μμ
npfjets

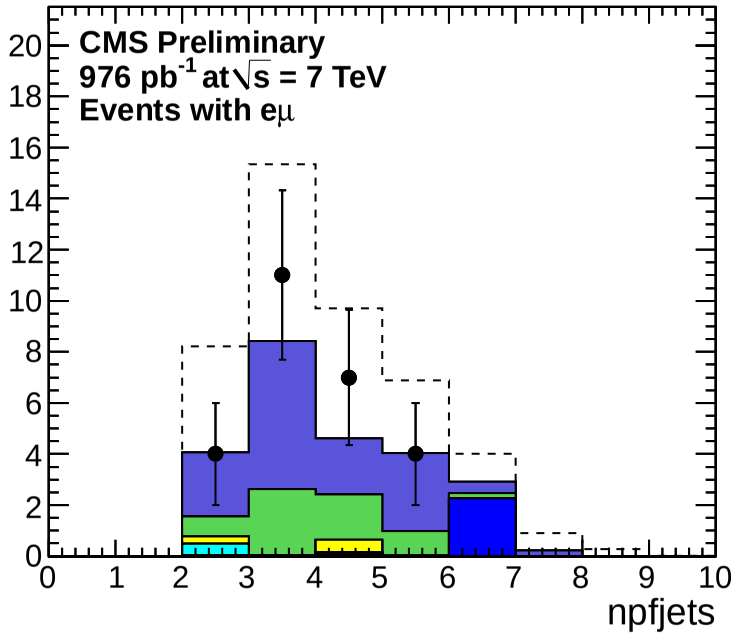
CMS Preliminary
976 pb-1 at √s = 7 TeV
Events with eμ
npfjets

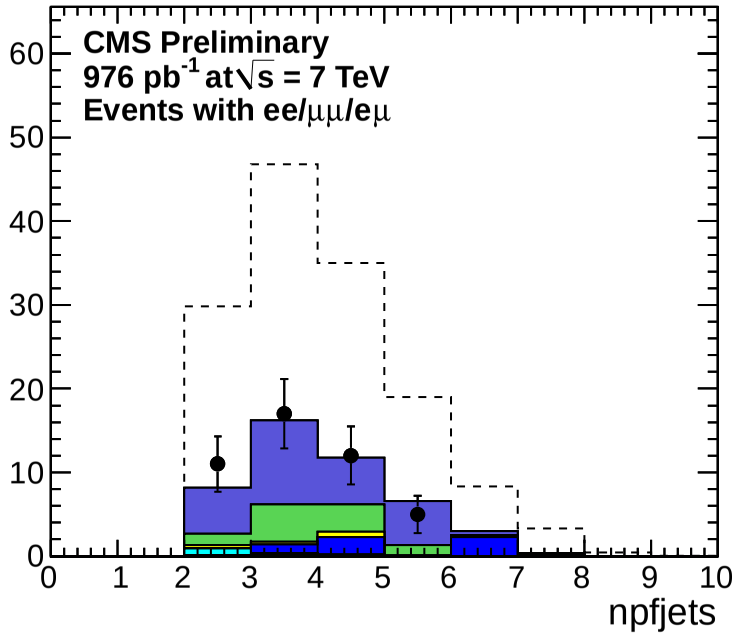
CMS Preliminary
976 pb-1 at √s = 7 TeV
Events with ee/μμ/eμ
npfjets

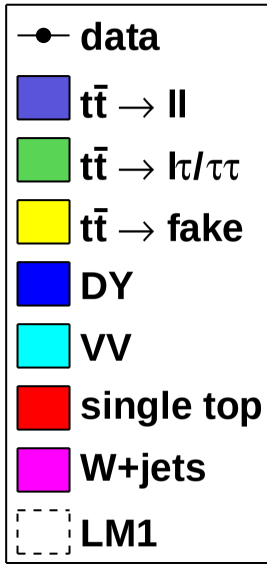
data
tt̄ → ll
tt̄ → lτ/ττ
tt̄ → fake
DY
VV
single top
W+jets
LM1

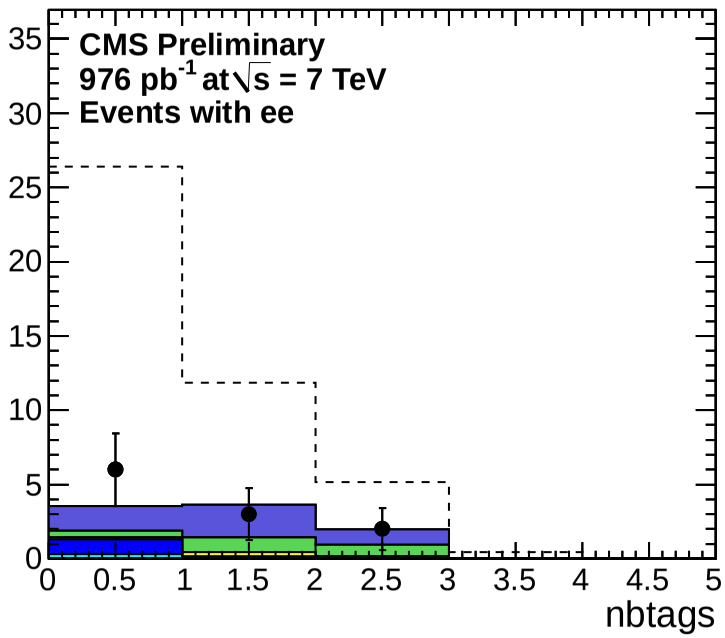
CMS Preliminary
976 pb-1 at √s = 7 TeV
Events with ee
nbtags

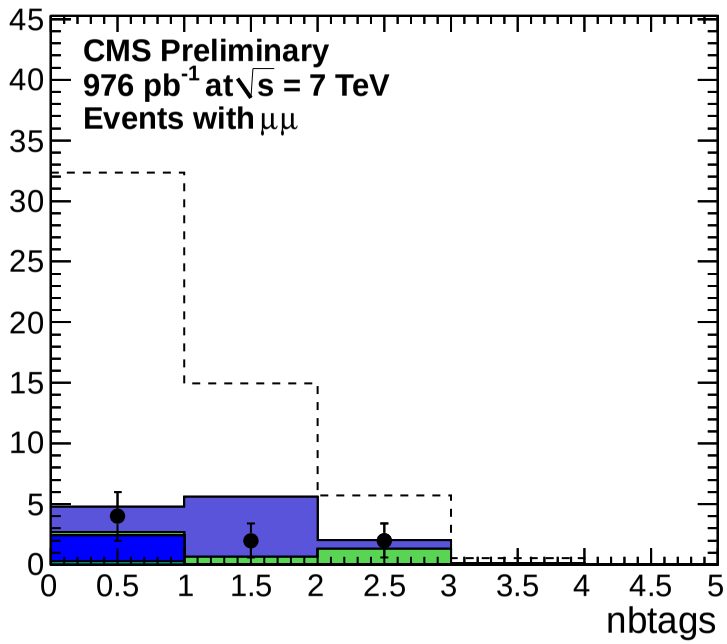
CMS Preliminary
976 pb-1 at √s = 7 TeV
Events with μμ
nbtags

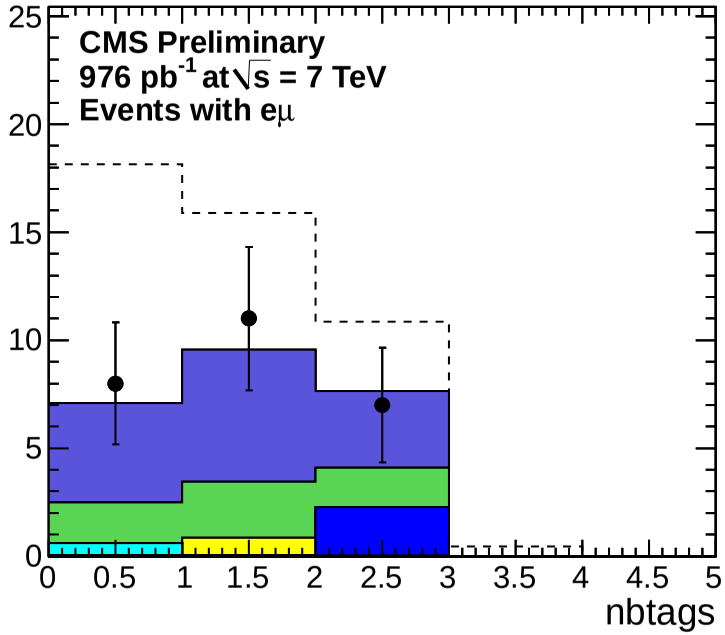
CMS Preliminary
976 pb-1 at √s = 7 TeV
Events with eμ
nbtags

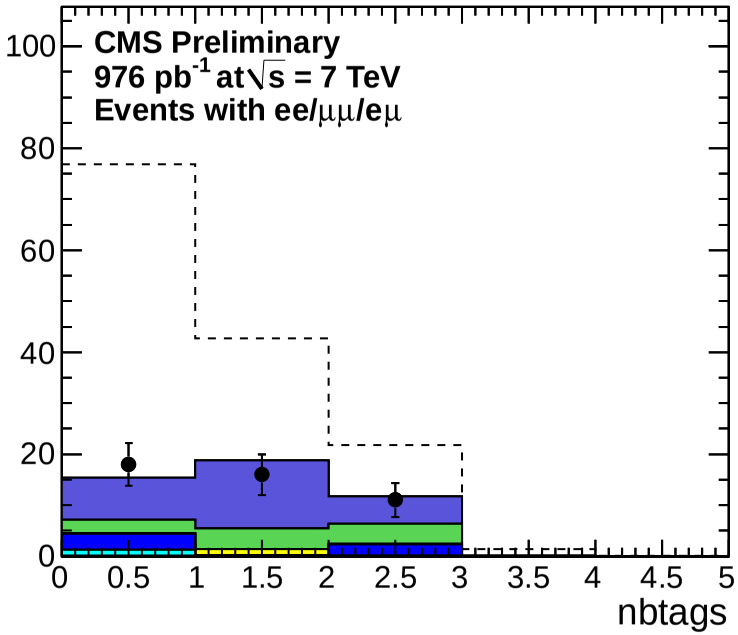
CMS Preliminary
976 pb-1 at √s = 7 TeV
Events with ee/μμ/eμ
nbtags

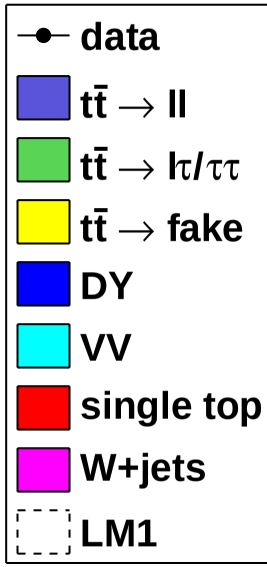
data
tt̄ → ll
tt̄ → lτ/ττ
tt̄ → fake
DY
VV
single top
W+jets
LM1

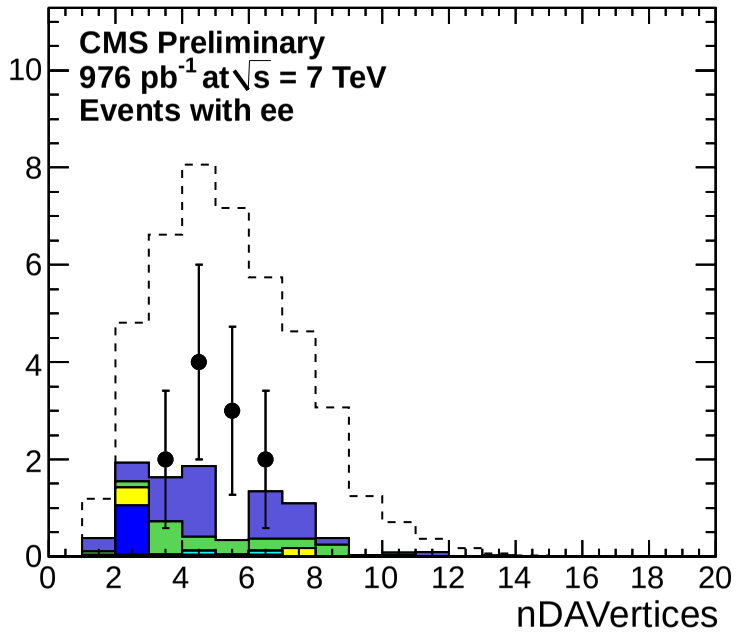
CMS Preliminary
976 pb-1 at √s = 7 TeV
Events with ee
nDAVertices

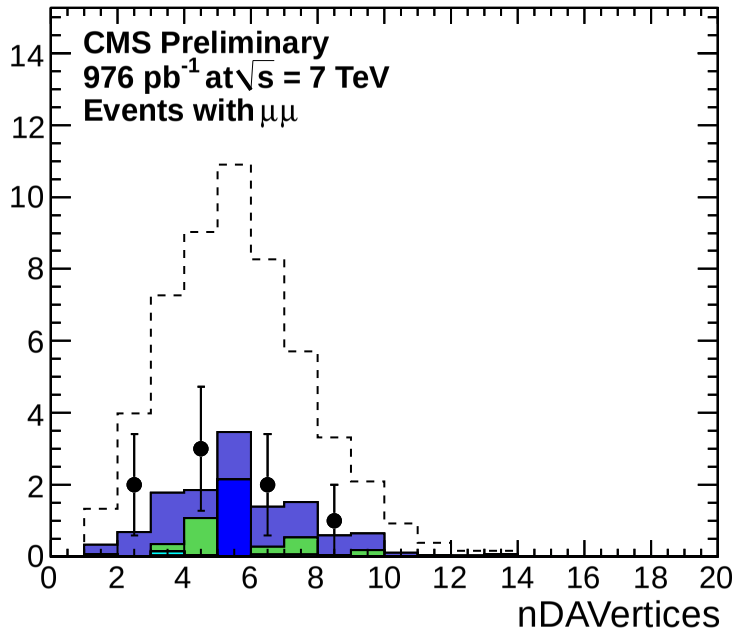
CMS Preliminary
976 pb-1 at √s = 7 TeV
Events with μμ
nDAVertices

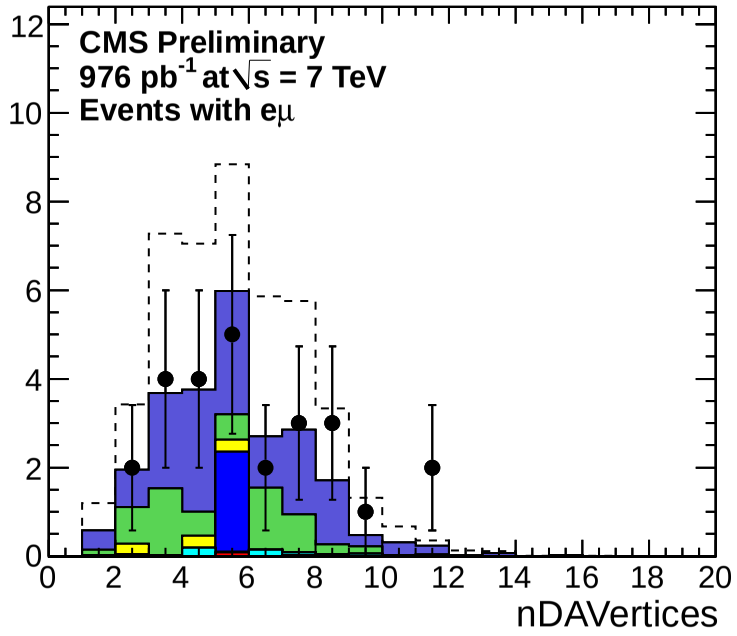
CMS Preliminary
976 pb-1 at √s = 7 TeV
Events with eμ
nDAVertices

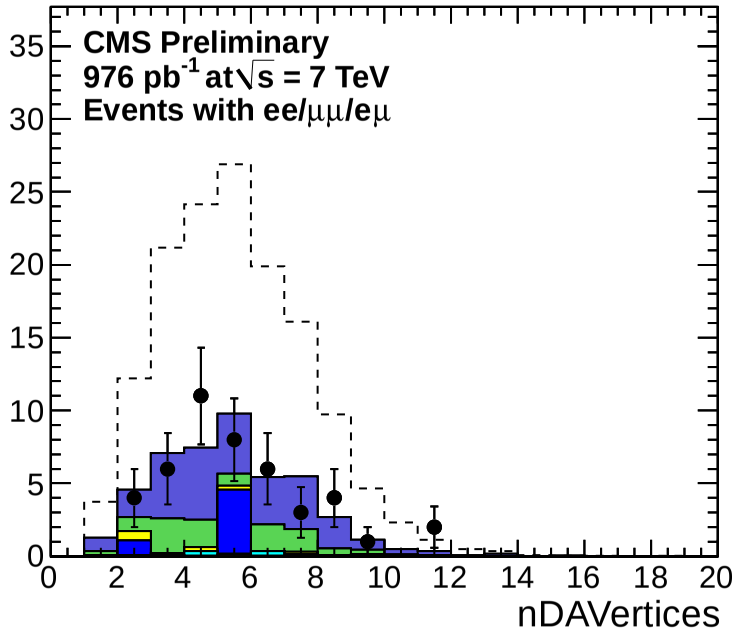
CMS Preliminary
976 pb-1 at √s = 7 TeV
Events with ee/μμ/eμ
nDAVertices

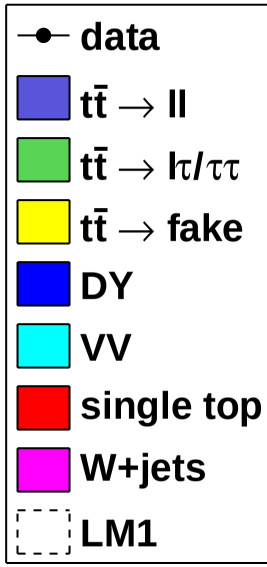
data
tt̄ → ll
tt̄ → lτ/ττ
tt̄ → fake
DY
VV
single top
W+jets
LM1

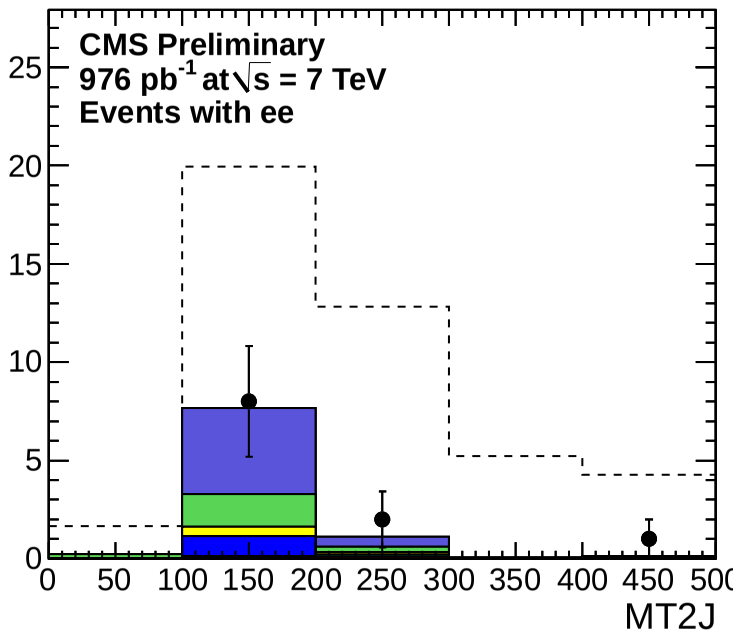
CMS Preliminary
976 pb-1 at √s = 7 TeV
Events with ee
MT2J

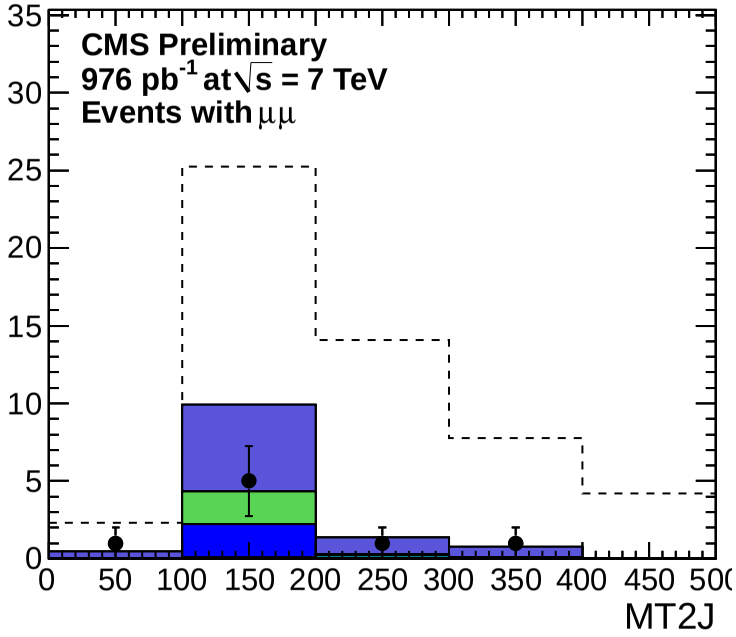
CMS Preliminary
976 pb-1 at √s = 7 TeV
Events with μμ
MT2J

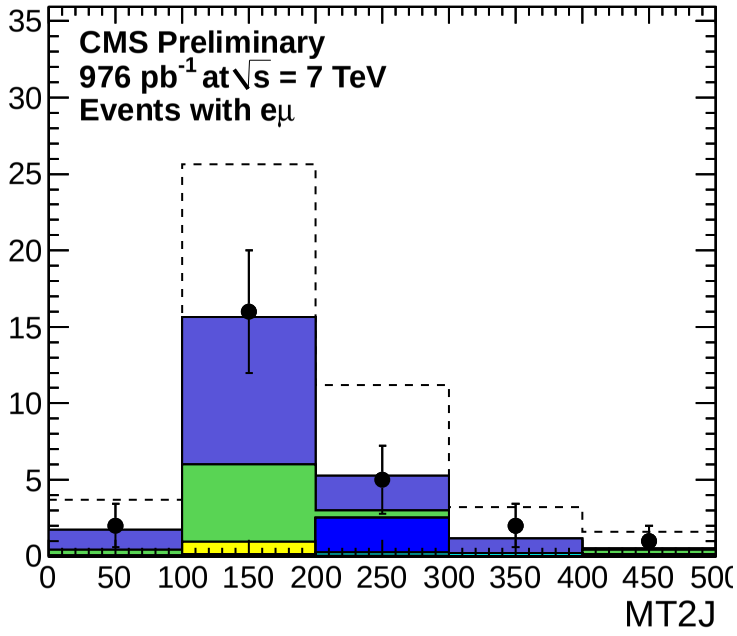
CMS Preliminary
976 pb-1 at √s = 7 TeV
Events with eμ
MT2J

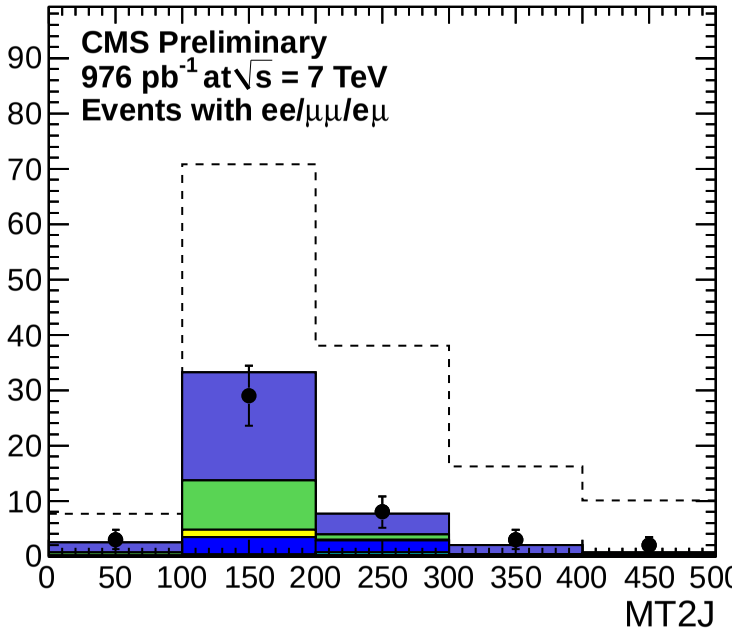
CMS Preliminary
976 pb-1 at √s = 7 TeV
Events with ee/μμ/eμ
MT2J

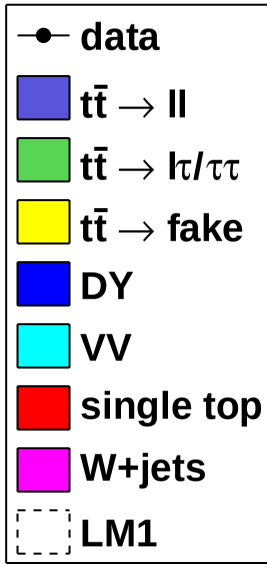
data
tt̄ → ll
tt̄ → lτ/ττ
tt̄ → fake
DY
VV
single top
W+jets
LM1

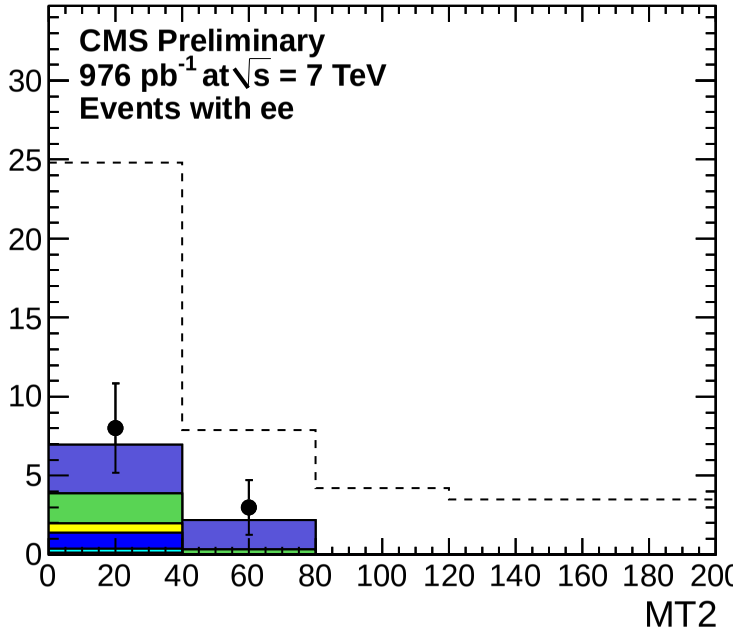
CMS Preliminary
976 pb-1 at √s = 7 TeV
Events with ee
MT2

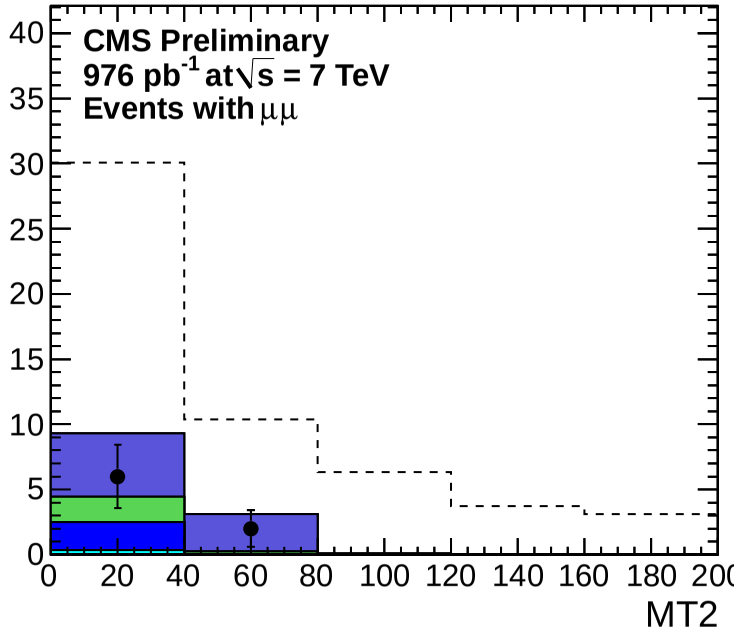
CMS Preliminary
976 pb-1 at √s = 7 TeV
Events with μμ
MT2

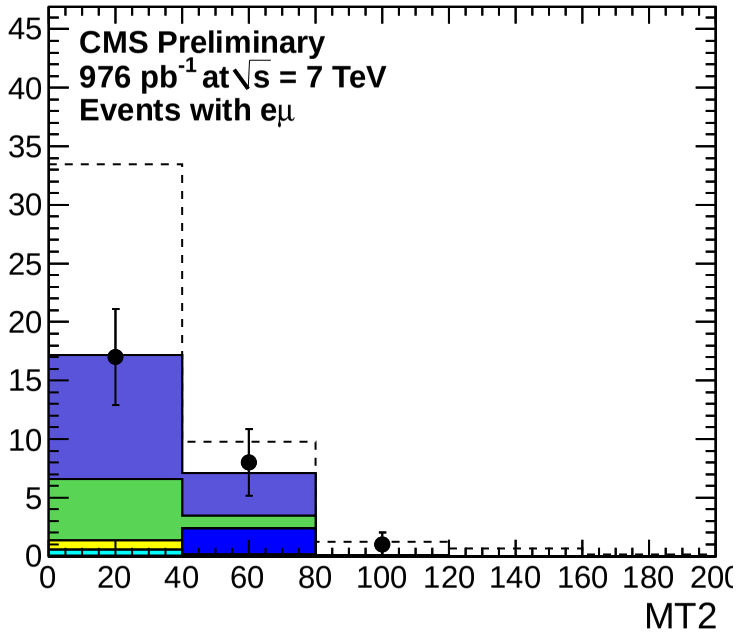
CMS Preliminary
976 pb-1 at √s = 7 TeV
Events with eμ
MT2

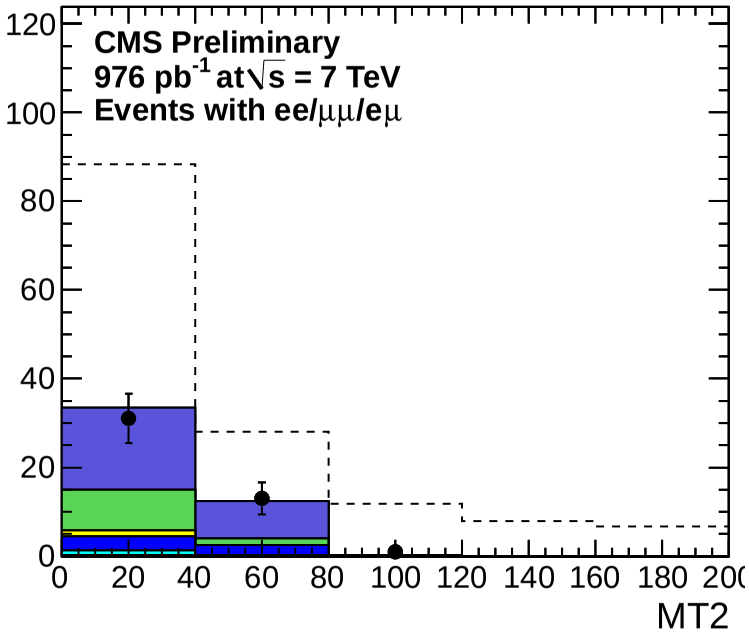
CMS Preliminary
976 pb-1 at √s = 7 TeV
Events with ee/μμ/eμ
MT2

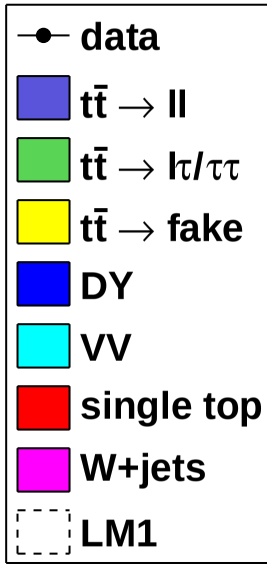
data
tt̄ → ll
tt̄ → lτ/ττ
tt̄ → fake
DY
VV
single top
W+jets
LM1

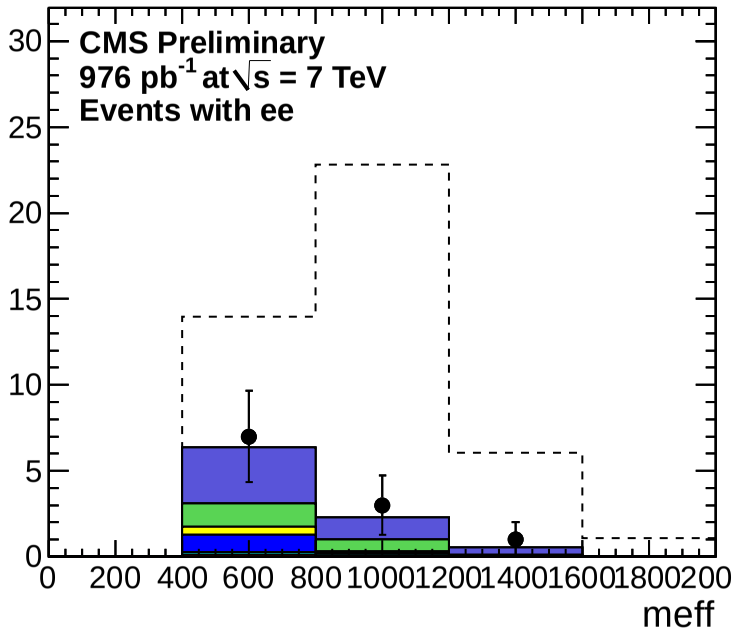
CMS Preliminary
976 pb-1 at √s = 7 TeV
Events with ee
meff

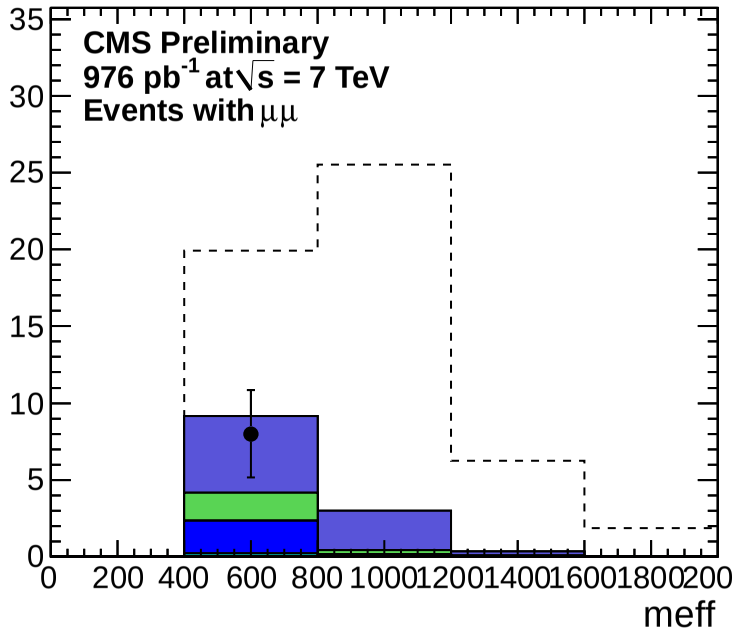
CMS Preliminary
976 pb-1 at √s = 7 TeV
Events with μμ
meff

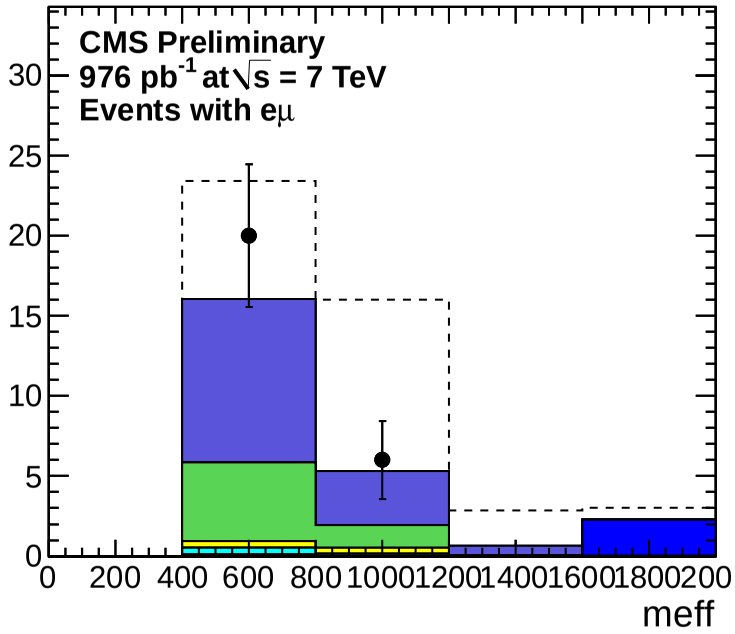
CMS Preliminary
976 pb-1 at √s = 7 TeV
Events with eμ
meff

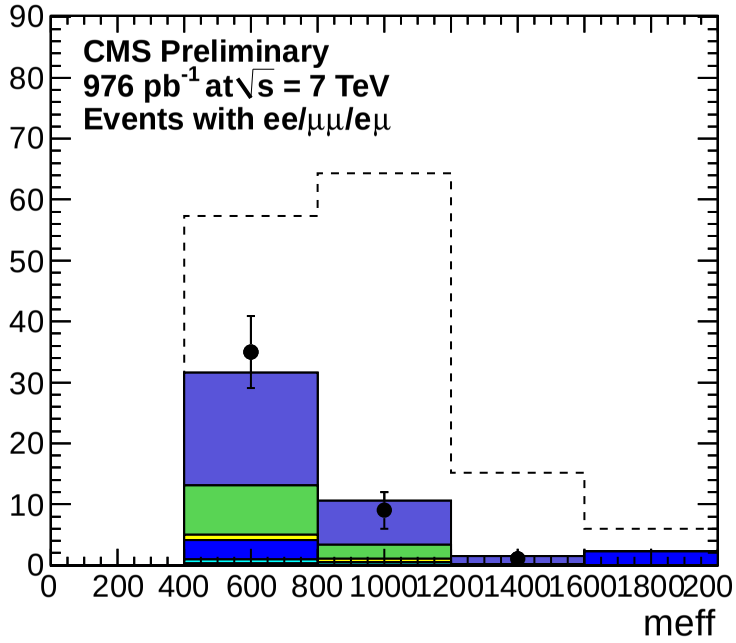
CMS Preliminary
976 pb-1 at √s = 7 TeV
Events with ee/μμ/eμ
meff

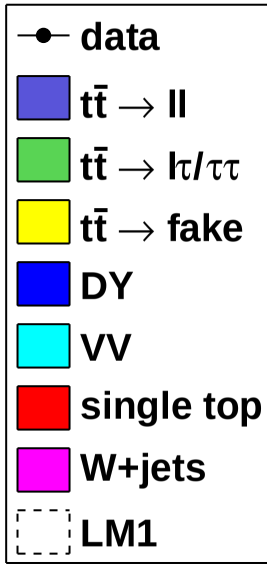
data
tt̄ → ll
tt̄ → lτ/ττ
tt̄ → fake
DY
VV
single top
W+jets
LM1